Composite Separators for Robust High Rate Lithium Ion Batteries

Botao Yuan, Kechun Wen, Dongjiang Chen, Yuanpeng Liu, Yunfa Dong, Chao Feng, Yupei Han, Jiecai Han, Yongqi Zhang,* Chuan Xia,* Andy (Xueliang) Sun, and Weidong He*

Lithium ion batteries (LIBs) are one of the most potential energy storage devices among various rechargeable batteries due to their high energy/power density, long cycle life, and low self-discharge properties. However, current LIBs fail to meet the ever-increasing safety and fast charge/discharge demands. As one of the main components in LIBs, separator is of paramount importance for safety and rate performance of LIBs. Among the various separators, composite separators have been widely investigated for improving their thermal stability, mechanical strength, electrolyte uptake, and ionic conductivity. Herein, the challenges and limitations of commercial separators for LIBs are reviewed, and a systematic overview of the state-of-the-art research progress in composite separators is provided for safe and high rate LIBs. Various combination types of composite separators including blending, layer, core–shell, and grafting types are covered. In addition, models and simulations based on the various types of composite separators are discussed to comprehend the composite mechanism for robust performances. At the end, future directions and perspectives for further advances in composite separators are presented to boost safety and rate capacity of LIBs.

1. Introduction

With the rapid development of the industrial revolution and technological innovation, traditional energy sources, such as fossil fuels (coal, oil, natural gas, etc.), are far from satisfying human beings needs, and cause serious environmental effects such as greenhouse effect and acid rain due to a large amount of carbon dioxide or sulfur dioxide production after burned.[1,2] Environmental pollution not only harms human health, but

also damages economic resources and ecological balance. Research interest and achievements in wind, solar, tidal and geothermal energy have surged to solve the energy issues, but the intermittence and uncontrollability of the aforementioned sustainable energy fail to meet large-scale applications.[3–6] Lithium ion batteries (LIBs), one of the electrochemical-storage-conversion devices with high mass/volume density and lower self-discharge properties, have attracted considerable attention due to the constant power supply.[7–13] In recent years, the aforementioned attractive properties of LIBs have promoted the utilization in a wide range of applications such as electric vehicle, electronic products, robot power, military power, emergency power, armarium power, wind energy storage and solar energy storage, as shown in **Figure 1**.

LIBs are mainly composed of four components: cathode, anode, electrolyte, and separator.[14] During the charging process, lithium ions (Li+) de-intercalate from the cathode and insert into the anode through the electrolyte and separator, and this process is reversed when discharging.[15,16] Separator provides channels for Li+ transfer and avoids the direct contact between cathode and anode.[17–21] The United States Advanced Battery Consortium requirements set operation standards for Li-ion battery separators, including suitable thickness (5–25 μm), uniform pore size (<1 μm), high wettability, excellent permeability (<0.025 s μm^{-1}), robust tensile mechanical

Dr. B. Yuan, Dr. K. Wen, Dr. Y. Liu, Dr. Y. Dong, Prof. J. Han, Prof. W. He
National Key Laboratory of Science and Technology on Advanced Composites in Special Environments
and Center for Composite Materials and Structures
Harbin Institute of Technology
Harbin 150080, China
E-mail: weidong.he@hit.edu.cn

Dr. D. Chen, Dr. C. Feng, Dr. Y. Han, Prof. W. He
School of Physics
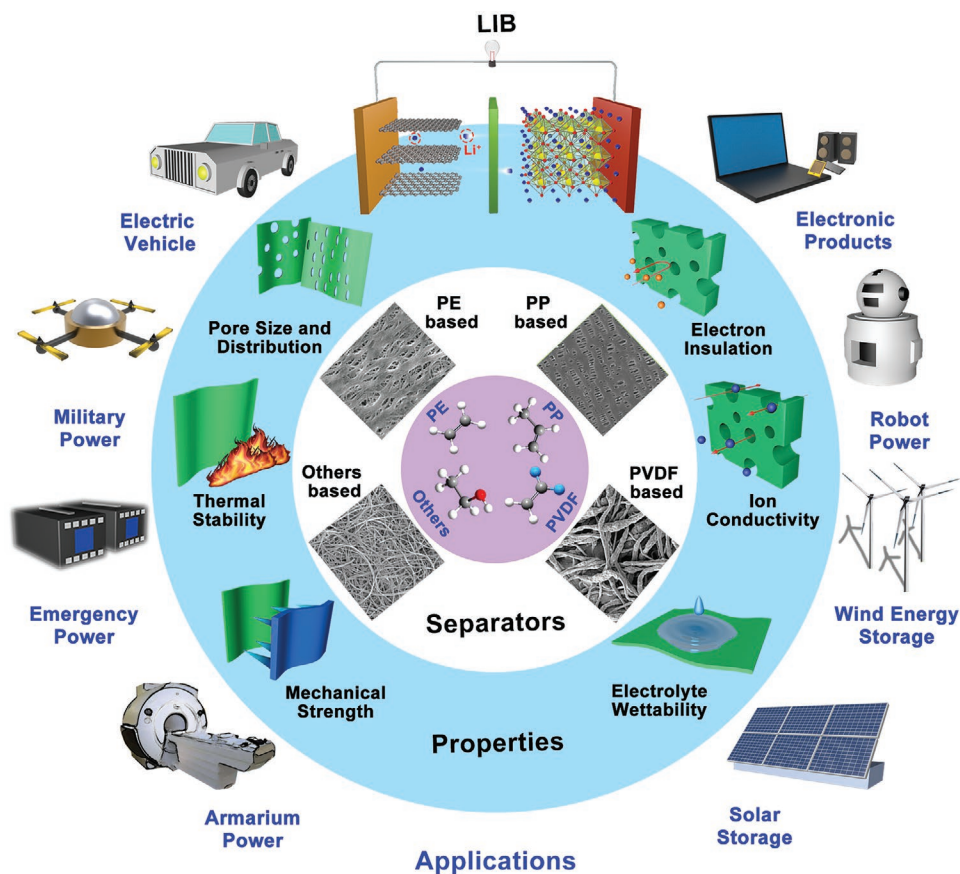University of Electronic Science and Technology of China
Chengdu 611731, China

Prof. Y. Zhang
Institute of Fundamental and Frontier Sciences
University of Electronic Science and Technology of China
Chengdu 611731, China
E-mail: yqzhang@uestc.edu.cn

Prof. C. Xia
School of Materials and Energy
University of Electronic Science and Technology of China
Chengdu 611731, China
E-mail: chuan.xia@uestc.edu.cn

Prof. A. Sun
Department of Mechanical and Materials Engineering
University of Western Ontario
London, Ontario N6A 5B9, Canada

ADVANCED
SCIENCE NEWS
www.advancedsciencenews.com

ADVANCED
FUNCTIONAL
MATERIALS
www.afm-journal.de

Figure 1. Diagram of the main properties required for the separators and the applications for LIBs. The microstructure of PE based separators is reproduced with permission.[144] Copyright 2012, Wiley-VCH GmbH. The microstructure of PP based separators is reproduced with permission.[229] Copyright 2019, Springer Nature. The microstructure of PVDF based separators is reproduced with permission.[92] Copyright 2017, American Association for the Advancement of Science (AAAS). The microstructure of others based separators is reproduced with permission.[157] Copyright 2017, Wiley-VCH GmbH.

strength (>1000 kg cm^{-2} or 98.06 MPa), high thermal stability (<5% shrinkage after 60 min at 90 °C), outstanding dimensional stability, chemical stability, and electrochemical stability.[22] Among the requirements for separators, the mechanical properties of separators are mainly characterized by the tensile strength in the machine direction (MD) and the transverse direction (TD).[23] All of the properties shown in Figure 1 are closely related to internal resistance, cycle performance, rate capacity, safety and commercial prospect for LIBs.[24,25]

Polyolefin separators (polyethylene (PE), polypropylene (PP)) have been commonly employed in commercial LIBs due to the electrochemical stability.[22,26] However, commercial polyolefin separators featured with inferior thermal stability and weak wettability fail to meet the burgeoning energy demands.[27,28] Separators experience thermal shrinkage as LIBs operate in severe environments, which induce short-circuit and thus lead to catastrophic LIBs failure due to their flammability and poor thermal stability.[23,29–32] Due to the poor electrolyte uptake of polyolefin separators, incomplete filling of the electrolyte in the separator pores results in the blockage of ion pathways, giving rise to uneven and irreversible Li$^+$ transport between anode and cathode.[33–36] Hence, polyolefin separator exhibits inferior compatibility with positive and negative electrodes. Further, the poor compatibility interface easily forms an unstable solid electrolyte interphase (SEI) associated with inhomogeneous lithium

dendrites growth.[37–41] The uneven lithium dendrites puncture the separator, inducing potential safety hazards.[42–46] The inferior wettability of the polyolefin-based separators owns poor rate performance due to the sluggish Li$^+$ transfer.[47–50] Recently, poly(vinylidene fluoride) (PVDF) and other polymers have also drawn extensive attention due to their superior wettability.[17,51] However, their thermal stability and mechanical strength still cannot satisfy the commercial demands.

To address the aforementioned issues, composite separators have been proposed and majorly focused which use various organic and inorganic materials as fillers with polymer matrices. Compared with commercial polyolefin separators or single component polymer separators, there are several advantages and disadvantages for composite separators. The mostly used fillers of composite separators are oxides or nitrides with high melting point and mechanical properties, polymers with high tensile strength and high decomposition temperature, or their combinations. The wettability, electrolyte uptake, mechanical properties, thermal stability, flame resistance, and ionic conductivity of separators have been significantly improved in composite form.[52,53] However, composite separators can also exhibit unfavorable disadvantages. For example, the thicker thickness and unsatisfactory pore structure of separators give rise to the large internal resistance increase of batteries. In addition, the fillers also cause the blockage of pores of polymer

**ADVANCED
SCIENCE NEWS**
www.advancedsciencenews.com

**ADVANCED
FUNCTIONAL
MATERIALS**
www.afm-journal.de

matrices, reducing the ionic conductivity and high rate capacity of LIBs. In view of the merits and drawbacks of composite separators, different improvement methods and technologies will be discussed in this review.

A number of methods have been proposed to improve the performances of composite separator, including introducing additives, creating new materials and constructing novel architectures. The formed composite separator structures are diverse, including the blending structure, layered structure, core–shell structure and grafting structure. Various composite separators have also been reported to improve the electrochemical performance of LIBs in an extreme environment and wider range of applications.

In this review, recent studies on composite separators for safe high rate LIBs are reviewed in terms of composite structure types and different materials. The composite structure types are comprehensively discussed to distinguish and integrate the types of the composite separators clearly. The models and simulations based on the various types of composite separators are also explored to explain the composite mechanism for robust performances. Future directions and development toward the composite separators for excellent electrochemical performance LIBs are also provided at the end.

2. Methods to Prepare Composite Separators

During the 30 years of development of LIBs, the preparation methodologies of separators are diverse and varied, and each method has a great impact on the performance of the separator. Due to the simple preparation process, short time consumption, and balanced performances, dry stretching method is usually applied to prepare commercial polyolefin separators through changing temperature, stretching force, stretching rate.[23] The pores of the polyolefin separators prepared with dry stretching methods tend to close at high temperatures to prevent thermal runaway and avoid short circuit risks.[54] In addition, the polyolefin separators through dry stretching methods have poor wettability with the electrolyte, thus causing sluggish Li+ transfer. Therefore, in addition to the dry stretching method, there are other methods that have been used to improve the separators, such as solution casting, dip coating, phase inversion, electrospinning, and surface grafting. The fabrication techniques of composite separators combine the above preparation methods. After the composite materials are added in the base materials, the safety performance of the separator could be enhanced, and the electrochemical performance of the battery could be also improved subsequently, due to the accurate, flexible and facile methods used in the composite processes.[55,56] The combination of different preparation techniques for composite separators have been provided and reported in the literature, then the most commonly used techniques are briefly explained in this section.

2.1. Solution Casting Method

Solution casting method has been mostly used to prepare the composite separators for LIBs because of its easy control of separators thickness, simple operation process and low cost.[57] In the method, polymer powder, and the additive are dissolved in a solvent under magnetic stirring to obtain a uniform solution, followed by heating at a certain temperature until the solution shows a translucent appearance gel, and then the solution is casted on a metal plate or a flat glass dish by using a scraper coating machine. Then the slurry of polymer and additive is evenly coated by a doctor blade, followed by drying at suitable temperature. After drying at the certain temperature, the film is then detached from the plate and the separator is obtained. The porosity, pore size and mechanical strength of the composite separator prepared through this mode depends upon the solubility of polymers and additives, the particle size of polymers and additives, types of solvent, water bath temperature, drying temperature, and slurry stability.[58]

2.2. Phase Inversion Method

Phase inversion method is also widely applied to fabricate the composite separators for LIBs. In this method, a composite homogeneous polymer solution is firstly formed. Then, the molecular dynamics equilibrium of the solution is disrupted and changed from a single phase to two phases by some physical ways, followed by forming a polymer-rich phase and a polymer-lean phase. At the end, composite separators are obtained from the polymer-rich phase with the evaporation of polymer-lean phase.[59] The preparation of composite separators through phase inversion method could be classified into three main different techniques: 1) nonsolvent-induced phase separation (NIPS); 2) thermally induced phase separation (TIPS); 3) vapor induced phase separation.[19] The phase inversion methods through NIPS and TIPS are the most widely used and explained in detail as follows.

The NIPS method could be easily controlled to avoid separators perforation, obtain a small and evenly distributed micropore size, and achieve high tensile strength, biaxial and puncture strength, compared to other methods such as the dry-spinning/ hot-drawing process.[60] In this method, the composite separators are prepared by dissolving polymer powders in a solvent at a certain concentration. After forming a transparent solution, the additive is then added into the solution under continuous stirring to form uniform slurry. Then the solution is casted on a smooth glass plate by using the scraper coating machine. Then the glass plate is immersed in water or other nonsolvent to achieve the phase inversion process, during which the solvent exchanges with water. Finally, the acquired composite separator could be peeled off from the plate and dried at a certain temperature. The key step of NIPS is that the solvent and nonsolvent exchange under the driving force caused by the gradient in chemical potential.[19] The dissolved polymer precipitates and transfers from one-phase regions to two-phase regions in polymer-solvent-nonsolvent system.[61] The transformation accompanied with thermodynamic variation of polymers has great impact on the formation and distribution of pores, which presents the formation of different morphologies such as sponge-like and fingerlike structures.[22] The process through this method is shown in **Figure 2**a, and to show the microstructure, for instance, the micrograph of the ZrO$_2$/poly(vinylidene fluoride-*co*-hexafluoropropylene) (PVDF-HFP) separator prepared by NIPS method is shown in Figure 2b.[62]
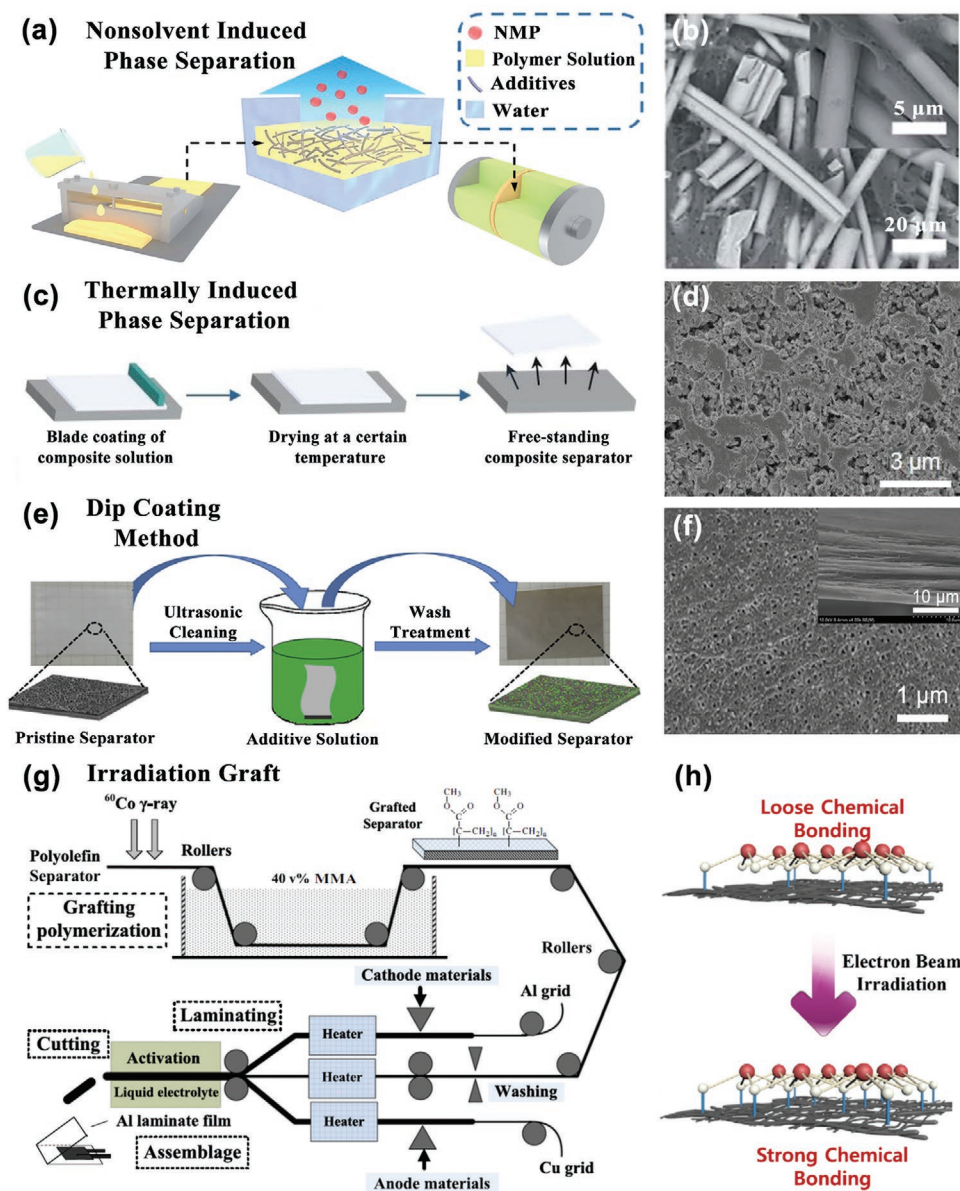
Figure 2. Pictorial illustration of processing steps for preparation of separators and scanning electron microscope (SEM) micrograph of the corresponding composite separators by a,b) nonsolvent-induced phase separation method. Reproduced with permission.[62] Copyright 2016, The Royal Society of Chemistry. c,d) Thermally induced phase separation method. Reproduced with permission.[64] Copyright 2020, American Chemical Society. e,f) Dip coating method. Reproduced with permission.[66] Copyright 2018, Elsevier B.V. g) Irradiation graft copolymerization technique. Reproduced with permission.[68] Copyright 2010, Springer-Verlag. h) Electron beam irradiation process. Reproduced with permission.[70] Copyright 2018, Elsevier B.V.

TIPS method is another kind of phase inversion method. TIPS process plays an important role in preparing porous membrane, especially in macromolecular polymer porous membrane. The porosity and the pore size distribution of separator can be easy to control through TIPS process compared with the dry or melt stretching method. Moreover, the performance of separator can be improved from aspects of raw material by adding additional components to the mixed system directly.[63] Importantly, TIPS method does not contain plasticizers as pore formation agents and does not require additional processing stages such as stretching, etching, or immersion in coagulation bath. It allows for the direct use of the free-standing composite separator immediately after drying. In this method,

the preparation process is similar to NIPS. The only difference is that TIPS needs to be sintered or dried at high temperature for phase inversion after forming the mixed slurry, as shown in Figure 2c, and the corresponding micrograph of the composite separator prepared by TIPS method is shown in Figure 2d.[64]

2.3. Dip-Coating Method

Different from the preparation process of the solution casting method, dip-coating method, as a surface modification method, is based on the original separators and coating the additive slurry on them. The conventional base separators (such as

**ADVANCED
SCIENCE NEWS**

www.advancedsciencenews.com

**ADVANCED
FUNCTIONAL
MATERIALS**

www.afm-journal.de

polyolefin separators or nonwoven mats) directly used as separators cannot meet the requirements of long cycle and high rate of LIBs. Their large nonuniform pore size results in the issues of leakage current and internal short circuit due to the particle penetration across them and the formation of dendrites in the LIBs system.[65] The dip-coating method could be applied to alleviate the above issues. In this method, the additive is firstly dissolved in a solvent to obtain uniform and stable slurry. Then the commercial separator or polymer separator is fixed on the metal plate or a flat glass dish, followed by coating with the slurry of the additive by doctor blade. Afterward, the dip-coating separator is dried at a certain temperature. After drying, the other side is probably coated by the same process to produce the composite membrane. The composite separators prepared by this method are mostly layered structures, and the basic materials are mostly commercial separators or polyolefin nonwovens. The preparation processes by this method are expressed in Figure 2e, and the micrograph of the composite separator prepared by the dip-coating method is shown in Figure 2f.[66,67]

2.4. Irradiation Treated Method

Irradiation treated PE separators by high energy irradiations such as plasma, gamma ray and electron beam technologies have very different pore and surface structures. The high energy irradiation can produce free radicals to initiate the crosslinking reaction of the polymer chains, so as to greatly improve the mechanical strength of the separator, as shown in Figure 2g.[68]

Surface grafting under appropriate low electron beam irradiation is a potential modification method to fabricate thermally stable composite separators without causing significant impairment of the polymer matrix.[69] In this technique, the base separator is firstly immersed in organic solution containing organic functional groups or corresponding surface-modified objects, and then irradiated by an electron beam under a certain dose and dose rate by electron accelerator. After the irradiation, the grafted separator is immersed in an acid for a long time to obtain surface-grafted composite separators. As the main merit, irradiated composite separators own stronger chemical bonding without change in thickness, as shown in Figure 2h.[70]

In addition, surface grafting under plasma treatment is also employed to prepare the separators with functional groups, which exhibits unique advantages including environment-friendly process, low production cost, and easy commercialization. In this technique, the plasma treatment system is composed of four main parts: a tubular-type Pyrex reactor equipped with several inner electrodes, a vacuum pump, a gasification grafting instrument, as well as a radio-frequency power supply. By controlling the pressure, generated plasma treats the base separator to obtain the composite separators with functional groups.

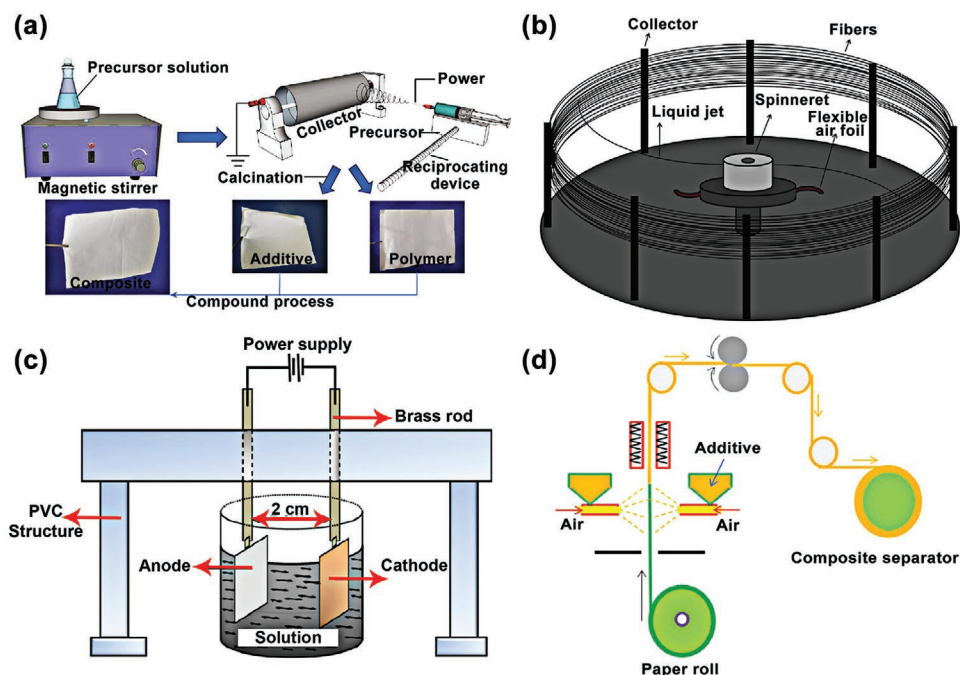## 2.5. Electrospinning Method

Electrospinning method, as a simple and effective approach to prepare the nanofibers separators, can solve the lack of flexibility of pure microporous membranes.[71] The nonwoven membrane prepared via electrospinning has many advantages as applied to separators of LIBs, including small pore size, high porosity, large specific surface area, and good gas permeability.[72] The multiple selectivity of polymer substrates, versatility of preparation process and controllability of morphology make it facile to fabricate composite separators with specific functionality via electrospinning technique.[73]

In this method, the slurry of polymer and additive is firstly prepared through stirring and heating in water bath at a certain temperature. And then the blended polymeric solution is filled in a syringe, which is pumped through the needle of a syringe and appeared at the needle tip in the form of droplet. As a high voltage is applied between the needle and the collector, the electrostatic force compete with the surface tension and forms a Taylor cone. After electrostatic force becomes greater than the surface tension of a droplet, the composite solution from syringe emits toward the collector in the direction of electric field, as shown in **Figure 3**a. The fibrous electrospun membranes have become an alternative option for separators due to their unique 1D structure and high porosity that ensures high electrolyte uptake and high ionic conductivity. More interestingly, the thickness of the electrospun separator can be tailored from tens of micrometers to hundreds of micrometers by adjusting the volume of the spinning solution.[74] However, the biggest challenge applied by electrospinning techniques is to prepare the separators with high mechanical strength.[75] As a result, preparing the composite separators employing this method depends on the properties of the additives.

2.6. Centrifugal Spinning Method

Centrifugal spinning has been studied as an electrospinning alternative to fabricate nanofibers membranes due to its fast, cost-effective, high safety performance.[76] In this technique, a high-speed rotary and perforated spinneret are used to fabricate nanofibers from polymer and additive solutions. During fiber spinning, high centrifugal force is generated on the polymer solution by rotating the spinneret. When the spinneret reaches a critical rotational speed, the centrifugal force is able to overcome the surface tension of the solution and liquid jets are ejected from nozzles. The liquid jets are stretched under the centrifugal force and the solvent evaporates. The resultant solidified composite fibers are deposited on the rod collectors, as shown in Figure 3b. The diameters of fibers can vary from several nanometers to micrometers and the production rate of the centrifugal spinning process could be more than 500 times faster than the conventional electrospinning technique. In an earlier study, it has been reported that the average production rate of a laboratory-scale centrifugal spinning device was around 50 g h^{-1}, which was at least two orders of magnitude higher than that of a typical laboratory-scale electrospinning process. Compared with electrospun separators, nanofiber separators made by centrifugal spinning are less expensive due to the faster production and lower solvent consumption. In centrifugal spinning, the morphology of nanofibers is affected by solution properties, including viscosity, surface tension, molecular structure, molecular weight, solution concentration,

Figure 3. Schematic illustration of processing steps for preparation of separators by a) electrospinning method. Reproduced with permission.[72] Copyright 2020, Hindawi. b) Centrifugal spinning method. Reproduced with permission.[77] Copyright 2015, Elsevier B.V. c) Electrophoretic deposition method. Reproduced with permission.[80] Copyright 2019, The Royal Society of Chemistry. d) Wet-laid method. Reproduced with permission.[84] Copyright 2018, Elsevier B.V.

solvent structure, additive, and operational conditions such as rotating speed, spinning head diameter, nozzle diameter, and nozzle-collector distance.[77]

2.7. Electrophoretic Deposition (EPD) Method

EPD method is known as a highly efficient approach for membrane assembly.[78,79] This technique enables efficient control over the structure, stoichiometry, and dimensionality at a low processing cost, and has been employed extensively in the biochemical, coating and ceramic industries. In addition, this technique is usually used to prepare composite separators for LIBs. In this method, the process consists of two steps in which polymer and additive particles are firstly uniformly dispersed in the solvent to form a stable colloid, and then deposited onto a conductive substrate for strong adhesion under an electrical field, as shown in Figure 3c.[80] A mussel-inspired, self-aligned, and hierarchically laminated structure can thus be achieved with EPD. EPD holds massive merits including superb efficiency, extreme convenience, short shaping time, and low cost, owning broad prospects for preparing composite separators and energy storage devices.[81]

2.8. Wet-Laid Method

Wet-laid method is applied to fabricate the separators by a facile papermaking process. The papermaking process could reduce the processing cost for a large scale application.[82,83] In this process, the additive particles and base polymer are firstly

dispersed into a solvent with a small amount of polymer binder. Then the resulting suspension is subsequently sprayed onto the paper using compressed air as shown in Figure 3d. This coating procedure involving the spraying of an aqueous suspension is environmentally friendly and highly effective for production. Additionally, the structure and thickness of the coating layer can be adjusted more easily with this spraying method than with the commonly used casting method.[84]

2.9. Summary

In this section, the preparation methodologies of the composite separators for LIBs have been discussed. The significance of using different methods to prepare composite separators is to achieve higher thermal resistance, higher safety performance, electrolyte wettability, better cycle performance, and higher rate performance after battery assembly than commercial LIBs separators or single separators under different basic material, different additives, and different synthetic conditions and environments.

Each method has some merits and inevitable drawbacks. Solution casting method and dip-coating method effectively promote the mechanical strength, thermal stability, and electrolyte uptake of the separators, and also have a relatively simple preparation process and do not require the assistance of large equipment or instruments. However, the particles or polymer fibers coated materials tend to easily detach from the separators, leading to the pore blockage and further deteriorating battery performance. Through heating at high temperatures or immersing in the nonsolution, phase inversion method could be applied to form separators with large porosity and high

wettability, yet it is difficult to ensure the mechanical strength. Like the phase inversion method, the pore size and pore distribution of composite separators could be easily and precisely controlled by electrospinning method without mechanical strength. However, EPD method could be used to prepare high mechanical strength, high porosity and uniform pore distribution composite separators, but it is inconvenient to prepare a uniform and stable suspension prior EPD. As a result, different methods should be selected according to the materials of the separators, the composition of the additives, and the needs of the properties of the composite separators, including other method such as irradiation treated method, self-assembly method, and papermaking process.

In addition, in the process of preparing the composite separators, these methods will be used in an orderly combination. For example, the selected base materials such as commercial polyolefin or polymer fibers are usually fabricated by dry stretching or electrospinning methods. Then the additive organics or inorganics will be composited through solution casting, dip-coating or surface grafting methods.[85,86] Other specific methods combining various preparation methods will be introduced respectively in detail in the next section.

3. Architectures for Composite Separator Design

High safety and rate LIBs with excellent performance separators have always been the focus of attention so far. Composite separators could greatly improve upon these two main performance indicators of LIBs by their distinctive composition, morphology, and internal structure. Composite separators for LIBs can be classified in terms of the materials types (like composite separators combined by polymers and organic, inorganic materials and natural raw materials), or time sequence (composite commercial separators, or composite new polymer separators). In this review, we will firstly introduce the challenges of separator without composite. Then the composite separators are classified as blending structure type, layered structure type, core–shell structure type, and grafting structure type according to the combined forms of separators, as shown in **Figure 4**. Several examples of different materials in different types are discussed. The types of combination between polymer molecules and other additives, such as polymer chains and ceramic particles, will be specifically reflected in this section. In addition, the recent development in composite separators technology on the basis of composite types for safe high rate LIBs will be summarized in detail.

3.1. Challenges toward Separators for LIBs

Among various separators developed so far, polyolefin separators, such as polyethylene and polypropylene, have been the most predominant ones in commercially available separators for LIBs due to their low cost, proper mechanical strength, pore structure, and chemical resistance. However, despite their success in current LIBs development, there is still plenty of room for improvement in the performance of polyolefin separators. Their intrinsically hydrophobic surface character and low surface energy result in poor wettability and retention to polar liquid electrolyte, which could directly impede Li-ions transport through separators, and consequently damage rate capacity performance and cycle life of LIBs. In addition, their poor thermal stability often results in the thermal deformation of separator surfaces, and eventually risks of the internal short circuit of LIBs, or even fire and explosion. In this section, the challenges toward separators for LIBs are briefly described, and the reasons for the issues are also reported.

3.1.1. Thermal Stability Issue

Thermal runaway is a threat to the long cycle and high rate LIBs. There are several reasons for the thermal runaway of lithium-ion batteries. The first is overcharge. As the battery is charged, branch-shaped lithium dendrites, caused by the surface deposition of lithium metal, grow and pierce the separator easily, causing the short circuit.[96] Moreover, the active lithium can cause exotherm by reacting with the electrolyte directly. The dissolved metal lithium would cause the safety accidents due to its low melting point.[97] In addition, a high ambient temperature (above 60°) will also cause the thermal runaway of the battery.[98]

The thermal stability is closely related to the charge state of the battery.[99] To show the thermal issue clearly, the simulation and calculation are provided below. Li et al.[100] proposed an adiabatic rate calorimetry, which has been used to conduct a detail thermal stability analysis for the battery of different charge state. In the adiabatic system, the heat generated by the battery itself was completely used for the temperature rise of the sample. Assuming that the reaction equation in the thermal runaway reaction conforms to the Arrhenius equation,[101] the following equation can be obtained by the heat balance Equation (1)

$$\frac{dT}{dt} = \frac{Q}{C_p} * A * C^n * e^{-\frac{E}{RT}} \tag{1}$$

wherein T is the reaction temperature, C is the sample mass, Q is the reaction heat evolution, C_p is the average heat capacity of the sample, A is a the factor before reaction, n is the reaction order, and E is the reaction activation energy. Assuming that the sample mass C has the relationship with the temperature T, and the maximum temperature T_{max} indicates the danger degree of the accident caused by thermal runaway. Then the time to maximum rate (TMR) represents the time required to reach the maximum reaction rate, also is the time before thermal runaway occur in this temperature, shown in following Equation (2)

$$TMR = \frac{R * T^2}{\frac{dT}{dt} * E} \tag{2}$$

As the temperature increases, the TMR will become smaller and smaller, indicating that the higher the temperature, the lower the thermal stability of the battery.[102]

To ensure the safety of LIBs and avoid the thermal runaway, the thermal stability of separator is firstly considered because the thermal shrinkage of the separator with a rise in temperature
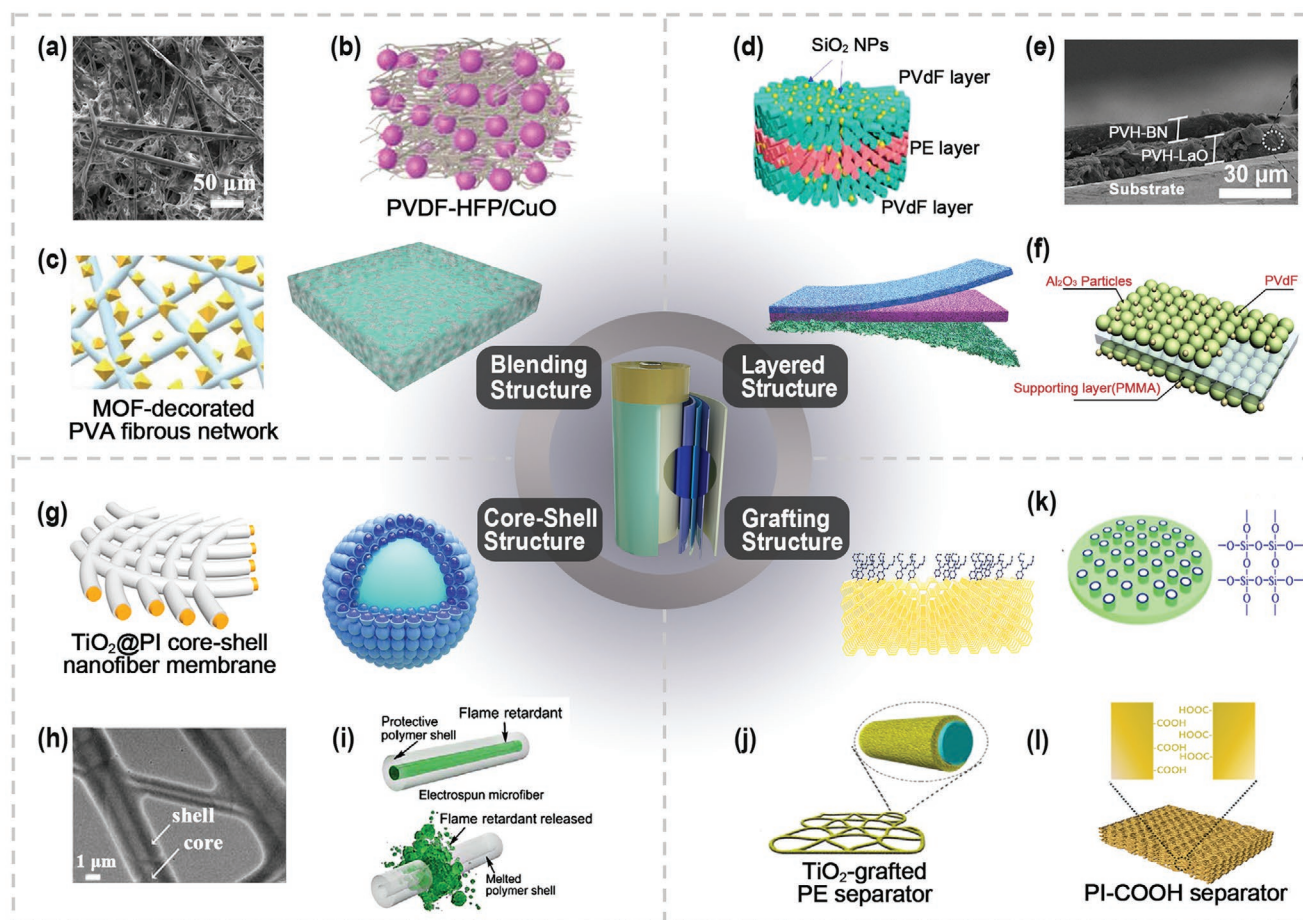
Figure 4. Categorization of composite separators for LIBs in terms of composite structure types and the several examples of different materials in different composite types. a) SEM image of PP/cotton blending fiber composite nonwoven. Reproduced with permission.[87] Copyright 2018, Elsevier B.V. b) Model of CuO/PVDF-HFP composite separator. Reproduced with permission.[17] Copyright 2019, Wiley-VCH GmbH. c) Model of metal organic framework (MOF)-polyvinyl alcohol (PVA) fibrous networks separator. Reproduced with permission.[88] Copyright 2019, Wiley-VCH GmbH. d) Model of silica-anchored layered PVDF/PE/PVDF separator. Reproduced with permission.[75] Copyright 2018, American Chemical Society. e) SEM image of PVDF-HFP (PVH)-LaO//PVH-BN bi-layer separator Reproduced with permission. [55] Copyright 2019, Elsevier Ltd. f) Model of Al$_2$O$_3$-PVDF-HFP/PMMA trilayer membranes. Reproduced with permission.[89] Copyright 2010, Elsevier B.V. g) Model of TiO$_2$@PI core–shell separator. Reproduced with permission.[90] Copyright American Chemical Society. h) SEM image of poly(lactic acid) (PLA)@poly(butylene succinate) (PBS) core–shell fibrous separator. Reproduced with permission.[91] Copyright 2013, The Royal Society of Chemistry. i) Model of triphenyl phosphate (TPP)@PVDF-HFP fibers separator. Reproduced with permission.[92] Copyright 2017, AAAS. j) Model of TiO$_2$-grafted PE separator. Reproduced with permission.[93] Copyright 2016, Elsevier B.V. k) Model of Celgard-SiO$_2$-TEOS separator. Reproduced with permission.[94] Copyright 2015, Science Press and Dalian Institute of Chemical Physics. l) Model of PI-COOH separator. Reproduced with permission.[95] Copyright 2018, The Royal Society of Chemistry

could cause serious issues inside the battery. The thermal shrinkage of the separator should be <5% at 100 °C h^{-1}.[103] The minimum thermal shrinkage ensures the safely working of LIBs at elevated temperatures. The thermal shrinkage of separators is calculated by measuring the dimensions of separator before and after annealing at a certain temperature for a specified time by using the formula given in Equation (3)[23]

$$\text{Thermal shrinkage (\%)} = \frac{D_i - D_f}{D_i} \times 100 \tag{3}$$

where D_i and D_f are the areas of the separator before and after annealing at different temperatures, respectively. Therefore, maintaining the dimensional stability at the certain temperature is the key to avoid the thermal runaway of LIBs. However, it is difficult for commercial separator to withstand the high temperature. For instance, Celgard 2325 (trilayer PP/PE/PP separator) starts to deform at 100 °C and completely melts at 150 °C after 300 s from the forward looking infrared (FLIR) images. From the thermogravimetry curves, Celgard 2325 separator starts to degrade from 260 °C and completely deform with a weight loss of 100% at 425 °C.[104] Therefore, to avoid the thermal deformation issue of separator surfaces, as well as even fire and explosion for LIBs, composite separators with improving thermal stability will be reviewed below.

3.1.2. Mechanical Behavior Issue

Mechanical behavior (tensile, puncture, and failure) is one of the most essential properties of separators. Since the stress level of separators has a great impact on the electrochemical

performances of lithium ion battery, such as capacity and charge/discharge behavior, it is important for separators to avoid the separator deformation that can cause internal short circuit.[105] Meanwhile, mechanical integrity is also of primary importance for the separator to withstand the stress induced by active material upon lithiation and delithiation.[106–108] They must be strong enough to endure the high tension forces during construction and work of battery.

Considerable efforts have been made in the measurements of mechanical strength of separators especially in the dry condition. The minimum strength requirement of separators is 1000 kg cm^{-2} or 98.06 MPa for 25 µm thickness to withstand the force during the assembly process.[109,110] The ultimate tensile strength of commercial separators (such as PP) in the MD is ten times higher than that in the TD.[111] However, the mechanical behavior of separators under the solvent electrolyte environment should be considered in the working system of LIBs.

Chen et al.[112] revealed the influencing factors of tensile strength for PP separators in the wetting condition. They proposed that the tensile properties of polymeric separators appear to be a function of loading rate and the relation between relaxation time and strain rate. The relaxation time is an essential physical quantity reflecting the hysteresis of the polymer under external loading. They delved into the influence mechanism of liquid electrolytes on the mechanical behaviors of separators and Equation (4) is about relaxation time of separators[113]

$$\sigma^* = \frac{\sigma}{\sigma_0}, \ \varepsilon^* = \frac{\varepsilon}{\varepsilon_0}, \ t^* = \frac{t}{t_0} \tag{4}$$

where σ^* is the normalized stress, σ is the stress, σ_0 is the maximum stress on the stress–strain curve, ε^* is the normalized strain, ε is the strain, ε_0 is the strain at σ_0, t^* is normalized time, t is time and t_0 is the time interval for stress increases from 0 to σ_0. Based on Equation (4), a nondimensional viscoelastic constitutive model derived from classical internal-variable theory of irreversible thermodynamics is employed in Equation (5)

$$\sigma^* = \sum_{i=1}^{n} \frac{E_i}{E^{(s)}} \int_0^{\varepsilon^*(t^*)} \exp\left[-\left(\frac{\varepsilon^*(t^*) - \varepsilon^*(\tau^*)}{\tau_{M_i}^*}\right)\right] d\varepsilon^*(\tau^*) \tag{5}$$

where E_0 and $E^{(s)}$ are the initial modulus and the secant modulus at instant t_0, respectively. $\tau_M^* = \tau_M / t_0$ represents the normalized relaxation time. The results show that the strain rate is independent of nondimensional stress–strain. Then comparing with the normalized Maxwell model, it is found that the magnitudes of $E_0/E^{(s)}$ and τ_M^* are rate independent. Numerical fitting results confirm that $\log t_0$ is directly proportional to $\log \dot{\varepsilon}$, which may deduce that the relaxation time (τ_M) varies in a power law with strain rate as

$$\tau_M = \kappa (\dot{\varepsilon} / \dot{\varepsilon}_r)^\lambda \tag{6}$$

where κ is the parameter of the material, $\dot{\varepsilon}_r$ is the reference strain rate, and λ is the effect factor of strain rate. The relaxation time decreases dramatically with increasing strain rate, and the relation between the relaxation time and strain rate obeys an inverse proportion ($\lambda = -1$). it can be further found

that this liquid electrolyte influence on τ_M is obviously larger than that on strength and stiffness. Thus, the relaxation time is a better option to reveal the coupling effect of liquid electrolyte and loading rate on polymer separators.

3.1.3. Wettability Issue

The wettability of separators determines the rate capacity for LIBs. The efficiency of Li ion transportation depends on the electrolyte absorption of separators, which displays the wettability of separators macroscopically. The superior electrolyte wettability could reduce ionic resistance and further increase the rate capacity of LIBs.[114]

In the experiment process, the electrolyte wettability is calculated by measuring the weight of separator before and after immersing into liquid electrolyte by using Equation (7)

$$\text{Electrolyte uptake (\%)} = \frac{W_{wet} - W_{dry}}{W_{dry}} \times 100 \tag{7}$$

where W_{dry} and W_{wet} are the weight of dry and wet separator.

To evaluate the wettability behavior, Schilling et al.[115] designed a soaking model to determine the electrolyte penetration rate K. They assumed that the pore structure is a bundle of capillaries and the wetting process of the porous separator with liquid electrolyte can be regarded as capillary movements. In this case, the capillary flow can be described by the modified Lucas–Washburn equation which are given in Equations (8) and (9)[116,117]

$$h = K \sqrt{t} \tag{8}$$

$$K = \sqrt{\frac{r\sigma \cos\theta}{2\eta}} \tag{9}$$

In Equation (8), h represents the height of the liquid front in the capillary, t is the imbibition time of the liquid into the pore structure of the porous layer, and K is the proportionality factor. As shown in Equation (9), the proportionality factor K is also dependent on the pore radius of the capillary bundle r, the surface tension σ and the contact angle θ. K is also declared as penetration rate, representing the speed of electrolyte penetration into the separator structure, which can be simply expressed as a velocity that the electrolyte soaks the separator.[115] Generally, the wettability behavior of separators are characterized through contact angle θ. The wettability of Celgard 2325 or Celgard 2400 cannot satisfy the demand for commercial LIBs since they exhibit high contact angle values, 48.9° and 45°, respectively.[118,119] The inferior surface wettability of separators will result in the lower speed of electrolyte penetration, further affecting the transportation of Li ion seriously. Therefore, it is necessary to introduce additives into commercial separators or replace with other composite separators directly.

3.1.4. Ionic Conductivity Issue

Except for the wettability, the ionic conductivity of separators also affects the rate capacity of LIBs. The ionic conductivity

ADVANCED
SCIENCE NEWS
www.advancedsciencenews.com

ADVANCED
FUNCTIONAL
MATERIALS
www.afm-journal.de

of separators is related to two driving forces for the motion of ions, which are concentration gradients and potential gradients. The concentration gradient causes diffusion and the potential gradient causes migration, corresponding to the mobility and diffusion coefficient, respectively. Diffusion properties of Li ion determine some key performance metrics of LIBs, including the charge and discharge rate, and cycling capacity. Therefore, it is indispensable to confirm the relationship among the ion mobility, diffusivity and ionic conductivity. Shokrollahi et al.[120] proposed that the diffusion coefficient is a suitable way to describe the mobility of Li ions and consequently ionic conductivity. Based on the Nernest–Einstein equation, relation between mobility and diffusion of ions is shown in Equations (10)–(12)

$$D_i = kTB_i \tag{10}$$

while D_i is diffusion of ions and B_i is the particle mechanical mobility

$$B_i = \frac{u_i}{z_i e} \tag{11}$$

z_i is the charge of the particle and u_i is the charge mobility. Relation of $B_i = \frac{u_i}{z_i e}$ and $\sigma_i = \frac{I_i}{E}$ is modeled as follows

$$D_i = \sigma_i \frac{kT}{c_i z_i^2 e^2} \tag{12}$$

where c_i is the concentration of particles. Thus, the ionic conductivity of separators is proportional to diffusion of ions within the homogeneous and this relation can be an approximate estimation where i particles of material is homogeneous.[121]

The ionic conductivity reflects the properties of the whole device, not only the separator. However, it is influenced by separator permeability. The permeability, κ, is used to describe how the geometric structure of the separator constricts Li$^+$-ion transport. Permeability is correlated with the electrical resistivity. For separators, the Gurley value (G) as a function of permeability, is generally used instead. The typical permeability values are between 10^{-17} and 10^{-16} m^2, and the Gurley values are between 200 and 600 s.[36]

Ionic conductivities are usually calculated from bulk resistances that are obtained with alternating current (AC) complex impedance analysis, where blocking-type cells are fabricated by sandwiching a separator between two stainless-steel electrodes.[36] The ionic conductivities of electrolyte filled separators required in LIBs for different application are in the range of 10^{-3} to 10^{-1} S cm^{-1} at room temperature.[22] The ionic conductivity of separator is calculated by using Equation (13)

$$\sigma = \frac{l}{R_b A} \tag{13}$$

where σ is the ionic conductivity (S cm^{-1}), R_b is the bulk resistance of the electrolyte, whereas l and A represent the thickness and area of the separator, respectively. The ionic conductivities of the PP separators with LP (LiPF$_6$ in ethylene carbonate/diethyl carbonate, 0.7 mS cm^{-1}) and with LC (LiClO$_4$ in propylene carbonate, 0.5 mS cm^{-1}) at ambient temperature cannot reach the performance requirements in large current density for LIBs. To enhance the ionic conductivity of commercial separators, additives are required to improve the Li ion transportation.

3.1.5. Section Summary

In this section, challenges toward separators for LIBs are briefly described and the reasons for the issues are also discussed from an experimental and theoretical perspective. Although the commercial Celgard separators own the strong mechanical strength, they still cannot avoid the limitation of thermal shrinkage at high temperature, inferior wettability and low ionic conductivity. LIBs with the commercial separators have the high risks of short circuit, fire and explosion. To avoid the issues mentioned above and improve the performance of separators in terms of high safety and rate capacity of LIBs, the composite separators with specific functional additives are urgently required and will be reviewed below.

3.2. Blending Structure Type

Blending polymers with additives in composite separators has generally been regarded as an effective approach to improve the performances of base polymers separators. Composite separators with blending type based on commercial separators, PVDF and its co-polymers and other polymers are designed and reviewed in this section to further improve the polyolefin separators.

3.2.1. Models and Simulations of Blending Composite Separators

To solve the challenges toward commercial separators especially in terms of thermal runaway and wettability issues, a variety of composite separators with blending structure type have been studied experimentally and theoretically.

Chen et al.[17] built the models of the anode/separator architecture including PVDF-HFP/CuO separator and calculated the atomic configuration and absorption energy through density functional theory (DFT) as shown in **Figure 5**a,b. They utilized fluorine-contained functional groups (CH$_2$CF$_2$, CH$_3$CHF$_2$, and CHF$_2$CHFCF$_3$) to represent PVDF-HFP and dimethyl carbonate (DMC) and ethylene carbonate (EC) represent the electrolyte, The adsorption energy values of CuO (1 1 0)-DMC (–1.28 eV) and CuO (1 1 0)-EC (–1.35 eV) are much larger than the adsorption energy values of CH$_2$CF$_2$-DMC (–0.03 eV), CH$_3$CHF$_2$-DMC (–0.18eV), CHF$_2$CHFCF$_3$-DMC(–0.09eV), CH$_2$CF$_2$-EC(–0.07eV), CH$_3$CHF$_2$-EC (–0.24 eV), and CHF$_2$CHFCF$_3$-EC (–0.08 eV). The atomic separations between Cu and O in DMC and EC are 2.09 and 2.21 Å, respectively, which are close to the Cu−O bond length (1.83 Å).[122] Owing to strong adsorption to DMC and EC, the separator incorporated with CuO owns a higher pronounced wettability and electrolyte uptake than pure PVDF-HFP separator, which is consistent with the contact angle measurement as shown in Figure 5c. To prove the superior thermal
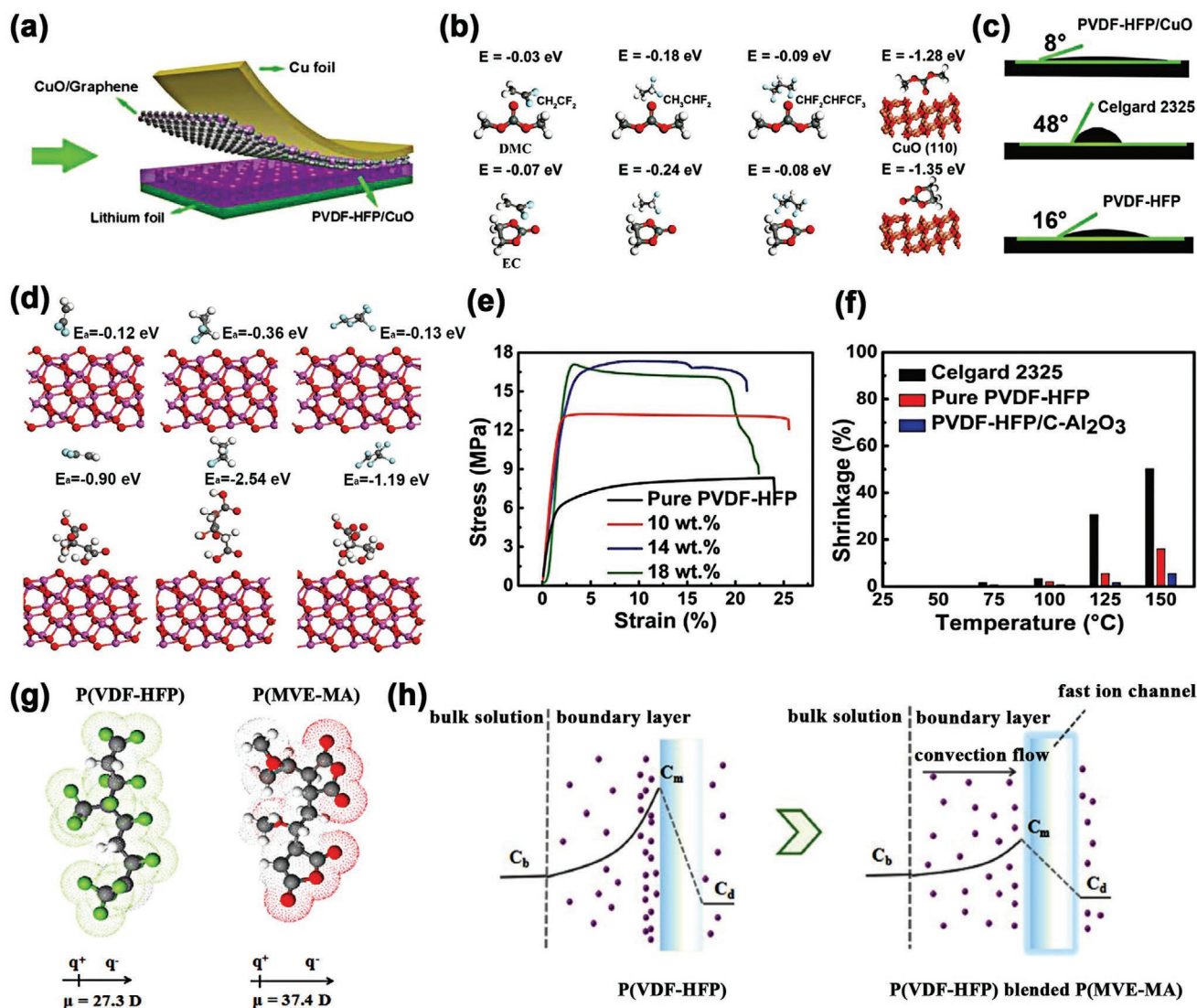
Figure 5. a) Schematic of the anode/separator architecture based on oxide anode and active-oxide-incorporated separator. b) Atomic model configuration and interaction for PVDF-HFP, electrolyte, and CuO. c) Contact angle images of PVDF-HFP/CuO, Celgard 2325, and pure PVDF-HFP separators. Reproduced with permission.[17] Copyright 2019, Wiley-VCH GmbH. d) DFT-calculated adsorption structures and energy values of PVDF-HFP functional groups on Al_2O_3 (001) surfaces. e,f) Stress–strain curves and thermal shrinkage of PVDF-HFP/colloidal Al_2O_3 and pure PVDF-HFP separators. Reproduced with permission.[123] Copyright 2018, Wiley-VCH GmbH. g) Pictorial model of static charge distribution of P(VDF-HFP) and P(MVE-MA). h) Schematic diagram of principle for the lithium ion transmission throughout the separators. Reproduced with permission.[125] Copyright 2018, Elsevier B.V.

stability and mechanical strength, Ali et al.[123] employed the DFT simulations to calculate the absorption energies of fluorine contained functional groups, Al_2O_3 (001) surface, and citrate acid group bound to Al_2O_3 surface as shown in Figure 5d. Al_2O_3 (001) surface has weak adsorption interaction with CH_2CF_2, CH_3CHF_2, and CHF_2CHFCF_3, varying from −0.12 to −0.36 eV, but the adsorption energy of PVDF-HFP groups is significantly enhanced from −0.90 and −2.54 eV when citrate acid group is bounded to Al_2O_3 surface.[124] The results indicate that colloidal Al_2O_3 particles and PVDF-HFP polymer chains have strong adsorption interactions and the composite separator improves the mechanical strength and thermal stability, which are proved by the experimental measurement results as shown in Figure 5e,f. To analyze the relationship between

ion conductivity and wettability or surface energy, Li et al.[125] firstly calculated the polarities of composite separator and then established the mechanism of the Li^+ transfer near the interface between the separator and anode. Taking poly(methyl vinyl ether-alt-maleic anhydride) (PMVE-MA) and PVDF-HFP as the example, they calculated the dipole moments which are 37.3 and 27.4 D, respectively, as shown in Figure 5g, indicating that the electronegativity and polarity of PMVE-MA are stronger than that of PVDF-HFP. The increased surface energy with the addition of PMVE-MA contributes to the attractive forces between polymer and solvent molecules, resulting in that the blended separator exhibits better electrolyte invasion. In addition, the mechanism of the Li-ion transfer near the interface between the separator and anode is described, as shown in

ADVANCED
SCIENCE NEWS

www.advancedsciencenews.com

ADVANCED
FUNCTIONAL
MATERIALS

www.afm-journal.de

Figure 5h. Introducing PMVE-MA reduces the differential concentration between C_m (outside the membrane concentration) and C_d (diffusion concentration). The blended separator with the interconnected and uniformed structure balances the osmotic pressure for the both sides of separator and proceeds with the smooth intercalation/de-intercalation of reversible Li^+.

3.2.2. Blending Type Based on Commercial Separators

Composite commercial polyolefin separators are prepared by modifying or doping the commercial separators in several ways. Recently, Wang et al.[126] demonstrated a simple and environmentally friendly self-assembly process of oppositely charged polymer PEI and inorganic oxide SiO_2 on the surface of PE separator. PEI/SiO_2-modified PE separator improves the electrolyte wettability. The water contact angle of PE separator decreasing from 124° to 24.6° after modification. The thermal and electrochemical stability are also improved significantly by the modification, endowing LIB with high C-rate capacity, which still holds 45.2% (65 mAh g^{-1}) of the discharge capacity at the current density of 5C. In addition, Hu et al.[127] fabricated aramid nanofibers (ANFs)-PP composite separator via a dip-coating process and took advantage of dopamine to improve the dimensional stability. The capacity retention of the cell equipped with it is twice that of the original PP separator at 5C discharge current density.

Zhang et al.[63] prepared a composite SiO_2/PE separators were via thermally induced phase separation. Through controlling the content of silica, the liquid electrolyte uptake increased from 30.2% to 63.2%, and the decomposition temperature of the composite PE separators was 40 °C higher than the pure PE separator. This is because the more stable space structures are induced by doping silica and increasing the tensile strength from 12 to 13.3 MPa.

3.2.3. Blending Type Based on PVDF or its Co-Polymers Separators

Apart from blending commercial materials with other additives, (PVDF) and its co-polymers-based composite separators have also drawn extensive attention due to the high electrolyte uptake, desirable polymer-solvent compatibility and electrochemical stability of PVDF or its co-polymers.[128] However, the intrinsic insufficient mechanical properties restrict the use of PVDF and its co-polymers, thus it is necessary to prepare the composite separators based on PVDF and its co-polymers.
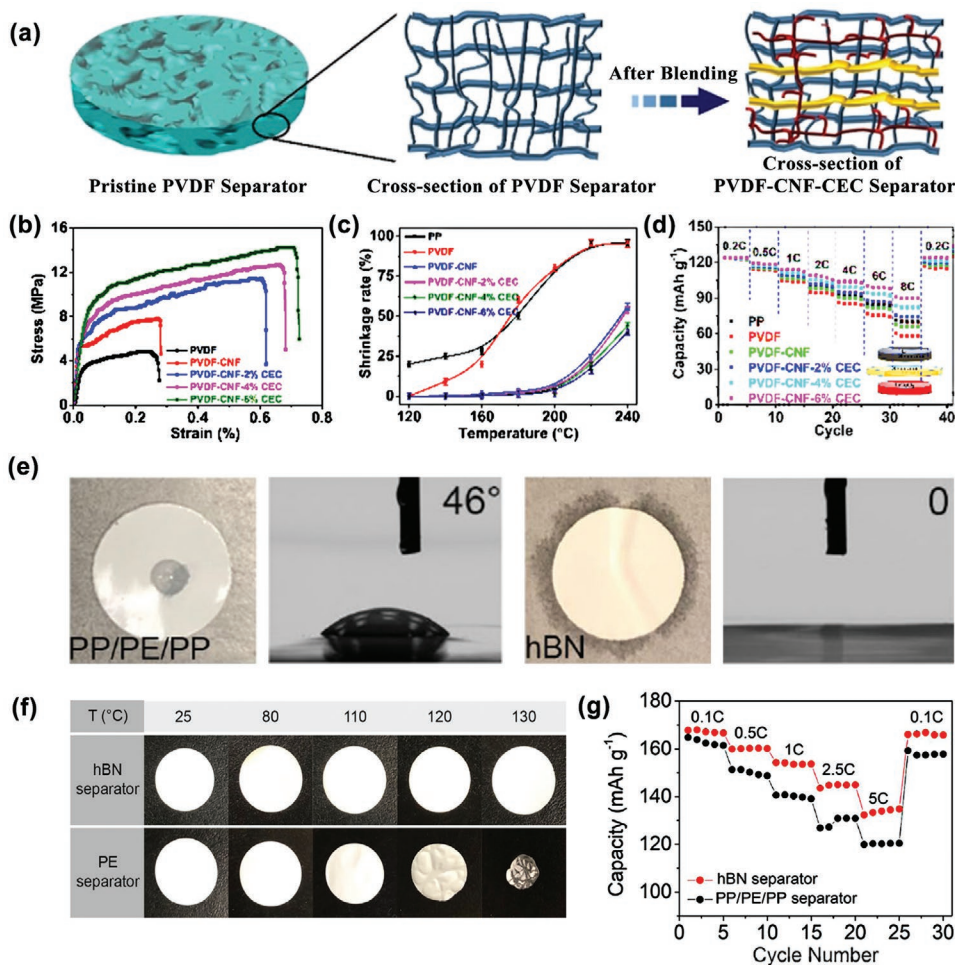
Compared with commercial separators, PVDF separators doped with the additives have high porosity, electrolyte wettability, and thermal stability. Fu et al.[129] introduced polymethyl methacrylate (PMMA) and nano SiO_2 into electrospun PVDF separator, thereby enhancing its mechanical strength (32.69 MPa) and thermal stability at 150 °C. The absorption of liquid electrolyte was also improved by decreasing the crystallinity of PVDF. The LIBs with the composite separator exhibits more stable cycle performance, higher discharge capacity (158 mAh g^{-1}) and excellent capacity retention. Cui et al.[130] reported a PVDF-CA/Al(OH)$_3$ separator that introduces cellulose acetate (CA) and Al(OH)$_3$ particles into PVDF. The separator presents a high porosity (68.6%), high electrolyte uptake (403.9%), especially

superior thermal stability (thermal shrinkage ratio was 4.6% at 160 °C) and excellent ionic conductivity (2.85 mS cm^{-1}). In addition, the rate capability (128.28 mAh g^{-1} at 8C) and cycle performance (151.97 mAh g^{-1} after 100 cycles at 1C) are also superior to the commercial PP separator. Costa et al.[61] prepared a mesoporous SiO_2/PVDF composite separator by the NIPS method. The enhanced thermal stability and electrolyte uptake give rise to an excellent rate discharge (118 mAh g^{-1}) capacity at 2C.

In addition, Li et al.[60] designed a PVDF separator by blending with cellulose nanofibers (CNFs) and cyanoethyl cellulose (CEC), as shown in **Figure 6**a. The PVDF/CNF/CEC composite separator exhibits enhanced mechanical properties (14.3 MPa) and superior thermal tolerance (almost no shrinkage at 200 °C) (see Figure 6b,c). In addition, the composite separator endows the LIBs with excellent rate capabilities from 0.2C to 8C compared to the PP membranes, as shown in Figure 6d. de Moraes et al.[64] prepared a composite separator based on carbon-coated hexagonal boron nitride (hBN) nanosheets and PVDF polymers. The contact angle of hBN/PVDF composite separator (0°) is significantly smaller than that of the shows the contact angle of PP/PE/PP separator (46°) (see Figure 6e). As the temperature increases, the hBN/PVDF separator has no significant thermal shrinkage at 130 °C compared to the commercial separator, as shown in Figure 6f. This combination of high thermal stability and electrolyte wettability enables the enhanced rate capability of the hBN/PVDF separator (130 mAh g^{-1} at 5C), as shown in Figure 6g.

PVDF co-polymer-based composite separators have also been widely developed, especially PVDF-HFP based separators. Among all of the additives, blending ceramic oxide with PVDF-HFP is considered to be an effective way to improve the performance of lithium ion batteries. Wang et al.[62] prepared a novel composite separator by blending inorganic ZrO_2 fibers with PVDF-HFP, which shows a skinless surface and a highly porous internal structure as shown in **Figure 7**a. Compared with Celgard 2400, pure PVDF-HFP separator and PVDF-HFP separator containing ZrO_2 powders, PVDF-HFP separator containing ZrO_2 fibers presents an excellent mechanical strength (over 5 MPa), superior thermal stability (no curling up), desired porosity (78.38%) and electrolyte uptake (252.5%), as shown in Figure 7b–e. The rate capacity of battery with the ZrO_2 fiber-doped PVDF-HFP separator is higher than that of Celgard 2400 or PVDF-HFP. In particular, this separator possesses 38% capacity retention at a discharge rate of 8C (see Figure 7f).

Chen et al.[17] reported a CuO-incorporated PVDF-HFP separator, which has a robust anode-separator architecture. The PVDF-HFP/CuO architecture owns an outstanding thermal conductivity, excellent mechanical properties and ensures structural integrity at high temperatures. The cells based on PVDF-HFP/CuO architecture have high rate capabilities of 637, 546, and 445 mAh g^{-1} from 0.5C to 2C in comparison to the Celgard 2325 or PVDF-HFP at all C rates. Boateng et al.[119] synthesized a PVDF-HFP/SiO_2 composite separator. The incorporation of SiO_2 nanoparticles leads to a reduced crystallinity (27%), enhanced wettability (14%), improved electrolyte uptake (420%), and enhanced mechanical strength (over 14 MPa) of the composite separator. The discharge capacities of the LiFePO$_4$(LFP)/Li half-cell with PVDF-HFP/SiO_2 separator are

ADVANCED
SCIENCE NEWS
www.advancedsciencenews.com

ADVANCED
FUNCTIONAL
MATERIALS
www.afm-journal.de

Figure 6. a) Schematic for PVDF/CNF/CEC separators. b) Stretching curves of PP, PVDF, PVDF/CNF/CEC separators. c) Thermal shrinkage properties of PP, PVDF, PVDF/CNF/CEC separators at 200 °C. d) Rate performance at a rate of 0.2C–8C in the voltage range of 2.8–4.2 V. Reproduced with permission.[60] Copyright 2017, American Chemical Society. e) Photographs and contact angle images of wetting properties of the hBN nanosheet composite separator and commercial separator. f) Thermal shrinkage properties for hBN separator and separator at 130 °C. g) Rate capability performance from 0.1C to 5C. Reproduced with permission.[64] Copyright 2020, American Chemical Society.

165 and 106 mAh g^{-1} at 0.5C and 5C, respectively, which are higher than cells with other separators.

In addition to blending ceramic powder with PVDF-HFP, introducing colloidal ceramic materials is another effective way to improve the performances of separators. Ali et al.[123] prepared a PVDF-HFP/colloidal Al$_2$O$_3$ composite separator. Dispersing the colloidal Al$_2$O$_3$ particles in the PVDF-HFP polymer matrix substantially enhance the mechanical strength of the PVDF-HFP separator. PVDF-HFP/colloidal Al$_2$O$_3$ separator only has a 4.5% thermal shrinkage at 150 °C. In addition, the composite separator owns a high electrolyte uptake of 372%, and delivers higher rate capacity at 2C. In addition, Waqas et al.[131] synthesized a PVDF-HFP/colloidal-TiO$_2$ composite separator. Colloidal TiO$_2$ forms strong adsorption interaction with PVDF-HFP, giving rise to advantageous mechanical robustness (11.13 MPa), electrolyte uptake (164.5%) and remarkable stability at 150 °C. PVDF-HFP/colloidal-TiO$_2$ exhibits an excellent rate performance (123.4 mAh g^{-1} at 2C).

Lithium salts are also often added to the PVDF-HFP separator for blending, which could improve its physical and chemical properties greatly. Shi et al.[132] incorporated Al-doped Li$_{6.75}$La$_3$Zr$_{1.75}$Ta$_{0.25}$O$_{12}$ suspension into PVDF-HFP gel to prepare a highly uniform quasi-solid composite separator. Adding the suspension increases ductility by three times as compared with pure PVDF-HFP separator. Batteries with the PVDF-HFP/LLZO separator give discharge capacities of 142.4, 111.1, and 93 mAh g^{-1} at 1C, 3C, and 5C, respectively, which are much higher than the specific capacities of batteries with pure PVDF-HFP and Celgard 2500 separators.

In addition to the aforementioned additives, polymers could be used in blending PVDF-HFP into composite separators. Luo et al.[133] prepared a 3D nanoporous PVDF-HFP composite separator with PE, of which the micromorphology is shown in **Figure 8**a. PE in the composite separator significantly enhances the mechanical strength and thermal stability of the separator, as well as improves electrolyte uptake (216%), as shown in Figure 8b–e. LiFePO$_4$/Li half cells with the composite separator deliver rate capacities of 146 mAh g^{-1} at 1C, 97 mAh·g^{-1} at 10C, and 57 mAh g^{-1} at 20C, as shown in Figure 8f,g.
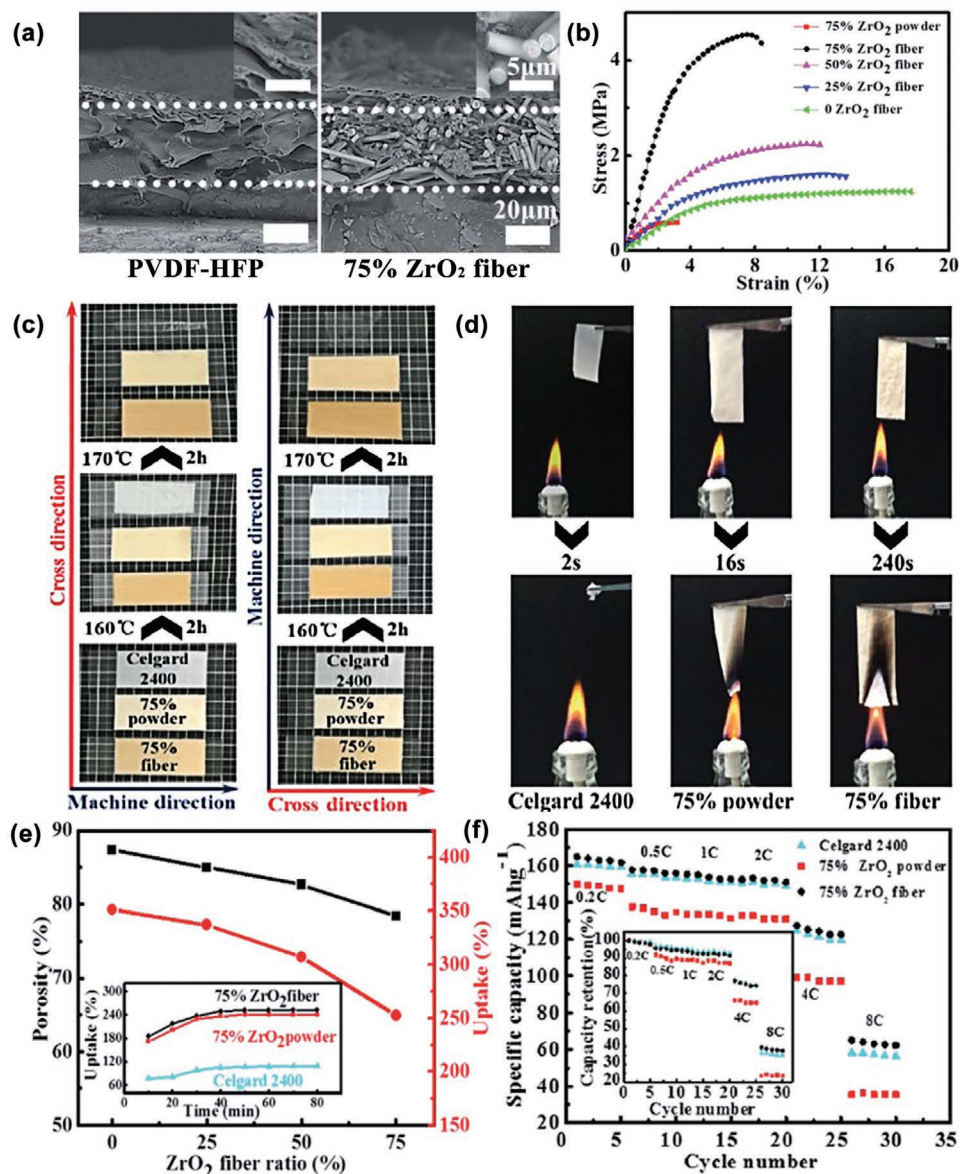
Figure 7. a) SEM micrographs of the membranes containing 0, 75% ZrO₂ fiber (scale bar = 20 mm for the large images and 5 mm for the inset). b) Stress–strain curves of membranes containing 0–75% ZrO₂ fiber and 75% ZrO₂ powder. c) Thermal contraction behavior. d) Combustion behavior of Celgard 2400, 75% ZrO₂ fiber separator and powder separator. e) Porosity and electrolyte uptake of Celgard 2400, ZrO₂ powder separator, ZrO₂ fiber separator. f) Rate capability under charge/discharge rates from 0.2C to 8C composed of Celgard 2400, 75% ZrO₂ powder and 75% ZrO₂ fiber separators. Reproduced with permission.[62] Copyright 2016, The Royal Society of Chemistry.

Clay or mineral materials have also been introduced into PVDF-HFP to form the stable separators for LIBs due to its unique self-hierarchy structure. Kim et al.[134] demonstrated a straightforward route to directly incorporate 2D clay sheets into the skeleton of PVDF-HFP. The generated pores can provide additional ionic transport pathways. Moreover, the addition of extremely low contents of 2D clay sheets in PVDF-HFP separators improves the thermal stability of the polymer separators.

In addition to PVDF-HFP, co-polymers of PVDF, including poly(vinylidene fluoride trifluoroethylene) (PVDF-TrFE) and poly(vinylidene fluoride-chlorotrifluoroethylene) (PVDF-CTFE), are also regarded as the based polymer separators to synthesize

the composite separators. Bicy et al.[135] fabricated a Al₂O₃ nanoparticle-decorated PVDF-TrFE membrane by the electro-spinning technique. The melting temperature of PVDF-TrFE is increased by adding the Al₂O₃ nanoparticles, and the membranes exhibit a superior thermal and dimensional stability compared to the Celgard 2320 separator. The fabricated cell with composite separators delivers a higher discharge capacity (95 mAh g⁻¹) at 1C, which is superior to the Celgard 2320 separator (85 mAh g⁻¹). Wang et al.[136] prepared a Sb₂O₃-modified PVDF-CTFE fibrous separator. Sb₂O₃ nanoparticles could effectively improve the mechanical strength (13.5 MPa), electrolyte uptake (356%) as well as thermal stability (without shrinkage at
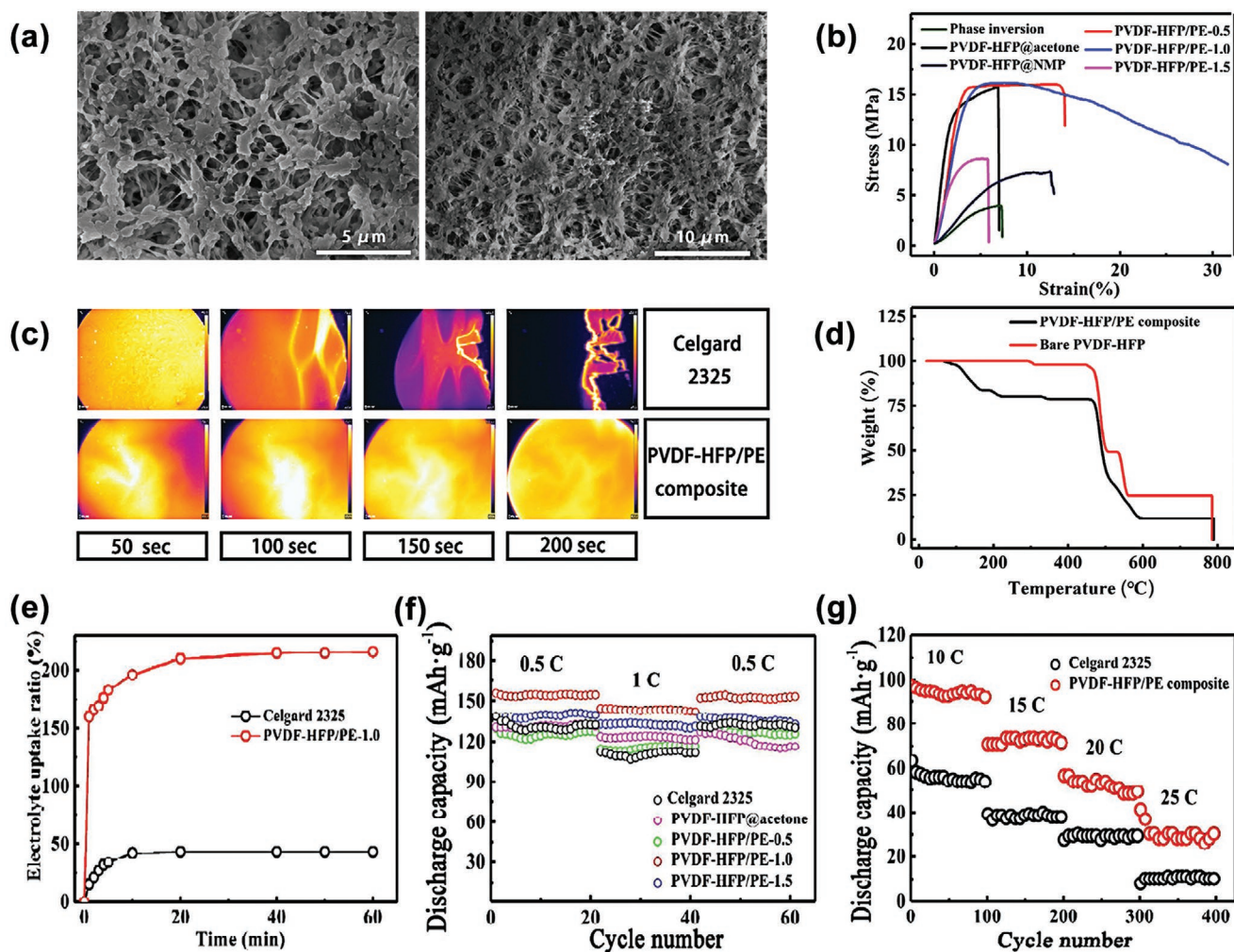
Figure 8. a) SEM images of PVDF-HFP/PE composite separators at different magnifications. b) Stress–strain curves of PVDF-HFP and composite separators. c,d) Thermography FLIR photographs and thermogravimetry curves of PVDF-HFP and composite separators. e) Electrolyte uptake ratio of composite separators and Celgard 2325. f) Rate performance curves of LiFePO₄ tested by Celgard 2325, PVDF-HFP, PVDF-HFP/PE-0.5, 1.0, 1.5 separators. g) High rate testing of LiFePO₄ with PVDF-HFP/PE-1.0 and Celgard 2325 separator at 10C–25C for 100 cycles. Reproduced with permission.[133] Copyright 2018, American Chemical Society.
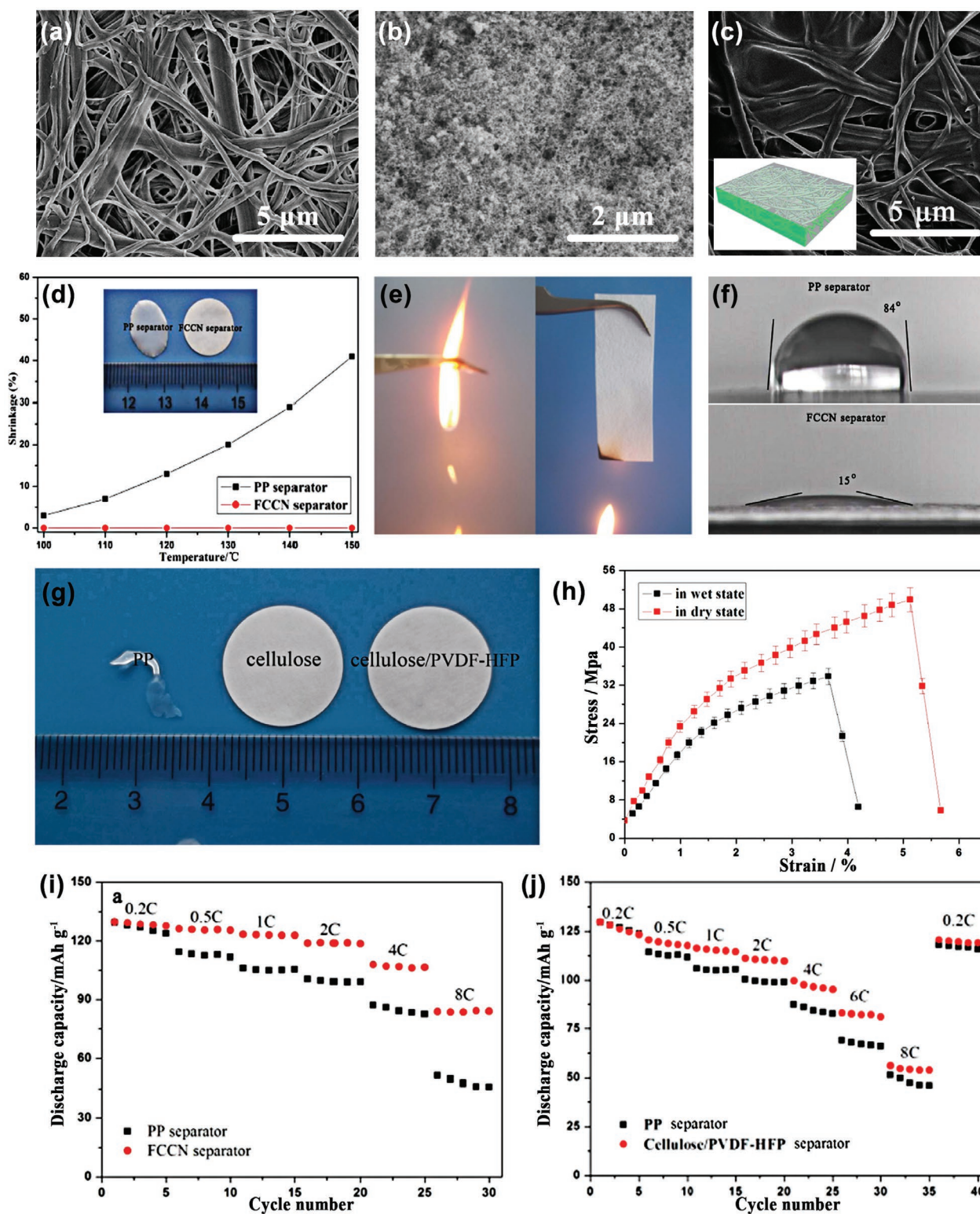
160 °C) of the PVDF-CTFE membrane. Especially, the cell with the Sb_2O_3/PVDF-CTFE separator has the discharge capacity of 93 mAh g^{-1} at 32C, while the cell containing the PE only has 19 mAh g^{-1}, which is due to the good wettability, high ionic conductivity, and low interfacial resistance of the Sb_2O_3/PVDF-CTFE separator.

3.2.4. Blending Type Based on Other Polymers Separators

Other polymers, such as cellulose, PVA, polyimide (PI), nylon 6,6 (PA66), polyacrylonitrile (PAN), could also have a good contact with the additives in the form of blending to fabricate the composite separators.[137] The composite separators could significantly improve the mechanical performance, thermal stability and wettability, as well as further enhance the safe and rate capacity of LIBs. Zhang et al.[138] fabricated a flame-retardant SiO_2/cellulose composite nonwoven (FCCN)

separator. The pore sizes are reduced tenfold after adding SiO_2, which prevents internal short-circuits and self-discharge, as shown in **Figure 9**a,b (before and after adding SiO_2). The SiO_2/cellulose separator exhibits a negligible thermal shrinkage under thermal treatment at 150 °C, inflame retarding property and better wettability, as shown in Figure 9d–f. As shown in Figure 9i, the SiO_2/cellulose composite nonwoven separator achieves a uniform current density especially for batteries operating at high charge/discharge rates (107 mAh g^{-1} at 4C and 83 mAh g^{-1} at 8C rate), which is higher than the cells employing PP separator (86 mAh g^{-1} at 4C and 47 mAh g^{-1} at 8C). In addition, Zhang et al.[85] also explored the cellulose based separator with PVDF-HFP, as shown in Figure 9c. Such nanofibrous composite nonwoven separator possesses an excellent heat tolerance at 200 °C, and high mechanical property (50 MPa) as shown in Figure 9g,h. The cells using the composite separator display a better rate capability at 8C discharge rate compared to those of commercial PP separator as shown in Figure 9j.

**ADVANCED
SCIENCE NEWS**

www.advancedsciencenews.com

**ADVANCED
FUNCTIONAL
MATERIALS**

www.afm-journal.de

Figure 9. a–c) SEM micrographs of CN separator and FCCN separator. d) Thermal shrinkage rate of PP separator and FCCN separator at 100–150 °C, and the inset photograph of PP separator and FCCN separator after thermal treatment at 150 °C for 0.5 h. e) Combustion behavior of PP separator and FCCN separator. f) Contact angle images of PP separator and FCCN separator. i) Rate capability of the LiCoO₂/graphite cells using PP separator and FCCN separator. Reproduced with permission.[138] Copyright 2014, Springer Nature. c) SEM image of cellulose/PVDF-HFP composite nonwoven. g) Photographs of separators after thermal treatment at 200 °C for 0.5 h. h) Stress–strain curves of the cellulose/PVDF-HFP composite nonwoven. j) Rate capability of the cells using PP separator and composite separator. Reproduced with permission.[85] Copyright 2012, American Chemical Society.

**ADVANCED
SCIENCE NEWS**

www.advancedsciencenews.com

**ADVANCED
FUNCTIONAL
MATERIALS**

www.afm-journal.de

Among the hydrophilic and heat-resistant polymers, PVA is a well-known membrane material with outstanding properties, such as excellent thermal stability, chemical stability, hydrophilicity and good film-forming property. Blending PVA membrane with different additives is well known ways to improve the safety and C-rate performance of LIBs. Zhang et al.[88] fabricated novel electrospun blending composite separators containing MOF particles and poly(vinyl alcohol) (PVA) denoted as EMP, as well as pure electrospun PVA denoted as EP, which are shown before and after blending in **Figure 10**a–c. The composite separators exhibit a lower thermal shrinkage at 200 °C and improved electrolyte uptake, as shown in Figure 10d,e. The MOF particles containing opened metal sites can spontaneously adsorb anions while allowing effective transport of lithium ions in the electrolyte,[139] leading to a dramatically improved lithium-ion transference number t_{Li+} (up to 0.79) and lithium-ion conductivity (2.9 mS cm^{-1}), as shown in Figure 10f,g. Implementation of such
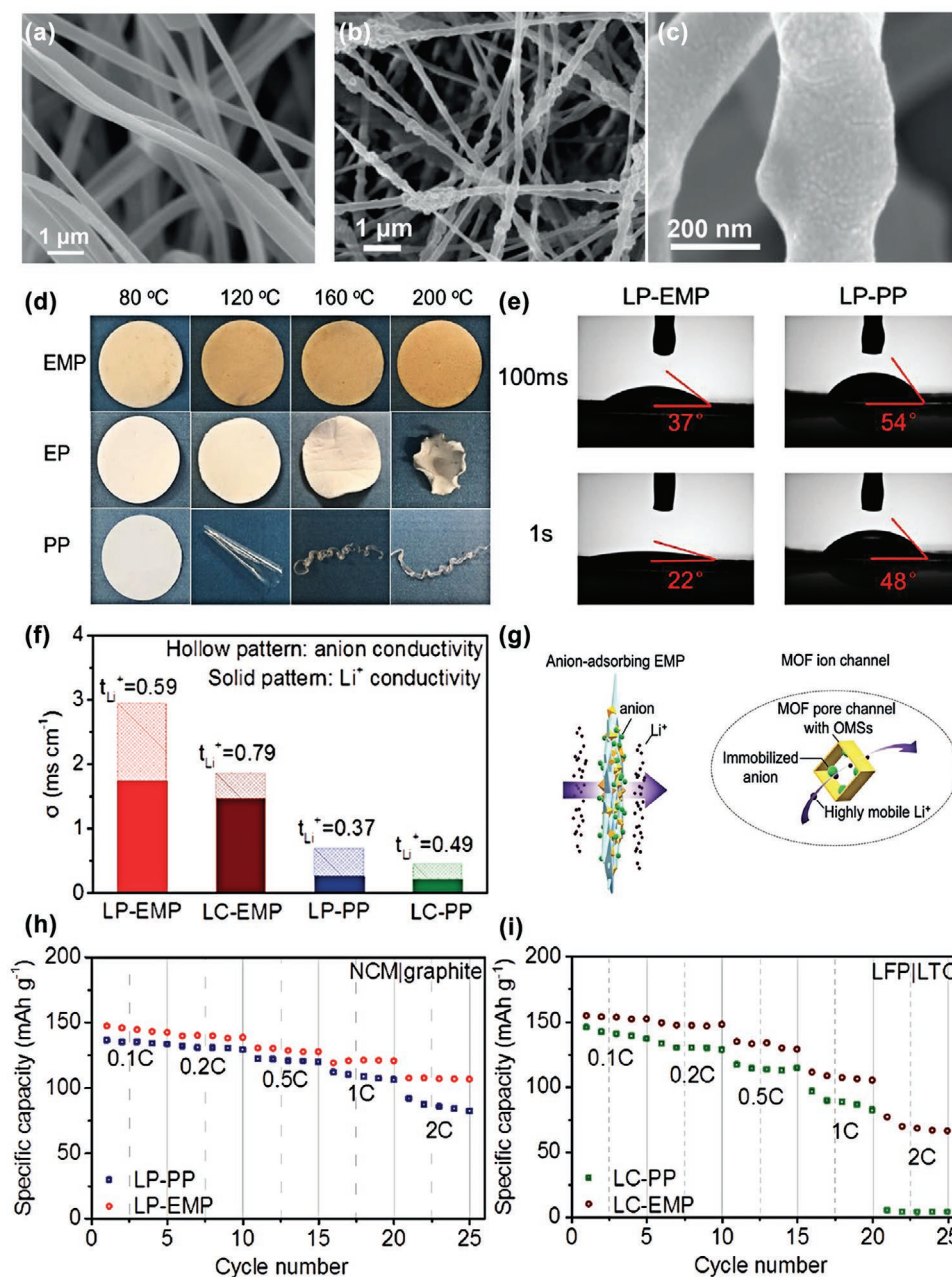
Figure 10. a–c) SEM images of EP and EMP. d) Optical photographs of separators after thermal treatment for 1 h. e) Contact angles of EMP and PP in 1 M LiPF$_6$ with ethylene carbonate/diethyl carbonate (LP). f) Comparisons on Li$^+$ transference number and separated ion conductivity. g) Schematic diagram of functional EMP for adsorbing anions and facilitating the transport of lithium ions. h) Rate performance with LiNi$_{0.33}$Co$_{0.33}$Mn$_{0.33}$O$_2$/graphite cells using LP electrolyte at 0.1C, 0.2C, 0.5C, 1C, and 2C. i) Rate performance with LFP/Li$_4$Ti$_5$O$_{12}$ cells using 1 M LiClO$_4$ in propylene carbonate (LC) electrolyte at 0.1C, 0.2C, 0.5C, 1C, and 2C. Reproduced with permission.[88] Copyright 2019, Wiley-VCH GmbH.

composite separators for LIBs leads to a significantly improved rate capability both for LiNi$_{0.33}$Co$_{0.33}$Mn$_{0.33}$O$_2$/graphite cell and LFP/Li$_4$Ti$_5$O$_{12}$ full cell, as shown in Figure 10h,i.

In addition, Chen et al.[140] fabricated a covalently bonded poly(vinyl alcohol)-silica (PVA-SiO$_2$) composite nanofiber separators. The PVA-SiO$_2$ separators possess a unique 3D interconnected porous structure and display a higher porosity (73%), better electrolyte affinity, higher electrolyte uptake (405%) and lower thermal shrinkage compared to PP separators.

PI has been selected as the separators materials for LIBs because of its intrinsic excellent thermal and mechanical properties. Shayapat et al.[141] fabricated thermally stable PI composite separators with Al$_2$O$_3$ nanoparticles. The separators show no thermal shrinkage at 200 °C, while commercial SV718 separators shrink at above 100 °C. The porosity and liquid-electrolyte uptake of the Al$_2$O$_3$/PI separators are over 90% and 790%, respectively, thus the separators assembled by LiCoO$_2$-Li exhibit higher rate discharge capacity (115.1 mAh g^{-1} at 5C) than that using the SV718 separator (98.4 mAh g^{-1}). In addition, nylon 6,6, which is well-known for high thermal stability and outstanding mechanical property, could also be synthesized into composite separators in the blending form. Yanilmaz et al.[142] fabricated electrospun SiO$_2$/nylon 6,6 (PA66) nanofiber separators, which enhanced the mechanical strength (22 MPa) and thermal stability (no change at 150 °C), as well as liquid electrolyte uptake (360%) compared to microporous polyolefin separators. The cells with SiO$_2$/PA66 separators have the similar discharge capacities (about 160 mAh g^{-1}) at 0.2C but higher rate capacities at 8C (78 mAh g^{-1}) compared with cells containing PP membranes (67 mAh g^{-1} at 8C). PAN has also been studied as a separator material and PAN-based separators show promising properties, including high ionic conductivity, good thermal stability, high electrolyte uptake and good compatibility with Li metal. Liang et al.[143] prepared lithium aluminum titanium phosphate (LATP)/PAN composite fiber-based separators. The electrospun LATP/PAN composite separators have a higher lithium ion conductivity, better electrochemical stability, and lower interfacial resistance with lithium electrode. Yanilmaz et al.[76] produced PMMA/PAN separators in a blending form through the centrifugal spinning technique. Compared with microporous PP membrane, centrifugally spun PMMA/PAN separators have a higher ionic conductivity, higher electrochemical oxidation limit, and lower interfacial resistance.

Except for above polymers, there are still a great number of porous polymers or fiber nonwoven polymers, such as polyurethane (PU), PMMA, polyethyleneglycol (PEG), polyphenylene sulfide (PPS), ANFs, which are also blended with additives to prepare the composite separators for high safety and superior electrochemical performance LIBs. **Table 1** shows the important characteristics of recently developed composite separators in the blending form for LIBs.

3.2.5. Section Summary

In this section, the recent development in the composite separators with the blending form has been demonstrated including blending based on commercial separators, blending based on PVDF and its co-polymers and blending based on other polymer

materials. It has been observed that commercial polyolefin separators on the basis of retaining the original mechanical properties and pore size are endowed with other excellent properties in order to improve their utilization efficiency for LIBs. With the development of composite separators, PVDF and its co-polymers could efficiently improve the wettability exceeding the polyolefin separators. PVDF and its co-polymers are commonly blended with the ceramic particles or polymer fibers to enhance the thermal stability and further avoiding safety issues when assembled in LIBs. Furthermore, other polymer materials have been studied because of their intrinsic excellent properties, such as better thermal stability and higher mechanical strength. The main reason for blending some additives in the polymers is to make up for inferior properties of the polymer, and to improve the electrochemical performance of LIBs on the basis of ensuring its safety. In addition, the blending form of the composite separators has a great number of potential advantages. It could be explained that organic polymer molecules can be combined with inorganic ceramic molecules or polymer chain molecules in the form of adsorption or covalent bonds in 3D space to form a denser composite structure, which reflects the optimal dual performance of raw materials and additives, as well as further improving the thermal stability and wettability. In addition, without increasing the thickness of the separators, the performance of separators could be controlled and balanced through adjusting the proportion of the amount of raw materials and additives in the blending form. In general, the composite separators with the blending form benefit for the high safety and high rate LIBs.

3.3. Layered Structure Type

Apart from the blending form between polymers and additives, a layered structure is usually synthesized and utilized to enable different materials, including polymers, ceramic particles, fiber nonwoven to perform their respective functions. The multilayer separator structure combining the advantages of each layer could improve the affinity to the electrolyte, ionic conductivity, and electrochemical performances.

3.3.1. Models and Simulations of Layered Composite Separators

To enable significant improvements in high-temperature cycling performance and fast-rate charge/discharge reactions, a great number of composite separators with layered structure were designed and meanwhile, molecular dynamic simulations have been used to predict and prove the relationship between the structure or composition of the separator and the performances of LIBs. Oh et al.[167] designed a Janus-faced, dual (ion/electron)-conductive/chemically active battery separator based on a heterolayered nanofiber mat architecture. They focused on the interaction between the polymers and multiwalled carbon nanotubes (MWNT) for the bulk and surface systems through MD simulations. The stronger van der Waals interactions were observed in the PEI/MWNT system, as shown in **Figure 11**a–c. In particular, the interaction area increases through wrapping motion of PEI on the MWNT surface. In addition, the

Table 1. Important characteristics of recently developed composite separators in the blending form for LIBs.

Materials	Additives	Fabrication method	Separator thickness [μm]	Thermal shrinkage [%]	Tensile strength [MPa]	Liquid electrolyte types	Electrolyte uptake [%]	Ionic conductivity [mS cm^{-1}] at RT	Cathode/anode	Rate performance	Refs.
PP	PEI/SiO$_2$	Self-assembly	14	25% at 130 °C for 0.5 h	–	LiPF$_6$-EC/DEC/EMC	398	0.49	LiCoO$_2$/Li	68 mAh g^{-1} (45.2%) at 5C	[126]
PE	PDA	Dip-coating	–	16% at 140 °C for 1 h	–	LiClO$_4$-EC/PC	112	0.3	LiCoO$_2$/Li	139.4 mAh g^{-1} (97.1%) at 0.5C	[144]
PP	AlPO$_4$/PVDF-HFP/PMMA	Solution casting	37	50% at 170 °C for 1 h	111.2	LiPF$_6$-EC/DMC	2.28	1.03	LiNiCoMnO$_2$/Li	112 mAh g^{-1} (67.5%) at 10C	[145]
PP	SiO$_2$/PDA	Dip-coating	–	22% at 160 °C for 0.5 h	–	Liquid Electrolyte	130	0.55	LiCoO$_2$/graphite	(50%) at 2C	[146]
PP	Aramid nanofiber	Dip-coating	20	20% at 150 °C for 1 h	71.7	LiPF$_6$-DMC/EC/PC	124.5	0.76	LiMn$_2$O$_4$/Li	(69.4%) at 5C	[127]
PE	CeO$_2$/P(MMA-BA-AN-St)	Phase inversion	75	36% at 135 °C for 1 h	52	LiPF$_6$-EC/DEC/EMC	81	2.5	LiNi$_{0.5}$Mn$_{1.5}$O$_4$/Li	110 mAh g^{-1} (90%) at 1C	[147]
PP	Cotton fiber	Solution casting	30	0% at 170 °C for 1 h	165	LiPF$_6$-EC/DMC	180	1.76	LiCoO$_2$/Li	139.3 mAh g^{-1} (82.5%) at 5C	[87]
PVDF-HFP	PE	Solution casting	20	0% at 150 °C for 1 h	16	LiPF$_6$-EC/DMC/EMC/DEC/VC	216	1.01	LiFePO$_4$/Li	97 mAh g^{-1} (59%) at 10C, 57 mAh g^{-1} (35%) at 20C	[133]
PVDF	hBN	Phase inversion	–	0% at 130 °C for 1 h	5.3	LiPF$_6$-EC/DEC	353	0.95	Li$_4$Ti$_5$O$_{12}$/Li	130 mAh g^{-1} (77%) at 5C	[64]
PVDF	CEC/CNF	Phase inversion	50	0% at 200 °C for 1 h	14.3	LiPF$_6$/EC/DEC/EMC	370	1.26	LiCoO$_2$/Li	92.5 mAh g^{-1} (75%) at 8C	[60]
PVDF-HFP	CuO	Solution casting	25	0% at 120 °C for 1 h	17	LiPF$_6$-EC/DMC	230	0.28	CuO(graphite)/Li	445 mAh g^{-1} (70%) at 2C	[17]
PVDF-HFP	clay	Solution casting	–	0% at 200 °C for 0.5 h	–	LiPF$_6$-EC/DEC/EMC	–	1.49	LiCoO$_2$/Li	67 mAh g^{-1} (45.9%) at 3C	[134]
PVDF-HFP	Colloidal Al$_2$O$_3$	Solution casting	40	4.5% at 150 °C for 0.5 h	18	LiPF$_6$-EC/DMC/EMC/DEC/VC	372	0.7	LiFePO$_4$/Li	120 mAh g^{-1} (76.4%) at 2C	[123]
PVDF-HFP	Colloidal-TiO$_2$	Solution casting	40	4.8% at 150 °C for 0.5 h	11.13	LiPF$_6$-EC/DMC/EMC/DEC/VC	164.5	1.57	LiFePO$_4$/Li	123.4 mAh g^{-1} (78.6%) at 2C	[131]
PVDF	PMMA/SiO$_2$	Electrospinning	30	0% at 150 °C for 1 h	32.69	LiPF$_6$ solution	406	4.0	LiFePO$_4$/Li	128 mAh g^{-1} (81.2%) at 2C	[129]
PVDF-HFP	ZrO$_2$ fiber	Phase inversion	30	0% at 170 °C for 2 h	>5	LiPF$_6$-DMC/DEC/EC	252.5	0.32	LiFePO$_4$/Li	(78%) at 4C (38%) at 8C	[62]
PVDF-HFP	Al(OH)$_3$/CA	Phase inversion	50	4.6% at 160 °C for 0.5 h	–	LiPF$_6$-EC/DMC/EMC	403.9	2.85	LiCoO$_2$/Li	128.28 mAh g^{-1} (81%) at 8C	[130]
PVDF-CTFE	Sb$_2$O$_3$	Electrospinning	42	0% at 160 °C for 2 h	13.5	LiPF$_6$-EC/DEC	356	2.88	LiFePO$_4$/Li	93 mAh g^{-1} (55.7%) at 32C	[136]
PVDF	SiO$_2$	Phase inversion	–	0% at 170 °C for 0.5 h	–	LiPF$_6$-EC/DMC	220	0.9	LiFePO$_4$/Li	118 mAh g^{-1} (74.7%) at 2C	[61]
PVDF	SiO$_2$	Electrospinning	–	0% at 150 °C for 0.5 h	13	LiPF$_6$-EC/EMC	370	2.6	LiFePO$_4$/Li	95 mAh g^{-1} (55.9%) at 8C	[148]
PVDF	Zeolite	Electrospinning	26	0% at 150 °C for 1 h	3.2	LiPF$_6$-EC/DMC/EMC	378	1.72	LiFePO$_4$/Li	110 mAh g^{-1} (72.4%) at 5C	[149]
PVDF	PDA	Phase inversion	30	0% at 150 °C for 0.5 h	–	LiPF$_6$-EC/DMC	1160	0.962	LiMn$_2$O$_4$/Li	45 mAh g^{-1} (42.8%) at 7C	[150]
PVDF-HFP	Li$_{6.75}$La$_3$Zr$_{1.75}$Ta$_{0.25}$O$_{12}$	Solution casting	25	0% at 160 °C for 0.5 h	18	LiPF$_6$-EC/DMC/EMC/DEC/VC	250.85	0.74	LiFePO$_4$/Li	93 mAh g^{-1} (56.4%) at 5C	[132]

ADVANCED
SCIENCE NEWS

www.advancedsciencenews.com

ADVANCED
FUNCTIONAL
MATERIALS

www.afm-journal.de

Table 1. Continued.

Materials	Additives	Fabrication method	Separator thickness [μm]	Thermal shrinkage [%]	Tensile strength [MPa]	Liquid electrolyte types	Electrolyte uptake [%]	Ionic conductivity [mS cm^{-1}] at RT	Cathode/ anode	Rate performance	Refs.
PVDF	SiO$_2$/cellulose	Phase inversion	25	0% at 250 °C for 0.5 h	15	LiPF$_6$-EC/DMC	–	1.25	LiNiCoMnO$_2$/Li	(50%) at 4C	[151]
PVDF-HFP	Cellulose	Phase inversion	115	2% at 200 °C for 0.5 h	3.87	LiPF$_6$-EC/DMC	310	1.89	LiCoO$_2$/Li	136 mAh g^{-1} (79.5%) at 8C	[152]
PVDF	MMT	Electrospinning	36	19% at 150 °C for 1 h	–	LiPF$_6$-EC/EMC/DEC	342	4.2	LiFePO$_4$/Li	118 mAh g^{-1} (81.7%) at 2C	[153]
PVDF-TrFE	Al$_2$O$_3$	Electrospinning	–	0% at 120 °C for 1 h	2.8	LiPF$_6$-EC/DMC	320	5.8	LiFePO$_4$/Li	98 mAh g^{-1} (63.6%) at 1C	[135]
PVDF-HFP	ZrO$_2$	Phase inversion	–	0% at 150 °C for 1 h	–	LiPF$_6$-EC/EMC	120	6.1	LiCoO$_2$/Li	(34.4%) at 3C	[154]
PVDF-HFP	SiO$_2$	Solution casting	30	4.5% at 160 °C for 1 h	14.7	LiPF$_6$-EC/DMC/EMC	420	1.28	LiFePO$_4$/Li	106 mAh g^{-1} (64.2%) at 5C	[119]
PVDF	POSS	Solution casting	50	0% at 170 °C for 1 h	12.7	LiPF$_6$-EC/DMC/EMC	974	4.2	LiCoO$_2$/Li	122 mAh g^{-1} (83%) at 2C	[155]
cellulose	PVDF-HFP	Electrospinning	27	0% at 200 °C for 0.5 h	50	LiPF$_6$-EC/DMC	280	1.04	LiCoO$_2$/Li	96 mAh g^{-1} (73.8%) at 4C	[85]
cellulose	Kraft/PSA	Wet-laid	35	0% at 180 °C for 1 h	48	LiPF$_6$-EC/DMC	333	1.58	LiCoO$_2$/Li	65.5 mAh g^{-1} (50%) at 8C	[156]
cellulose	PSA	Wet-laid	40	0% at 200 °C for 0.5 h	17	LiPF$_6$-EC/DMC	260	1.2	LiCoO$_2$/graphite	(47.5%) at 8C	[82]
cellulose	Hydroxyapatite	Self-assembly	56	0% at 200 °C for 1 h	13.21	LiPF$_6$-EC/DMC	253	3.07	LiCoO$_2$/graphite	120 mAh g^{-1} (85.7%) at 5C	[157]
PVA	MOF	Electrospinning	60	0% at 200 °C for 1 h	–	LiPF$_6$-EC/DEC	230	2.9	LiFePO$_4$/LiTiO$_2$	75 mAh g^{-1} (44%) at 2C	[88]
cellulose	Al$_2$O$_3$	Solution casting	30	0% at 180 °C for 0.5 h	140	LiPF$_6$-EC/DMC/DEC	625	4.91	LiFePO$_4$/Li	130 mAh g^{-1} (80%) at 1C	[158]
PVA	SiO$_2$	Electrospinning	25	0% at 150 °C for 0.5 h	11.2	LiPF$_6$-EC/DMC	405	1.81	LiFePO$_4$/Li	123.3 mAh g^{-1} (90.3%) at 2C	[140]
PI	Al$_2$O$_3$	Electrospinning	20	0% at 200 °C for 1 h	38.6	LiPF$_6$-EC/DMC	864.2	–	LiCoO$_2$/Li	117 mAh g^{-1} (70%) at 5C	[141]
glass microfiber	Melamine formaldehyde	Wet-laid	40	0% at 150 °C for 0.5 h	21.2	LiPF$_6$-EC/DMC	280	0.52	LiFePO$_4$/Li	91 mAh g^{-1} (65%) at 4C	[159]
nylon 6,6	SiO$_2$	Electrospinning	65	0% at 150 °C for 0.5 h	22	LiPF$_6$-EC/EMC	360	3.8	LiCoO$_2$/Li	78 mAh g^{-1} (48.8%) at 8C	[142]
PI	PEO	Dip-coating	40	0% at 180 °C for 1 h	–	LiPF$_6$-EC/PC/DMC/EA	178	0.65	LiFePO$_4$/Li	117 mAh g^{-1} (74.5%) at 3C	[160]
PEI/PU	SiO$_2$	Electrospinning	50	2% at 170 °C for 0.5 h	6.22	LiPF$_6$-EC/EMC/DMC	795.61	6.25	LiFePO$_4$/Li	147 mAh g^{-1} (88.5%) at 1C	[161]
glass microfiber	TiO$_2$/PVDF-HFP	Solution casting	65	0% at 150 °C for 1 h	–	LiPF$_6$-EC/DMC/EMC	330	3.45	LiCoO$_2$/Li	122 mAh g^{-1} (85%) at 10C	[162]
PAN	Agarose/PAA	Electrospinning	25	0% at 150 °C for 0.5 h	–	LiPF$_6$-EC/DEC	–	0.87	LiMn$_2$O$_4$/Li	45 mAh g^{-1} (42.9%) at 5C	[163]
PPS	Aramid nanofibers	Wet-laid	56	0% at 200 °C for 1 h	9.8	LiPF$_6$-EC/DMC	238.6	1.43	LiFePO$_4$/Li	115 mAh g^{-1} (70%) at 2C	[58]
PAN	SiO$_2$	Electrospinning	65	0% at 150 °C for 0.5 h	3.5	LiPF$_6$-EC/EMC	337	2.6	LiFePO$_4$/Li	82 mAh g^{-1} (50.3%) at 8C	[164]
cellulose	POM	Phase inversion	29	0% at 180 °C for 1 h	116	LiPF$_6$-DMC/DEC/EC	412	1.56	LiFePO$_4$/Li	(86.6%) at 4C	[165]
PAN	PU	Electrospinning	50	0% at 170 °C for 0.5 h	10	LiPF$_6$-EC/EMC/DMC	776.09	2.07	LiFePO$_4$/Li	147 mAh g^{-1} (86.5%) at 1C	[166]
cellulose	SiO$_2$/sodium alginate/flame retardant	Wet-laid	40	0% at 150 °C for 0.5 h	45	LiPF$_6$-EC/DMC	270	2	LiCoO$_2$/graphite	107 mAh g^{-1} (82.9%) at 4C 83 mAh g^{-1} (64.3%) at 8C	[138]
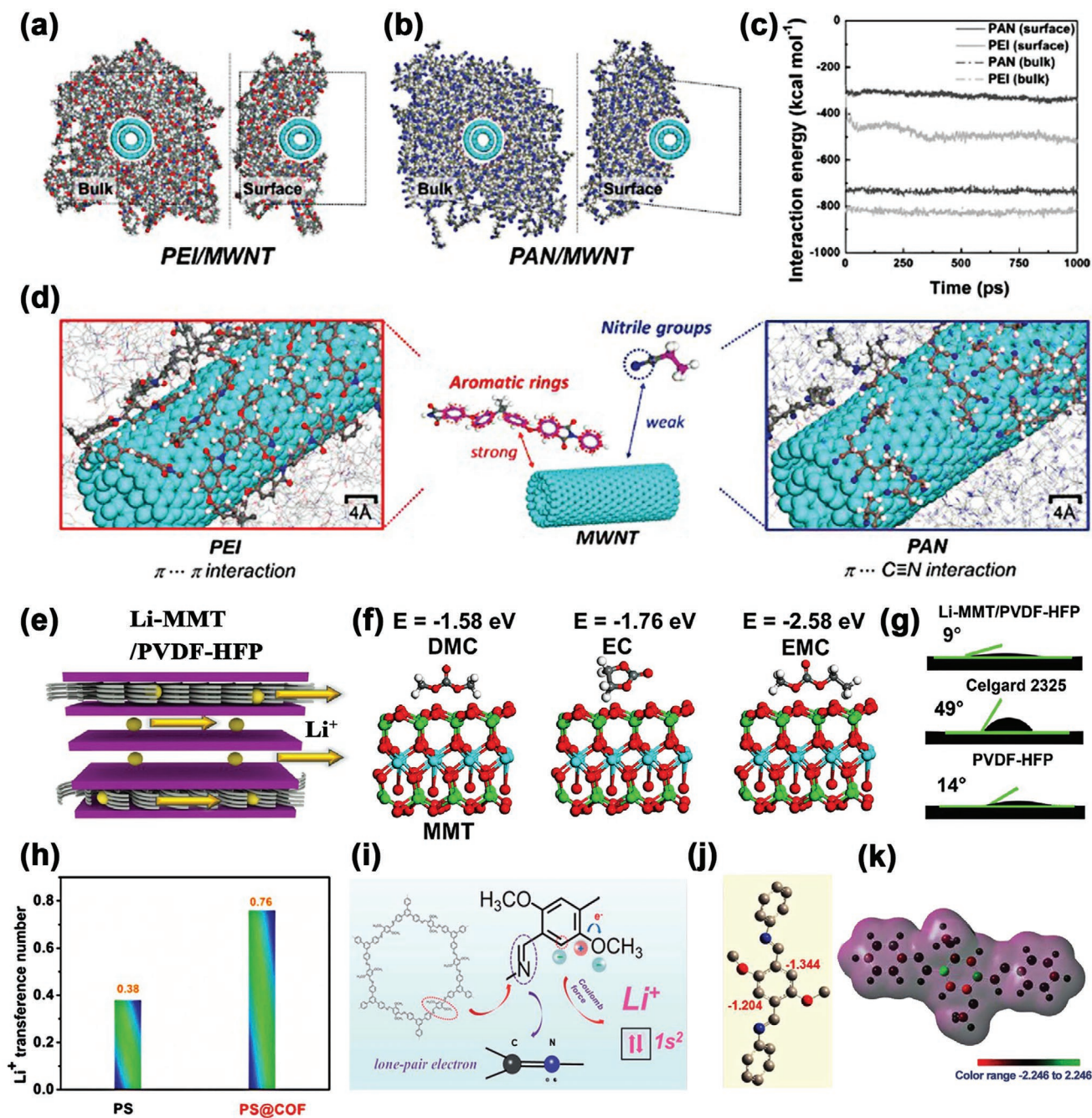
Figure 11. a) Model systems of PEI/MWNT coating layer for bulk and surface. b) Model systems of PAN/MWNT coating layer for bulk and surface. c) Interaction energy profiles between the polymers (PEI vs PAN) and MWNT with respect to simulation time. d) Snapshots of atomistic configurations of the PEI (or PAN)/MWNT systems. The major interaction sites of PEI (or PAN) with MWNTs are shown in the middle. Reproduced with permission.[167] Copyright 2016, Wiley-VCH GmbH. e) Illustration of the structure of Li-MMT/PVDF-HFP separator. f) Atomic model configuration and interaction between MMT and electrolyte. g) Contact angle images of Li-MMT/PVDF-HFP, PVDF-HFP, and Celgard-2325 separators. Reproduced with permission.[44] Copyright 2020, Elsevier B.V. h) Comparison of Li+ transference number at room temperature. i) Ionic transportation regulation mechanism of the COF-modified separator. j) Optimized structure of the COF subunit and the distributed electronegativity on the adjacent carbon atom. k) Surface electrostatic potential distribution of COF molecular fragments. Reproduced with permission.[168] Copyright 2019, The Royal Society of Chemistry.

atomistic configurations of the PEI (or PAN)/MWNT systems were investigated as shown in Figure 11d. The aromatic rings of PEI tended to align parallel to the MWNT surface because of strong intermolecular π-π stacking interactions. compared with

the weak van der Waals interactions of PAN/MWNT coating layer. Zhao et al.[44] fabricated PVDF-HFP/Li-montmorillonite (MMT) composite separators, as shown in Figure 11e. By DFT calculations, the adsorption energy values between MMT and

**ADVANCED
SCIENCE NEWS**

www.advancedsciencenews.com

**ADVANCED
FUNCTIONAL
MATERIALS**

www.afm-journal.de

electrolyte are –1.58 eV for MMT-DMC, –1.76 eV for MMT-EC, and –2.58 eV for MMT-EMC, which are much larger than PVDF-HFP/electrolyte adsorption energies (–0.03 to –0.24 eV), as shown in Figure 11f. The results are consistent with the contact angle measurements, as shown in Figure 11g. Owing to the strong affinity to DMC, EC, and EMC, the separator incorporated with Li-MMT owns much more pronounced, electrolyte uptake and wettability, as compared with Celgard 2325 and pure PVDF-HFP separators. Wen et al.[168] coated a custom-designed covalent organic framework (COF) on commercial separators. The lithium ion transference number (t_{Li+}) of the as-fabricated separator (PS@COF) is two times that of the uncoated PS as shown in Figure 11h. The construction mechanism of the lithium ion channel is shown in Figure 11i. The electronegativity of O is stronger than that of C, causing the shared electron pair between O and benzene to shift toward O, which results in the C of the benzene being connected to –OCH₃ with a positive charge. Naturally, the C in the ortho position is negatively charged. A large number of sites in the COF are connected to form this highly selective channel for Li⁺. The surface electrostatic potential map can prove that the ortho position of –OCH₃ carries a more negative potential, which provides a theoretical basis for the construction of the channel (Figure 11j,k). The contribution of the COF to the improved Li⁺ transference number of the separator can be verified by the effect of PVDF.

3.3.2. Layered Structure Based on Commercial Separators

Commercial polyolefin separators are regarded as the most common separators for LIBs because of their relatively high mechanical strength and greatly uniform pore structure. However, poor thermal stability and low liquid electrolyte uptake lead to the inferior discharge capacity at high rate current.[36] Therefore, combining with other additives in the layered form is favorable for commercial polyolefin separators to achieve the excellent supporting substrate and simultaneously demonstrate other superior properties of the coating layers.
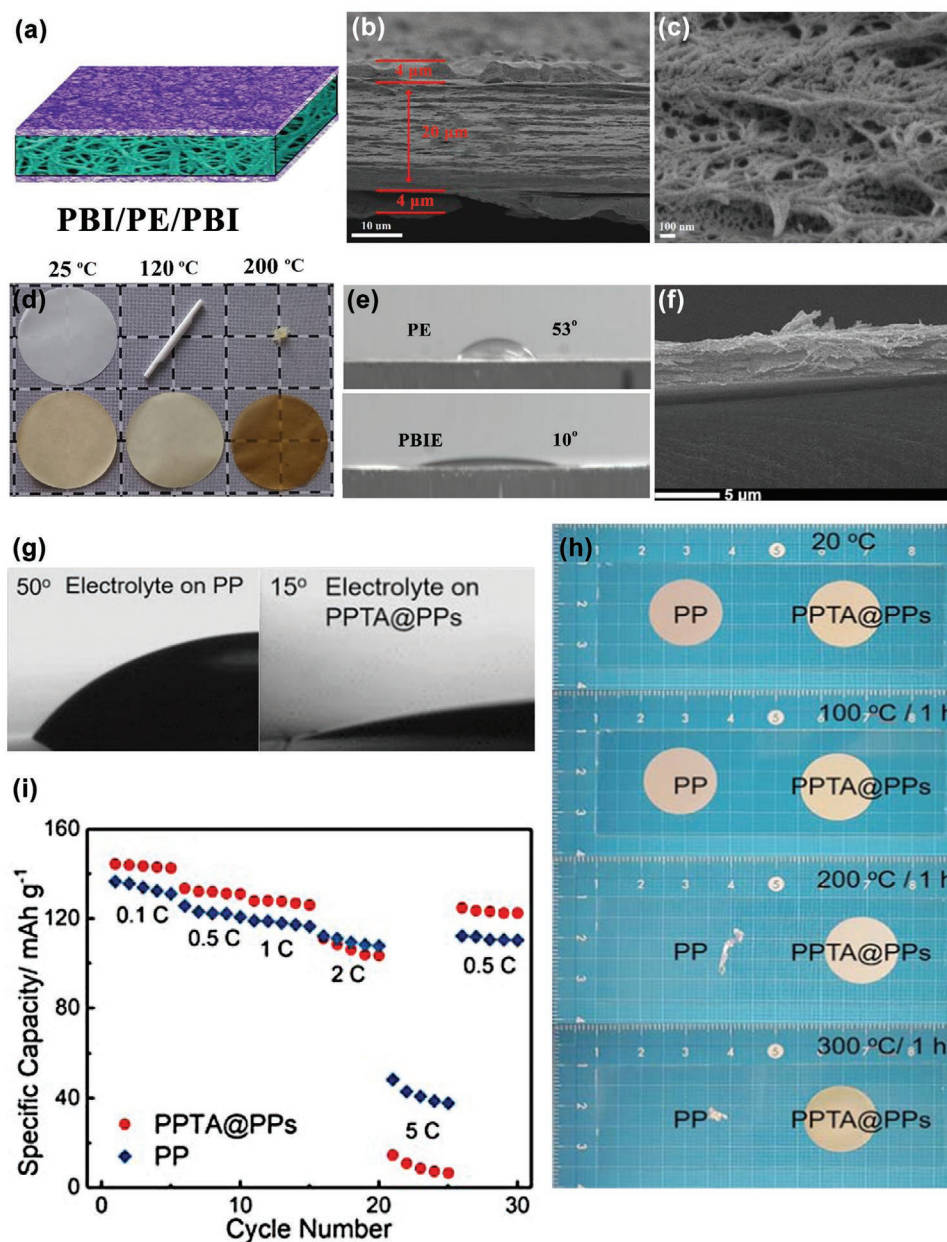
Using ceramic particles as a coating layer can effectively improve the thermal stability of the membrane surface. Feng et al.[169] fabricated a composite separator through combining hydrophobic silica aerogel and PP separator, effectively increasing the thermal stability (the area retention rate is 30% higher than that of the PP separator after being heated for 30 min at 160 °C). In addition, the hydrophobic silica aerogel layer significantly improves the wettability (close to 0° of contact angle), owing to the introduced hydrophobic functional group of –Si(CH₃)₃ and porous structure. The LIBs with SAC separator exhibit a higher rate capacity of 124 and 100 mAh g⁻¹, while that with PP separator is 108 and 45 mAh g⁻¹, when high-rate of 4C and 8C were applied, respectively. Jung et al.[170] coated a thin Al₂O₃ layer (<10 nm) on every surface of the porous PP framework without significantly increasing the total separator thickness by the atomic layer deposition (ALD). The thin Al₂O₃ ALD coating results in suppressed thermal shrinkage and the enhanced wettability, leading to improved safety of the batteries, and more importantly, without any decrease in electrochemical performances such as capacity and rate capability.

The commercial separators also can be combined with the polymers in the layered structure form. Li et al.[171] designed a sandwich-like composite separator with superhigh thermal stability, which including porous polybenzimidazole (PBI) layers on both sides of a PE separator denoted as PBIE separator, as shown in **Figure 12a–c**. The PBI/PE/PBI sandwich-like composite separator exhibits no dimensional shrinkage up to 200 °C, and improved liquid electrolyte uptake (10° of contact angle), as shown in Figure 12d,e. The composite separator with superhigh thermal stability and the shut-down function will be highly suitable for improving the safety of LIBs. He et al.[172] demonstrated coating poly-*p*-phenylene terephthamide (PPTA) layer onto commercial PP separators (Figure 12f). Without any additional binder, PPTA layer acting as a framework sticks to the porous PP separators, endowing the composite separators with enhanced heat resistance and wettability, as shown in Figure 12g,h. Moreover, the cells equipped with the PPTA/PP separators show a better rate discharge capacity, as shown in Figure 12i.

Combining ceramic materials and polymers could further improve the various properties of composite separators for high safety and rate LIBs. Waqas et al.[104] prepared a highly efficient and thermally stable PE-hBN/PVDF-HFP bilayer separator. The incorporation of hBN in PE matrix promotes the interfacial interaction between PE and PVDF-HFP layers to prevent separation of layers, as shown in **Figure 13a**. The PVDF-HFP layer provides an additional thermally stable backbone and its inherent hydrophilic property and highly porous structure improve the overall performance of the separator. The bilayer separator owns a thermal shrinkage of 6.6% upon annealing at 140 °C for 1 h and a high electrolyte uptake of 348%, as shown in Figure 13b,c. To achieve uniform deposition of lithium ions to further control safety for LIBs, Zhao et al.[49] proposed an ion redistributors with LLZTO coated PP separators to eliminate dendrites, as shown in Figure 13d–f. The cells with LLZTO composite separators render a high coulombic efficiency above 98% over 450 cycles, while the ones with PP decline rapidly after 200 cycles, as shown in Figure 13g, indicating that the Li metal loss resulted from electrolyte depletion and nonuniform Li deposition.

In addition, Pan et al.[75] demonstrate an ultrathin silica-anchored layered (PVDF/PE/PVDF) porous fiber separator. The separator displays both ultrathin thickness (≈20 μm thick) and high mechanical strength of approximately 11.2 MPa, as well as high porosity, which results in high electrolyte uptake (≈380%) and ionic conductivity (≈2.5 mS cm⁻¹). When deployed in a LiFePO₄/Li cell, the cell can deliver a discharge capacity of 134.3 mAh g⁻¹ at a high rate of 10C and maintain a capacity of 129.2 mAh g⁻¹ after 300 charge–discharge cycles, showing an excellent high-rate performance. Similarly, Xu et al.[173] applied the layer-by-layer (LbL) self-assembly process of poly(acrylic acid) (PAA) and ZrO₂ to construct functional ultrathin multilayers on PE separators without sacrificing the excellent porous structure of original separators. Such PAA/ZrO₂-PE separators possess good electrolyte wettability, excellent electrolyte uptake, high ionic conductivity and large Li⁺ transference number. More importantly, the top layer of LbL self-assembly could affect the dissociation of electrolyte and the formation of stable SEI layer. Compared with the pristine PE, the composite

ADVANCED
SCIENCE NEWS
www.advancedsciencenews.com

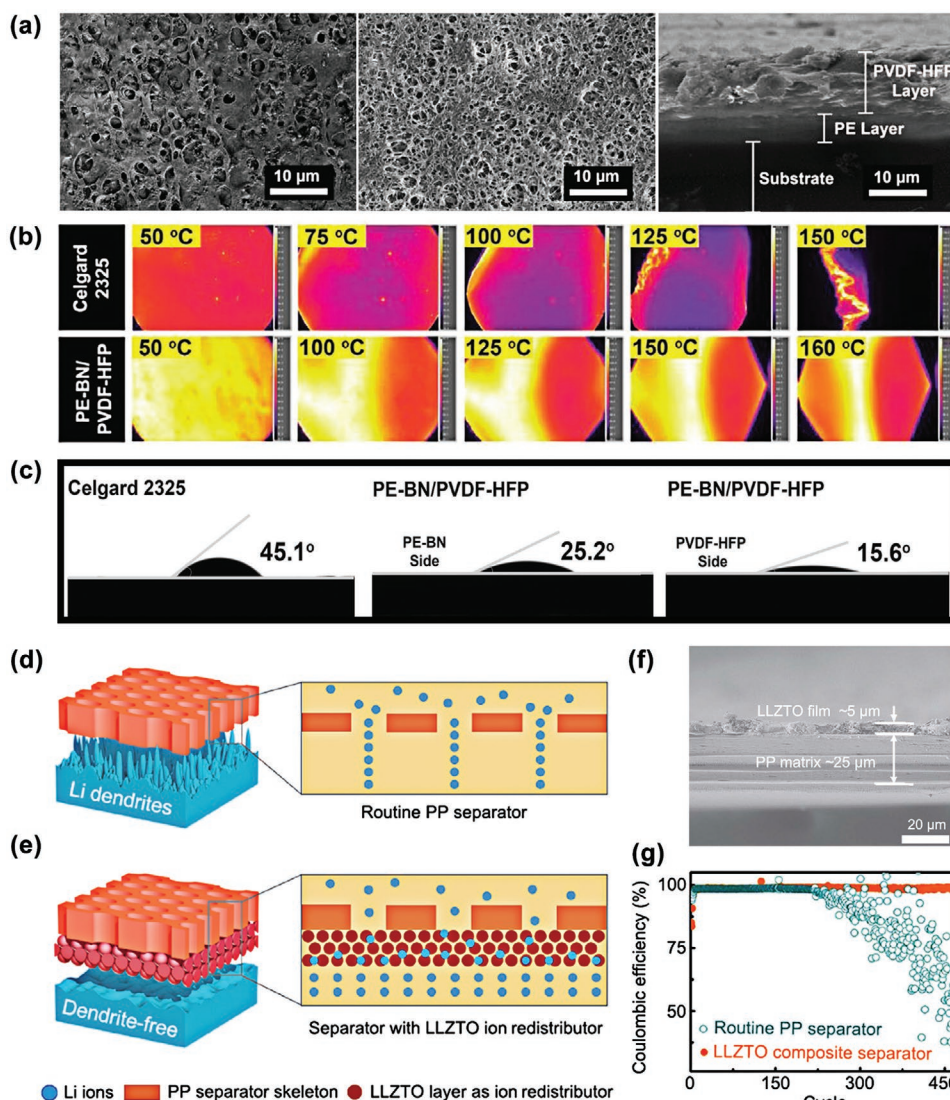ADVANCED
FUNCTIONAL
MATERIALS
www.afm-journal.de

Figure 12. a) Model diagram of PBIE separator. b) The cross-section and magnified cross-section SEM images of PBIE separator. c) Photographs of the PE and the PBIE separator after heat treatments at 120 and 200 °C. d) Contact angle images of the PE and the PBIE. Reproduced with permission.[171] Copyright 2017, Elsevier B.V. e) Cross-section SEM image of the PPTA@PPs. f,g) Contact angle and heat resistance pristine PPs and PPTA@PPs. h) Rate capacities of the cells with pure PP and PPTA@PPs at discharge rates of 0.1C, 0.5C, 1C, 2C, and 5C. Reproduced with permission.[172] Copyright 2018, Wiley Periodicals, Inc.

separator endows the cells with an excellent capacity retention at high C-rates and superior cycling performance.

3.3.3. Layered Structure Based on Other Polymers Separators

Apart from commercial polyolefin separators as the base of layered structure, many other polymers, such as PVDF, PVDF-HFP, PET and PI could be combined with additive layer to prepare the composite separators with high and strong properties.

In particular, PVDF and its co-polymers are the greatly common materials as the substrate due to their intrinsic superior pore distribution and wettability. However, the use of pure PVDF polymer is rarely developed as the substrate for layered structure. The co-polymers of PVDF, such as PVDF-HFP have been commonly reported to prepare the composite separators in the form of layered structure. Recently, Zeng et al.[174] developed a robust bilayer separator by using MoO_3 and Al-doped $Li_{6.75}La_3Zr_{1.75}Ta_{0.25}O_{12}$ (LLZTO). Combination between MoO_3/PVDF-HFP and LLZTO/PVDF-HFP endows the composite

ADVANCED
SCIENCE NEWS
www.advancedsciencenews.com

**ADVANCED
FUNCTIONAL
MATERIALS**
www.afm-journal.de

Figure 13. a) SEM images of bottom surface, top surface and cross-section view of PE-BN/PVDF-HFP separator. b) FLIR images of Celgard 2325 and PE-BN/PVDF-HFP separators under annealing. c) Contact angle measurement images of Celgard 2325 and PE-BN/PVDF-HFP separators with liquid electrolyte. Reproduced with permission.[104] Copyright 2018, Wiley-VCH GmbH. d,e) Schematic illustration of the electrochemical deposition behaviors of the Li metal anodes using a routine PP separator and a composite separator with the LLZTO layer. f) Cross-section SEM of the composite separator with the LLZTO. g) Coulombic efficiencies with cycle numbers in Li I Cu cells at a current density of 0.5 mA cm^{-2} in ether-based (DOL/DME) electrolytes. Reproduced with permission.[49] Copyright 2018, AAAS.

separator with strong interfacial adhesion, as shown in **Figure 14**a. The bilayer separator owns a high mechanical strength (22.3 MPa), low thermal shrinkage (5%) after annealing at 160 °C for 4 h and improved electrolyte retention, as shown in Figure 14b–d. Based on the bilayer separator, Li/LiFePO$_4$ cells deliver a high ion conductivity of 6.33×10^{-4} S cm^{-1} and remarkable discharge rate capacities of 91 and 71 mAh g^{-1} at 7C and 10C, respectively, as shown in Figure 14e,f.

Recently, Gonzalez et al.[175] prepared a nano composite Janus separator, which includes partially electronically conductive (PEC) layer and SiO$_2$/PVDF-HFP layer. By using the single-layer separators, dendrites completely penetrating separator after long cycles, causing high short circuit current and large cell temperature increase; conversely, negligible short

circuit current and temperature rise occurs with the Janus separator, indicating that the PEC layer successfully intercepts dendrites.

Polyethylene terephthalate (PET), a well-known membrane material, has also attracted much attention as the separators of Li-ion batteries because of its good mechanical properties, thermal stability, and excellent electronic insulation. However, its intrinsic poor wettability and large pore size restrict the application of separators in high safety and electrochemical performance LIBs, thereby it is necessary to prepare composite separators based on PET, particularly in the form of layered structure. Zhu et al.[176] proposed a novel membrane via a mechanically pressed process with PVDF nanofiber based on PET microfiber support. The improved physical
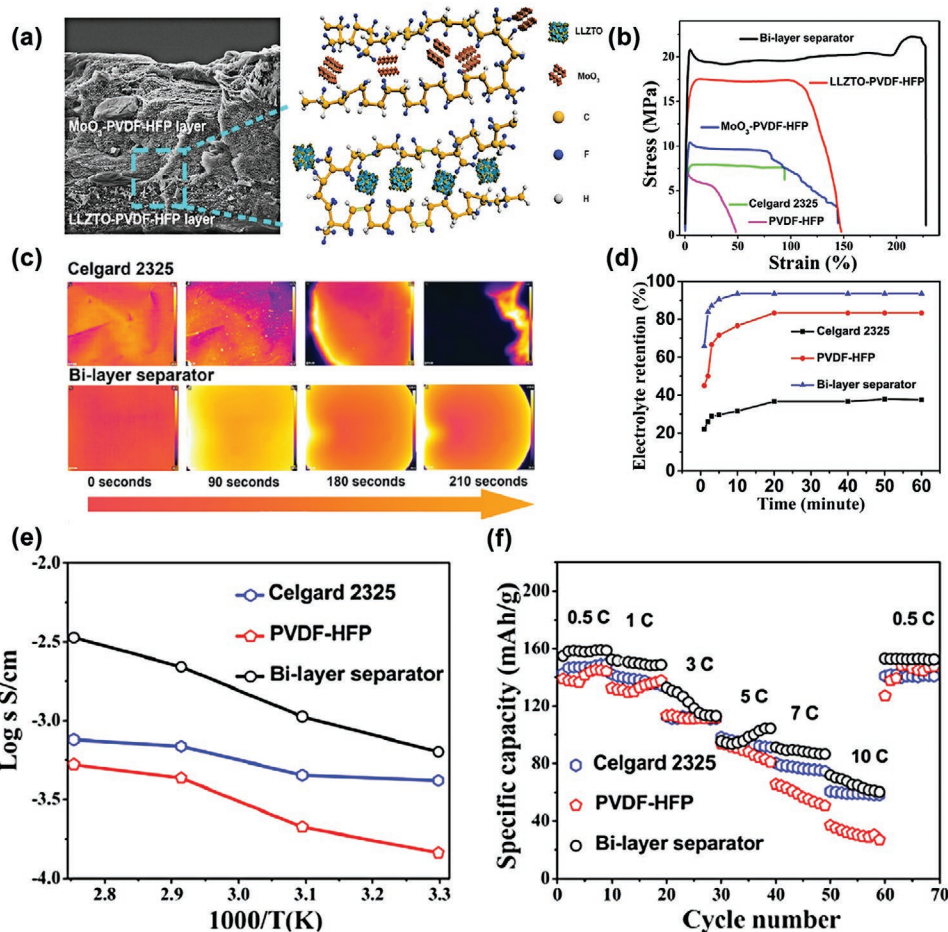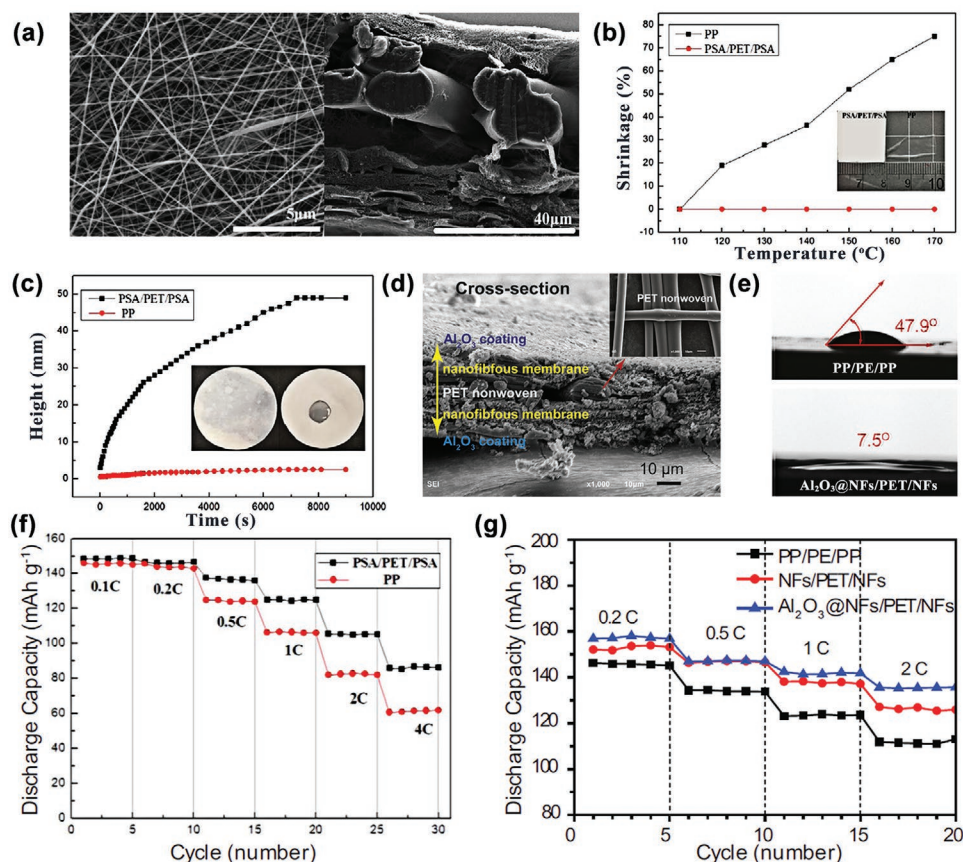
Figure 14. a) Cross-sectional SEM images of the bilayer separator and the schematic illustration for the bilayer structure. b) Stress–strain curves of PVDF-HFP, Celgard 2325, MoO_3-PVDF-HFP, LLZTO-PVDF-HFP, and bilayer separators. c) FLIR thermal distributed images (left) and the corresponding time-resolved temperature curves (right) of Celgard 2325 and bilayer separators. d) Electrolyte retentions of Celgard 2325, PVDF-HFP and bilayer separators after soaking in liquid electrolyte. e) Ion conductivities of Celgard 2325, PVDF-HFP, and bilayer separators. f) Rate performance of Li/LFP cells with Celgard 2325, PVDF-HFP, and bilayer separators. Reproduced with permission.[174] Copyright 2019, American Chemical Society.

properties, such as surface morphology, wettability, and heat stability endow LIBs containing the PET-reinforced PVDF composite separators with high safety performance. Jeong et al.[83] fabricated a SiO_2/PVDF-HFP coated PET nonwoven layered composite separator, in which PVDF-HFP serves as a binder to interconnect SiO_2 and PET. PET is also employed as a mechanical substrate to suppress the thermal shrinkage of the composite separators. Moreover, enhanced thermal stability and wettability via coating layers greatly increase the rate discharge capacities at 2C compared with commercial separators. Peng et al.[177] developed a PET nonwoven sandwiched electrospun polysulfonamide (PSA) fibrous separator. The PET nonwoven served as a mechanical support, and the PSA layers provided the separators with nanoporous structures, as shown in **Figure 15**a. This novel composite separator possessed a better thermal stability (no change at 150 °C) and electrolyte wettability than commercial polypropylene separator, which endows the cells with excellent discharge C-rate capacity (86.7 mAh g^{-1}) compared with the PP (61.8 mAh g^{-1}) at 4C., as shown in Figure 15b,c,f. Liu et al.[178] designed a

Al_2O_3@NFs/PET/NFs multilayer separator possessing hierarchically 3D tortuous structure, which comprises a PET nonwoven sandwiched between two PVA-*co*-PE nanofibrous membrane and inorganic Al_2O_3 coating layers on both sides for surface modification, as shown in Figure 15d. The layered separator shows high porosity and impressively superior electrolyte affinity, thus resulting in excellent rate capabilities, compared to the NFs/PET/NFs separator and commercial PP/PE/PP separator, as shown in Figure 15e–g.

The composite separators for LIBs are widely formed in a layered structure. Therefore, in addition to the above-mentioned separators that can be used as substrates of layered structure, other polymers have been developed, such as PI, glass fiber (GF), poly(isophthaloyl metaphenylene diamine) (PMIA), and cellulose. The PI nanofibrous membranes fabricated via electrospinning also possess a high porosity, good electrolyte wettability, and excellent flame retardancy. Nevertheless, they have poor mechanical properties due to the loose and random overlapping structure of the nanofibers without strong interactions. Fabricating the composite separators based on PI is required
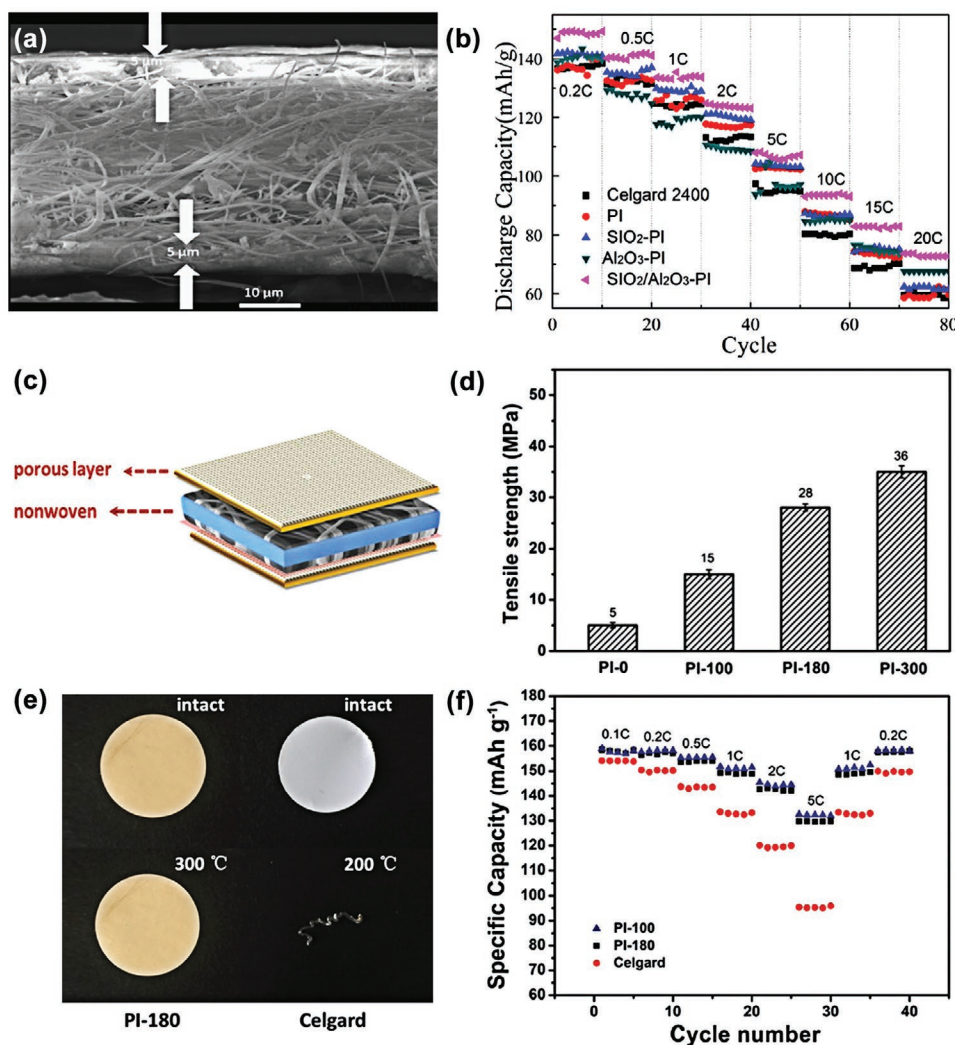
Figure 15. a) Typical SEM images of PSA/PET/PSA separator (surface) and PSA/PET/PSA separator (cross-section). b) Thermal shrinkages of separators under heat treatment, wherein the inset is photographs of the separators after exposure to 150 °C for 0.5 h. c) Immersion-height evolution of liquid electrolyte for PP and PSA/PET/PSA separator wherein the inset is showing electrolyte wetting behavior of separators. f) Discharge C-rate capability of cells using the PSA/PET/PSA separator and the PP separator. Reproduced with permission.[177] Copyright 2017, Wiley Periodicals, Inc. d) Cross-sectional SEM morphologies of Al_2O_3@NFs/PET/NFs separator with inset image of PET nonwoven. e) Electrolyte contact angle of PP/PE/PP separator and Al_2O_3@NFs/PET/NFs separator. g) C-rate capability of cells with PP/PE/PP, NFs/PET/NFs, Al_2O_3@NFs/PET/NFs separator. Reproduced with permission.[178] Copyright 2015, Elsevier Ltd.

to meet the needs of industrial LIBs. Liang et al.[179] prepared a SiO_2/Al_2O_3-coated electrospun PI membrane (**Figure 16**a). The SiO_2/Al_2O_3-coated PI membrane exhibits the best rate capability (especially at 15C and 20C respectively) as shown in Figure 16b. Sun et al.[180] also prepare the PI based layered composite separators, by spraying on both sides of a poly(amic acid) (PAmA) nonwoven membrane to form a novel nanofibrous membrane with porous layer coated morphology (see Figure 16c). The layered PI/PAA/PI separators improve the tensile strength (28 MPa) by forming a crosslinked network structure, and enhance the wettability toward the electrolyte, and outstanding thermal stability (5% weight loss at 528 °C), as shown in Figure 16d,e. Notably, LIBs using porous-layer-coated polyimide separators exhibits a much higher discharge rate capabilities (129.9 mAh g^{-1} at 5C) than that using a Celgard 2400 separators (95.2 mAh g^{-1} at 5C) (shown in Figure 16f).

Glass fiber and cellulose could also be used to fabricate the composite separators for LIBs as the substrate in a layered structure, due to their intrinsic mechanical strength and relatively high wettability. Xiao et al.[181] prepared a composite polymer membrane by coating PVDF on the surface of methyl

cellulose (MC) membrane, as shown in **Figure 17**a. The porous outer PVDF layers make PVDF/MC/PVDF separators exhibit higher mechanical strength, enhanced ion conduction. The lithium ion transference number is much larger than that of the pure MC (see Figure 17b–d). In addition, some composite separators in layered structure could efficiently suppress the growth of lithium dendrites and greatly improve the safety of LIBs. Pan et al.[182] prepared sandwich-structured separators composed of two 2.5 μm thick CNF surface layers and an intermediate 15 μm thick glass microfiber (GMF). The CNF/GMF/CNF separators exhibit a much better electrolyte wettability and thermal stability compared to Celgard separator due to the use of the hydrophilic and thermally stable CNFs and GMFs. Moreover, the separators with pore structure and tensile strength endow LIBs with high safety and enhanced electrochemical performances. Recently, Pan et al.[183] also designed a novel double-sided conductive (DSC) separator consisting of two 5 μm thick carbon nanotube (CNT)/CNF composite layers coated on each side of a 20 μm thick GF/CNF composite membrane, as shown in Figure 17e,f. More stable Li anodes can be realized by depositing Li within the porous
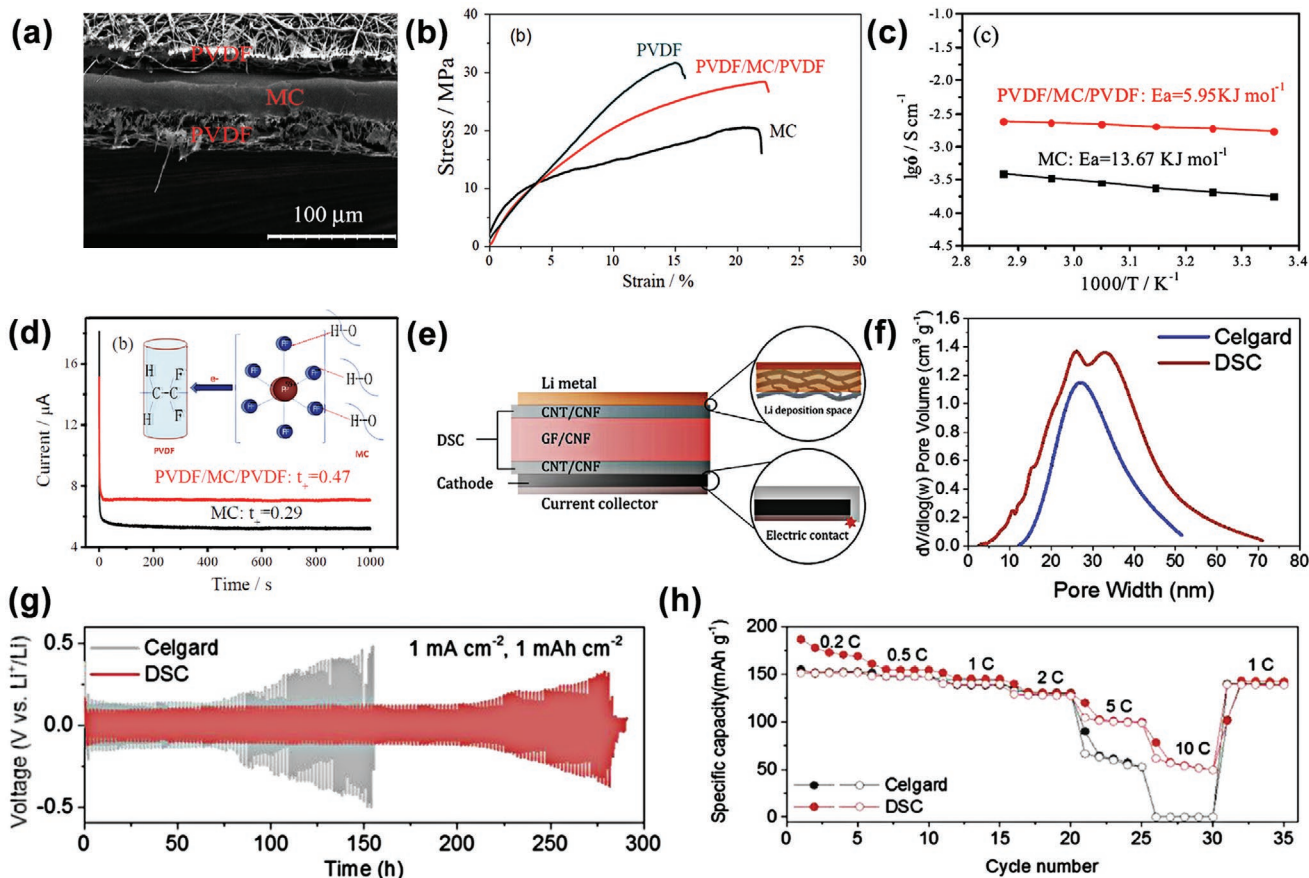
**ADVANCED
SCIENCE NEWS**

www.advancedsciencenews.com

**ADVANCED
FUNCTIONAL
MATERIALS**

www.afm-journal.de

Figure 16. a) Cross-sectional SEM images of SiO_2/Al_2O_3 (1:1)-coated PI membrane. b) The high rate capabilities of Li/separator/LiFePO$_4$ cells with separators based on the PI composite membrane that the quality of SiO_2 and Al_2O_3 ratio were 2:1, 1:1, and 1:2, respectively. Reproduced with permission.[179] Copyright 2015, Elsevier B.V. c) Model diagram of the porous layer coated PI nanofiber membrane. d) Tensile strength of the PI-x serial membranes. e) Thermal dimensional stability of the Celgard-2400 membrane and the composite separator. f) Rate capability of the composite separators and Celgard-2400 membranes (0.1C–5C). Reproduced with permission.[180] Copyright 2018, The Royal Society of Chemistry.

electronically conducting CNT/CNF matrix at the DSC separator anode side due to the decreased current density. The CNT/CNF layer of the DSC separator facing the cathode, which is in direct electric contact with the current collector, decreases the over-potential for the cathode. Improving its capacity and rate performance significantly. The LMBs containing LFP cathode and DSC separators show significantly improved rate capability about 110 mAh g^{-1} at 5C and 80 mAh g^{-1} at 10C (see Figure 17g,h). **Table 2** shows the important characteristics of recently developed composite separators with the layered structure for LIBs.

3.3.4. Section Summary

In this section, recent development in the composite separators with layered structure has been demonstrated. Coating the ceramic layer or polymer chain layer on the commercial polyolefin separator is a common approach to improve the thermal stability. Furthermore, a substantial number of polymers could be used as the substrate layer because of their intrinsic excellent properties, such as PVDF-HFP, PI, and PET. Based on the support provided by the substrate layer, the properties of the additive layers can be greatly highlighted in the layered composite membrane. The reason for coating the additive layers on the substrate polymer layer is mostly to improve the thermal stability, mechanical strength, wettability, and pore distribution, further increasing the safety, Li$^+$ ion conductivity, and rate capacity for LIBs. In addition, conductive layers or other special materials layers as the additive layers could be laminated on the substrate to retard and even suppress the growth of lithium dendrites, further enhancing the safety for long-term charge and discharge cycles or at extremely high current density. However, it is

ADVANCED
SCIENCE NEWS
www.advancedsciencenews.com

ADVANCED
FUNCTIONAL
MATERIALS
www.afm-journal.de

Figure 17. a) Cross-sectional SEM image of the sandwiched PVDF/MC/PVDF separator. b) Stress–strain curves of the PVDF, PVDF/MC/PVDF and MC separators. c) Ion conductivities of MC and PVDF/MC/PVDF separators. d) Ion transference numbers of MC and PVDF/MC/PVDF separators. Reproduced with permission.[181] Copyright 2014, Elsevier B.V. e) Schematic illustration of the DSC separator with respect to the two electrodes. f) Pore size distribution curves of the DSC separator. g) The cell voltage as a function of time equipped with Celgard and DSC separator cycled at a current density of 1 mA cm^{-2} with Li deposition and stripping. h) Capacity at the indicated cycling rates. Reproduced with permission.[183] Copyright 2019, Elsevier B.V.

inevitable for composite separators with the layered structure that the thickness of separators increases as laminated by the additive layers. Besides, the connection between layers has to be affected during the battery operation. Therefore, solving the thickness and layers connection issues are crucial to achieve high-performance composite separators for LIBs.

3.4. Core–Shell Structure Type

The composite separators constituted in the blending form between polymers and additives could significantly improve the physical properties of the commercial separators or single-component separators. However, it is difficult to achieve the uniform pore sizes and pore distribution. In addition, composite separators with layer structure usually show their multifunctional performances due to different characters revealed by substrate layer and additive layers. The structure between layers requires strong chemical bonding or physical adsorption, which is extremely easy to desorb or produce side reactions during long-term cycling or high-current charge and discharge. Recently, a core–shell structure has

been utilized to form the composite separators. Since the different characteristics of the core and the shell material could be exhibited easily and the connection between the core and the shell is relatively tight. The LIBs with composite separators with the core–shell structure would have a high safety and electrochemical performance.

3.4.1. Models and Simulations of Core–Shell Composite Separators

To obtain the thermally stable and significant improvements of electrochemical performances, molecular dynamic simulations for the composite separators with core–shell structures were designed to predict and prove the reasons for the performance improvements of LIBs. Yang et al.[214] analyzed the heat transfer and measured the thermal conductivity of each component including Al_2O_3/PVDF-HFP core–shell separator inside LIBs. Joule heat and entropy change in electrochemical processes are evaluated through both in-plane and cross-plane directions, represented by thermal conductivities of $k_\parallel$ and $k_\perp$, respectively. The $k_\perp$ was measured by differential steady

Table 2. The important characteristics of recently developed composite separators with the layered structure for LIBs.

| Substrate materials	Additives	Layered structure	Fabrication method	Separator thickness [µm]	Thermal shrinkage [%]	Tensile strength [MPa]	Liquid electrolyte types	Electrolyte uptake [%]	Ionic conductivity [mS cm⁻¹] at RT	Cathode/anode	Rate performance	Refs.
PE	PVDF	PVDF/PE/PVDF	Electrospinning	20	0% at 200 °C for 1 h	11.2	$LiPF_6$-EC/EMC/DMC	380	2.5	$LiFePO_4$/Li	134.8 mAh g⁻¹ (81.7%) at 10C	[75]
PE	PAA/ZrO_2	PAA/ZrO_2-PE	Self-assembly	14	–	–	$LiPF_6$-EC/EMC-DMC	325	0.51	$LiCoO_2$/Li	(33.3%) at 6C	[173]
PE	ZrO_2	ZrO_2/PE	Dip-coating	20	9.4% at 140 °C for 1 h	–	$LiPF_6$-EC/DEC/DMC	312.9	1.61	$LiFePO_4$/Li	100 mAh g⁻¹ (60.8%) at 5C	[184]
PP	Al_2O_3	Al_2O_3/PP	Atomic layer deposition	25	0% at 160 °C for 0.5 h	–	$LiPF_6$-PC	–	–	$LiFePO_4$/$LiTiO_2$	(56.7%) at 10C	[170]
PE	BN/PVDF-HFP	PE-BN/PVDF-HFP	Wet chemistry	40	6.6% at 140 °C for 1 h	22.01	$LiPF_6$-EC/EMC/DMC/DEC	348	4.4	$LiFePO_4$/Li	108 mAh g⁻¹ (70%) at 4C	[104]
PP	Al_2O_3/SiO_2	Al_2O_3/SiO_2-PP	Dip-coating	22	30% at 170 °C for 1 h	109.3	$LiPF_6$-EC/DMC	120	0.78	$LiCoO_2$/Li	100 mAh g⁻¹ (72.5%) at 2C	[185]
PE	Imidazole-SiO_2	Imidazole-SiO_2/PE	Dip-coating	29	0% at 150 °C for 0.5 h	–	$LiPF_6$-EC/DEC	220	1.03	$LiNi_{0.5}Co_{0.2}Mn_{0.3}O_2$/Li	92 mAh g⁻¹ (52.6%) at 5C	[186]
PE	PDA/POSS	PDA/POSS-PE	Dip-coating	–	0% at 150 °C for 0.5 h	–	$LiPF_6$-EC/DMC/EMC	301	0.45	$LiCoO_2$/Li	50 mAh g⁻¹ (32.9%) at 5C	[66]
PE	$Al(OH)_3$/PVDF-HFP	$Al(OH)_3$/PVDF-HFP-PE	Dip-coating	32	6.6% at 140 °C for 0.5 h	–	$LiPF_6$-EC/EMC	127	1.001	$LiCoO_2$/Li	66 mAh g⁻¹ (48.5%) at 10C	[187]
PP	PVDF	PVDF/PP/PVDF	Dip-coating	180	0% at 170 °C for 0.5 h	25	$LiPF_6$-EC/DMC/EMC	83.2	0.3	$LiFePO_4$/Li	120 mAh g⁻¹ at 0.2C	[67]
PE	SiO_2/PDA	SiO_2/PDA-PE-SiO_2/PDA	Dip-coating	26	0% at 220 °C for 0.5 h	–	$LiPF_6$-EC/DEC/DMC	80	0.98	$LiCoO_2$/Li	(68.7%) at 10C	[188]
PP	PPTA	PPTA/PP	Phase inversion	40	0% at 200 °C for 0.5 h	35	$LiPF_6$-EC/EMC/DMC	–	1.00	$LiCoO_2$/Li	45 mAh g⁻¹ (32.8%) at 10C	[172]
PE	Dickite	Dickite/PE	Dip-coating	297	0% at 160 °C for 0.5 h	8.9	$LiPF_6$-EC/DEC	861	3.157	$LiFePO_4$/Li	120 mAh g⁻¹ (77.9%) at 4C	[189]
PE	Al_2O_3/PVDF	Al_2O_3/PVDF/PE	Electrospinning	32	7.8% at 180 °C for 0.5 h	77	$LiPF_6$-EC/DEC	314	1.23	$LiCoO_2$/Li	42 mAh g⁻¹ (30.4%) at 3C	[190]
PE	Al_2O_3/emulsion paraffin wax	Al_2O_3/PE	Dip-coating	16	0% at 130 °C for 0.5 h	–	$LiPF_6$-EC/DEC	–	0.8	$LiCoO_2$/Li	70 mAh g⁻¹ (50.7%) at 4C	[191]
PE	PVDF/HEC	PVDF/HEC/PE	Dip-coating	16	0% at 150 °C for 0.5 h	90	$LiPF_6$-EC/DEC	–	0.78	$LiNi_{0.5}Mn_{1.5}O_4$/Li	123 mAh g⁻¹ (91.1%) at 5C	[192]
PE	Al_2O_3/PI	Al_2O_3/PI/PE	Dip-coating	10	0% at 160 °C for 0.5 h	0.5	$LiPF_6$-EC/DEC	85	0.89	$LiMn_2O_4$/Li	92.5 mAh g⁻¹ (86%) at 4C	[193]
PE	PBI	PBI/PE/PBI	Dip-coating	28	0% at 200 °C for 1 h	–	$LiPF_6$-EC/DMC/EMC	225	0.6	$LiFePO_4$/Li	122.6 mAh g⁻¹ (80%) at 5C	[171]

Table 2. Continued.

Substrate materials	Additives	Layered structure	Fabrication method	Separator thickness [μm]	Thermal shrinkage [%]	Tensile strength [MPa]	Liquid electrolyte types	Electrolyte uptake [%]	Ionic conductivity [mS cm⁻¹] at RT	Cathode/anode	Rate performance	Refs.
PP	Al_2O_3/PI	Al_2O_3/PI/PP	Dip-coating	25	10% at 150 °C for 0.5 h	–	$LiPF_6$-EC/DEC	–	0.95	$LiMn_2O_4$/Li	(66%) at 20C	[194]
PP	$Li_{1.5}Al_{0.5}Ge_{1.5}(PO_4)_3$	LAGP/PP	Dip-coating	25	0% at 160 °C for 1 h		$LiPF_6$-EC/DMC	132	2.67	$LiNi_{0.5}Mn_{1.5}O_4$/Li	103.5 mAh g⁻¹ (84.5%) at 5C	[195]
PE	SiO_2@PI	SiO_2@PI/m-PE/SiO_2@PI	Electrospinning	32	0% at 400 °C for 1 h	180	$LiPF_6$-EC/DEC	575	0.941	$LiCoO_2$/Li	135.6 mAh g⁻¹ at 0.2C	[196]
PE	Silica tubes	Silica tubes/PE	Dip-coating	30	18.95% at 150 °C for 0.5 h	1.13	$LiPF_6$-EC/DEC/DMC	112.5	0.82	$LiMn_2O_4$/Li	102.5 mAh g⁻¹ (95.3%) at 2C	[197]
PE	ZSM-5/PVDF	ZSM-5/PVDF/PE	Dip-coating	3	0% at 130 °C for 0.5 h	–	$LiPF_6$-EC/DMC/EMC	430.9	0.54	$LiCoO_2$/Li	95 mAh g⁻¹ (67.9%) at 3C	[198]
PP	Silica-aerogel	Silica-aerogel/PP	Solution casting	25	0% at 160 °C for 0.5 h	–	$LiPF_6$-EC/DMC	346	0.63	$LiFePO_4$/Li	100 mAh g⁻¹ (62.5%) at 8C	[169]
PE	ZrO_2/POSS	ZrO_2/POSS/PE	Phase inversion	14	0% at 150 °C for 0.5 h	–	$LiPF_6$-EC/DEC/EMC	340	0.46	$LiCoO_2$/Li	89 mAh g⁻¹ (59.3%) at 7C	[199]
PP	SiO_2/PVA	SiO_2/PVA/PP	Dip-coating	25	8.3% at 170 °C for 0.5 h	–	$LiPF_6$-EC/DMC/DEC	201.2	1.26	$LiCoO_2$/Li	121 mAh g⁻¹ (91.7%) at 2C	[200]
PVDF-HFP	MoO_3 and LLZTO	MoO_3/PVDF-HFP/LLZTO/PVDF-HFP	Dip-coating	30	5% at 160 °C for 4 h	22.3	$LiPF_6$-EC/DMC	372.6	0.633	$LiFePO_4$/Li	71 mAh g⁻¹ (44.7%) at 10C	[174]
PVDF	LiPVAOB	PVDF/LiPVAOB/PVDF	Dip-coating	40	0% at 100 °C for 0.5 h	32.4	$LiPF_6$-EC/DMC/EMC	88.5	0.26	$LiFePO_4$/Li	86.7 mAh g⁻¹ (66.7%) at 1C	[201]
PVDF-HFP	Electronically conductive layer	PEC/PVDF-HFP	Dip-coating	35	0% at 280 °C for 0.5 h	4.2	$LiPF_6$-EC/DMC	–	1	$LiNi_{0.5}Co_{0.2}Mn_{0.3}O_2$/Li	138 mAh g⁻¹ at 1C	[175]
PVDF-HFP	La_2O_3 and BN	PVDF-HFP-La_2O_3/PVDF-HFP-BN	Dip-coating	25	6.2% at 150 °C for 1 h	28	$LiPF_6$-DEC/EMC/DMC/EC/VC	214.6	0.75	$LiFePO_4$/Li	81 mAh g⁻¹ (51.3%) at 10C	[55]
PVDF	SiO_2	SiO_2/PVDF	Electrospinning	45	0% at 200 °C for 0.33 h	5	$LiPF_6$-DMC/EC/DEC	483	–	$LiMn_2O_4$/Li	55 mAh g⁻¹ (50%) at 10C	[72]
PVDF-HFP	PMMA	PMMA/PVDF-HFP	Dip-coating	10	0% at 150 °C for 0.5 h	–	$LiPF_6$-EC/DMC	342	1.31	$LiFePO_4$/Li	130 mAh g⁻¹ (86.7%) at 2C	[202]
PVDF-HFP	PVDF-PTFE	PVDF-PTFE/PVDF-HFP	Solution casting	62	4.7% at 160 °C for 0.5 h	6.9	$LiPF_6$-EC/DEC/DMC	151	1.29	$LiFePO_4$/Li	106 mAh g⁻¹ (66%) at 2C	[203]
PET	PVDF-HFP	PVDF-HFP/PET	Solution casting	35	–	–	$LiPF_6$-EC/DEC	185	0.81	$LiCoO_2$/Li	68 mAh g⁻¹ (51.5%) at 2C	[204]
PET	SiO_2/PVDF-HFP	SiO_2/PVDF-HFP/PET	Dip-coating	30	0% at 150 °C for 0.5 h	–	$LiPF_6$-EC/DEC	–	0.91	$LiCoO_2$/Li	67 mAh g⁻¹ (48.5%) at 2C	[83]
PET	PSA	PSA/PET/PSA	Electrospinning	50	0% at 150 °C for 0.5 h	17.7	$LiPF_6$-EC/DEC	423	1.06	$LiCoO_2$/Li	86.7 mAh g⁻¹ (57.8%) at 4C	[177]

Table 2. Continued.

Substrate materials	Additives	Layered structure	Fabrication method	Separator thickness [μm]	Thermal shrinkage [%]	Tensile strength [MPa]	Liquid electrolyte types	Electrolyte uptake [%]	Ionic conductivity [mS cm^{-1}] at RT	Cathode/ anode	Rate performance	Refs.
PET	SiO$_2$/PVDF-HFP	SiO$_2$/PVDF-HFP/PET	Solution casting	22	0% at 150 °C for 1 h	–	LiPF$_6$-EC/DEC	285	2.57	LiFePO$_4$/Li	87.5 mAh g^{-1} (62.5%) at 8C	[205]
PET	PMMA	PMMA/PET	Solution casting	21	0% at 150 °C for 1 h	–	LiPF$_6$-EC/DEC	160	0.96	LiCoO$_2$/Li	90 mAh g^{-1} (66.7%) at 2C	[206]
PET	PVA-PE	PVA-PE/PET/PVA-PE	Solution casting	44	0% at 150 °C for 0.5 h	35	LiPF$_6$-EC/DMC	159.7	0.55	LiFePO$_4$/Li	125 mAh g^{-1} (81.7%) at 2C	[207]
PET	PE	PE/PET	Dip-coating	22	0% at 200 °C for 1 h	111.8	LiPF$_6$-EC/EMC	105	0.58	LiCoO$_2$/Li	68 mAh g^{-1} (67.9%) at 5C	[65]
PET	Alumin-silicates zeolite/PVDF-HFP	Alumin-silicates zeolite/PVDF-HFP/PET	Solution casting	32	2% at 170 °C for 1 h	–	LiPF$_6$-EC/DEC	194	2.1	LiFePO$_4$/Li	(69%) at 6C	[208]
PI	SiO$_2$/Al$_2$O$_3$	SiO$_2$/Al$_2$O$_3$/PI	Electrospinning	40	–	–	LiPF$_6$-EC/DMC/EMC	519	2.92	LiFePO$_4$/Li	75 mAh g^{-1} (53.2%) at 20C	[179]
PI	Al$_2$O$_3$	Al$_2$O$_3$/PI/Al$_2$O$_3$	Electrospinning	27	0% at 200 °C for 0.5 h	–	LiPF$_6$-EC/DEC	440.21	0.364	LiNi$_{0.5}$Co$_{0.2}$Mn$_{0.3}$O$_2$/graphite	102 mAh g^{-1} (73.91%) at 10C	[209]
PI	PE	PE/PI	Electrospinning	26	0% at 200 °C for 0.5 h	–	LiPF$_6$-EC/DMC	400	1.34	LiMn$_2$O$_4$/Li	107 mAh g^{-1} (96.8%) at 2C	[210]
PI	Glass fiber	Glass fiber/PI	Dip-coating	46	0% at 200 °C for 0.5 h	10.4	LiPF$_6$-EC/DEC	210	0.38	LiFePO$_4$/Li	68.6 mAh g^{-1} (48%) at 8C	[118]
PI	PAA	PAA/PI/PAA	Electrospinning	–	5% at 528 °C for 0.5 h	28	LiPF$_6$-EC/DMC/DEC	341.51	1.84	LiFePO$_4$/Li	144.7 mAh g^{-1} (91.5%) at 5C	[180]
HEC	PVDF	PVDF/HEC/PVDF	Electrospinning	58	0% at 290 °C for 0.5 h	21.5	LiPF$_6$-EC/DMC/EMC	165.4	0.88	LiFePO$_4$/Li	140 mAh g^{-1} at 0.2C	[211]
PEI-PU	SiO$_2$	SiO$_2$/PEI-PU	Dip-coating	35	0% at 180 °C for 0.5 h	15.65	LiPF$_6$-EC/DMC/EMC	188.88	2.33	LiFePO$_4$/Li	144.5 mAh g^{-1} (87.7%) at 1C	[86]
PMIA	PVDF	PVDF/PMIA/PVDF	Electrospinning	20	0% at 180 °C for 1 h	13.96	LiPF$_6$-EC/DMC/EMC	–	0.81	LiCoO$_2$/Li	135 mAh g^{-1} (90%) at 1C	[212]
paper	Al$_2$O$_3$	Al$_2$O$_3$/paper/Al$_2$O$_3$	Wet-laid	48	0% at 130 °C for 0.5 h	5.3	LiPF$_6$-EC/DMC	–	1.64	LiCoO$_2$/graphite	95 mAh g^{-1} (62.5%) at 8C	[84]
PAN	SiO$_2$/TEGDA	SiO$_2$/TEGDA/PAN	Dip-coating	35	0% at 200 °C for 0.5 h	7.7	LiPF$_6$-EC/EMC/DEC	–	2.1	LiNi$_{0.6}$Co$_{0.6}$Mn$_{0.2}$O$_2$/Li	85 mAh g^{-1} (85%) at 5C	[213]
PMMA	Al$_2$O$_3$/PVDF	Al$_2$O$_3$/PVDF/PMMA/Al$_2$O$_3$/PVDF	Dip-coating	–	0% at 150 °C for 0.33 h	35	LiPF$_6$-EC/DEC/EMC	500	0.535	LiCoO$_2$/Li	(50%) at 3C	[89]
MC	PVDF	PVDF/MC/PVDF	Electrospinning	60	0% at 300 °C for 0.5 h	28.4	LiPF$_6$-EC/DEC/EMC	138.6	1.5	LiFePO$_4$/Li	110 mAh g^{-1} (69.6%) at 1C	[181]
glass microfiber	Cellulose nanofiber	CNF/GMF/CNF	Solution casting	20	0% at 200 °C for 0.5 h	–	LiPF$_6$-EC/DEC	–	1.14	LiFePO$_4$/Li	110 mAh g^{-1} (70%) at 5C	[182]
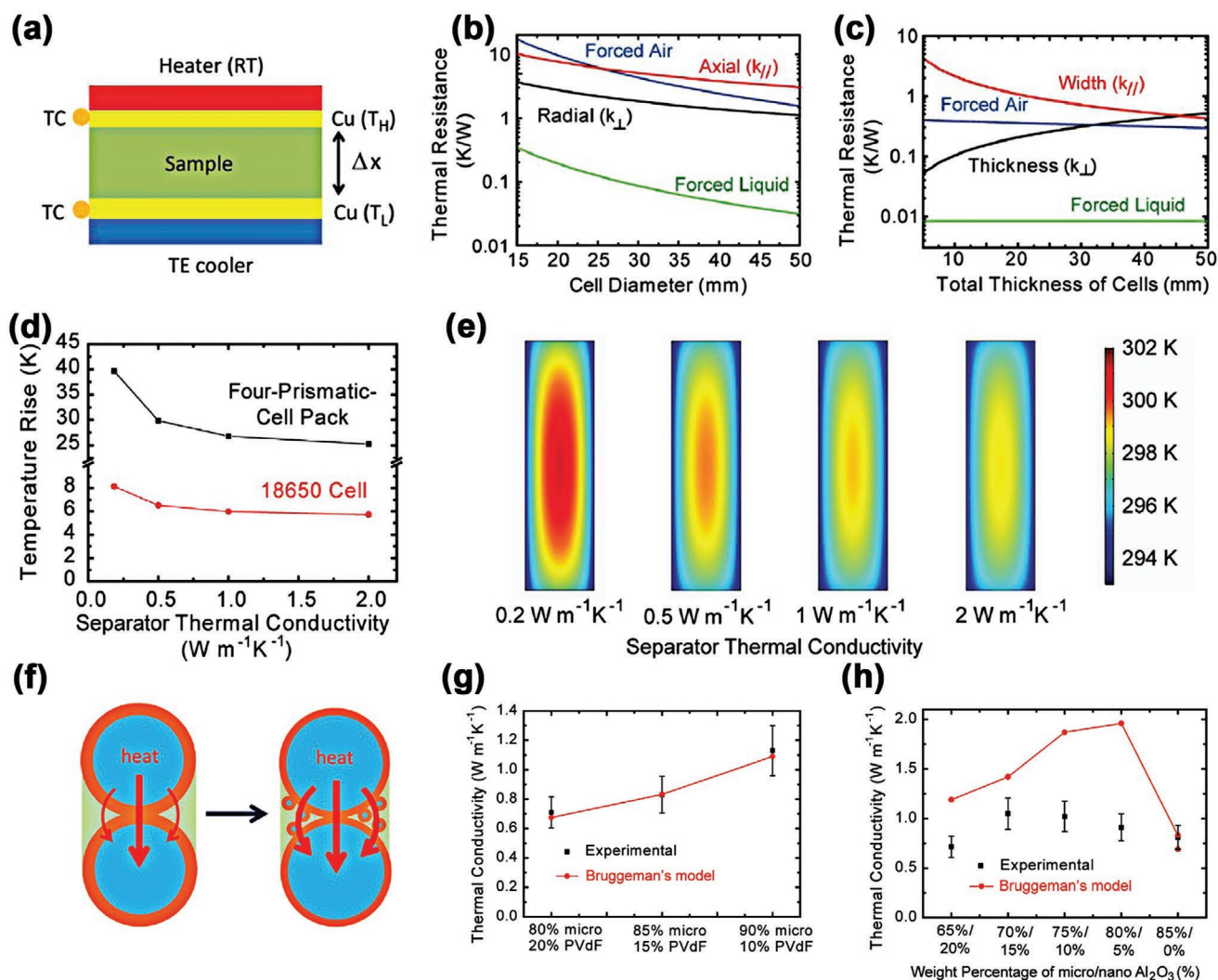
Figure 18. a) Schematic of the differential steady state method to measure thermal conductivity. b,c) Calculated thermal resistances. d) Numerical simulation by COMSOL Multiphysics on temperature rise against thermal conductivity of separator in a four-prismatic-cell pack and a 18650 cell, respectively. e) Corresponding temperature distribution in the cross-section of an 18650 cell. f) A conceptual schematic of adding Al_2O_3 nanoparticles to improve thermal conductivity. g,h) k_{eff} calculated by the Bruggeman's model of micro-Al_2O_3/PVDF-HFP composite separators and nano/micro-Al_2O_3/PVDF-HFP composite separators. Reproduced with permission.[214] Copyright 2016, Elsevier Ltd.

state method, as shown in **Figure 18**a. The heat flux was used to derive $k_\perp$ by applying to the sample and sample geometry based on the Fourier's law. Thermal resistances along different directions are estimated based on 1D heat conduction along the corresponding direction. It is defined as $\Delta T/Q$ at a steady state with uniform heat generation inside the cell, where ΔT is the temperature difference between the center and surface of the cell, and Q is the total heat transfer red at cell surface. The thermal resistance of external heat transfer is estimated as $1 = h/A$, where h is the heat transfer coefficient, and A is the surface area for external convection. Calculation results are shown as Figure 18b–d for cylindrical and prismatic cell configuration, respectively. The cross-plane direction has a larger cross-sectional area and smaller length for heat transfer, indicating that heat dissipation along the cross-plane direction is actually more efficient than in-plane. Therefore, improving $k_\perp$ of the triple layer structure in batteries can effectively enhance

total heat dissipation in batteries, especially when forced liquid cooling is used. In addition, COMSOL simulation was carried out to understand the effect of $k_\perp$ on temperature rise (*T* rise) of a battery in operation. These values correspond to reduction of 33% and 25% in *T* rise, respectively. Higher thermal conductivity of separator also leads to more uniform temperature distribution inside the cell, as shown in Figure 18e. The addition of Al_2O_3 facilitates heat transport of the PVDF-HFP separator as shown in Figure 18f. To better understand thermal transport in the composite, they use effective medium theory to model the dependence of k_{eff} on separator composition. The Bruggeman's model with spherical inclusion is used here and it is applied to micro-Al_2O_3/PVDF-HFP separator saturated with DEC first. The Bruggeman's model indicates that

$$\sum \lambda_i \frac{k_i - k_{eff}}{k_i + 2k_{eff}} = 0 \tag{14}$$

**ADVANCED
SCIENCE NEWS**
www.advancedsciencenews.com

**ADVANCED
FUNCTIONAL
MATERIALS**
www.afm-journal.de

where λ is the volume portion and subscript i means different phases in the composite. k_{eff} of the micro-Al_2O_3/PVDF-HFP composite separator predicted by the Bruggeman's model fits well with the experimental results as shown in Figure 18g,h. In addition, the higher k_{eff} predicted by the model also implies that further optimization of particle dispersion and polymer coating may boost.

3.4.2. Core–Shell Structure Based on PVDF or its Co-Polymers Shell

The commercial polyolefin-based composite separators with the core–shell structure are rarely studied. However, using PVDF and its co-polymers as the shell structure has become increasingly common due to their excellent physical properties, such as high wettability, proper pore size and pore distribution, and tight connection of the functional group with cores. The materials of core structure are usually the oxide ceramic materials. Shen et al.[215] fabricated a core–shell separator with high safety insurance through ALD of 30 nm Al_2O_3 on the PVDF-HFP

nonwoven fibers. The Al_2O_3/PVDF-HFP core–shell separators show a pretty high heat resistance up to 200 °C without any shrinkage and an excellent fire-resistant property. Besides, with higher uptake and ionic conductivity, cells with the novel separator shows better rate capacities.

He et al.[81] prepared a gel separator with core–shell structure through a single-step electrophoretic deposition on a stable surfactant-free colloid of PVDF-HFP and Al doped LLZTO, as shown in **Figure 19**a. The LLZTO/PVDF-HFP separator owns a mechanical strength of 28.6 MPa, enhanced wettability, improved thermal stability, and a room-temperature ionic conductivity of 7.13×10^{-4} S cm^{-1} (Figure 19b–e). LiFePO$_4$ LIBs with the composite separator deliver excellent discharge capacities of 167, 144, and 100 mAh g^{-1} at 0.1C, 1C, and 5C, respectively, demonstrating an outstanding rate capability as shown in Figure 19f.

Except for the ceramic materials as the core, the polymers with high thermal stability and mechanical strength could also be utilized to form core–shell structures. Flame retardant materials can effectively guarantee the safety for
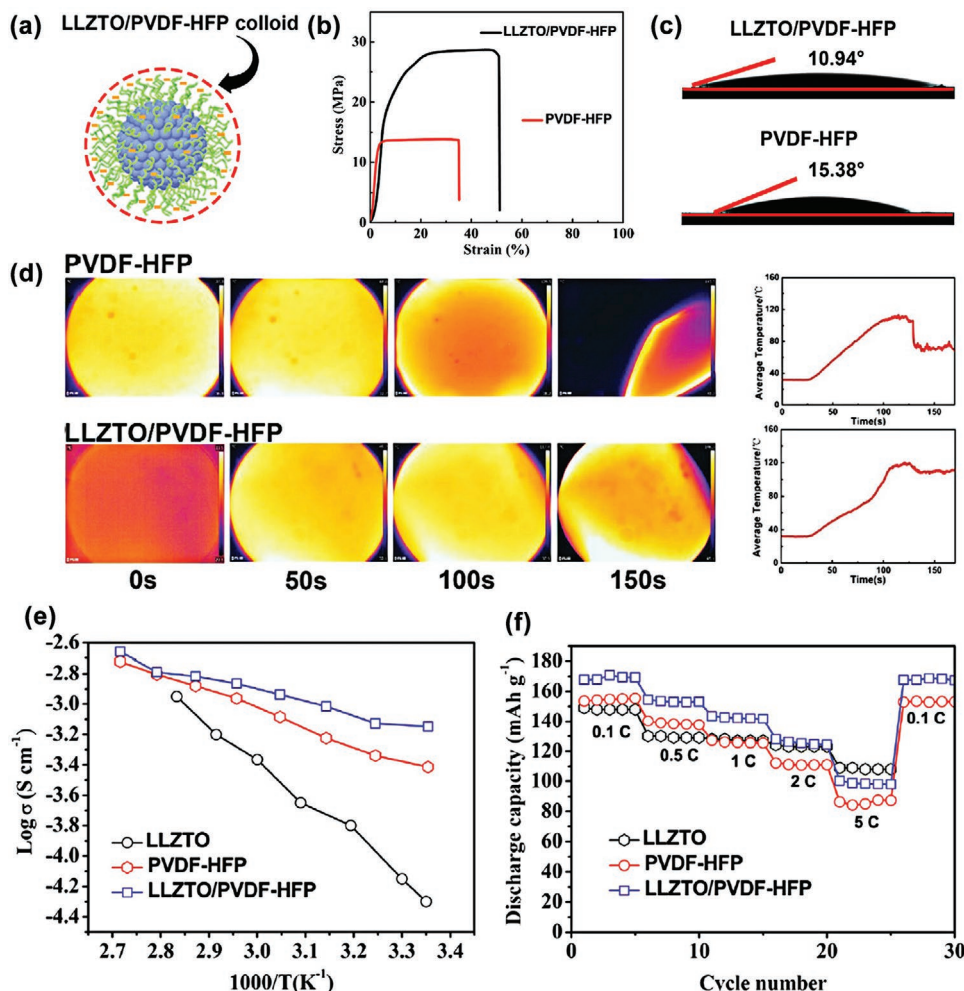
Figure 19. a) Schematic illustration of LLZTO/PVDF-HFP colloid molecule. b) Tensile tests of LLZTO/PVDF-HFP and PVDF-HFP separators. c) Contact angle tests of LLZTO/PVDF-HFP and PVDF-HFP separators. d) Infrared thermography and average temperature curves of PVDF-HFP and LLZTO/PVDF-HFP separators. e,f) Ionic conductivities and rate performances of batteries with LLZTO, PVDF-HFP and LLZTO/PVDF-HFP. Reproduced with permission.[81] Copyright 2019, Elsevier B.V.

**ADVANCED
SCIENCE NEWS**

www.advancedsciencenews.com

**ADVANCED
FUNCTIONAL
MATERIALS**

www.afm-journal.de

LIBs, such as TPP. The TPP is a popular organophosphorus-based flame retardant. Liu et al.[92] fabricated a novel core–shell microfiber separator where the TPP is the core and PVDF-HFP is the shell. The encapsulation of TPP inside the PVDF-HFP protective polymer shell (TPP@PVDF-HFP) has prevented direct exposure of the flame retardant to the electrolyte, preventing negative effects during the electrochemical reaction. Moreover, PVDF-HFP shell will melt as temperature increases and then the encapsulated TPP will be released into

the electrolyte, thus effectively suppressing the combustion. In addition, Huang et al.[216] extracted CA from waste cigarette filter to construct a cellulose-based core–shell separator, as shown in **Figure 20**a,b. The cellulose-core/PVDF-HFP-shell fibrous membrane shows a good tensile strength (34.1 MPa), excellent thermal stability (to 200 °C) and the more superior rate capabilities (from 0.2C to 5C) (see Figure 20c,d), demonstrating the cellulose/PVDF-HFP core–shell structures to be promising separators for a high-rate and more secure LIBs.
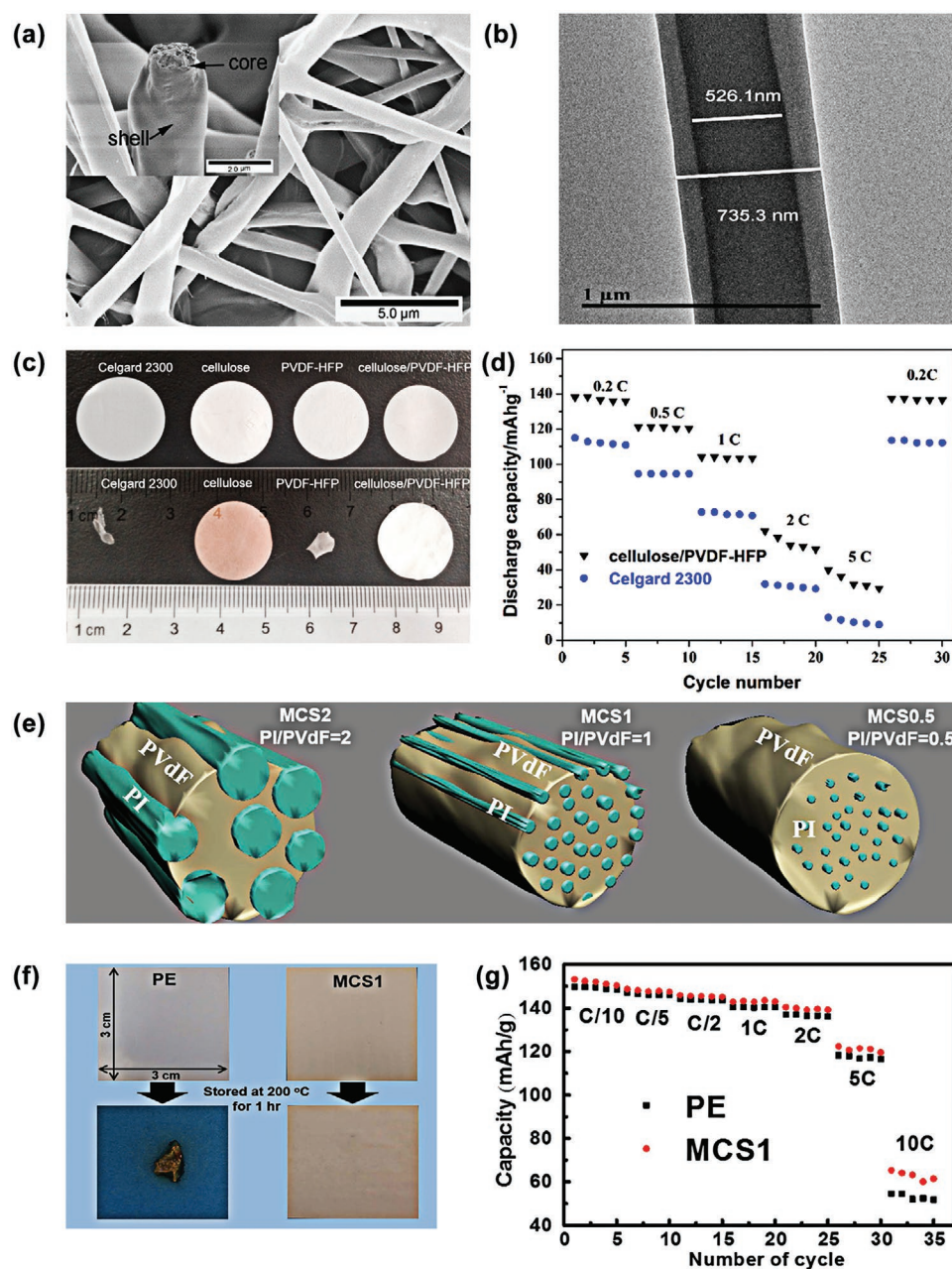
Figure 20. a,b) SEM and TEM images of coaxial CA/PVDF-HFP nanofibers with varying core/shell flow rate ratios: 2:3. c) Photographs of the separators before and after thermal treatment at 200 °C for 1 h. d) Rate performances of LiCoO$_2$ cells using Celgard 2300 and cellulose/PVDF-HFP separators. Reproduced with permission.[216] Copyright 2016, American Chemical Society. e) Schematics of the multicore–shell structure with different ratio. f) Photos of the MCS and the PE separator before and after the thermal stability. g) C-rate performance of prototype cells with the MCS composite separator. Reproduced with permission.[218] Copyright 2016, Springer Nature.

To further improve the performances of the shell structure, Huang et al.[217] also synthesized $Li_{0.33}La_{0.557}TiO_3$ (LLTO) incorporated PVDF-HFP as the shell structure, as well as cellulose as the core. The cellulose/LLTO-PVDF-HFP core–shell composite separators show a good wettability (16.5°, contact angle), high porosity (69.77%), and super electrolyte compatibility (497%, electrolyte uptake). In addition, the ionic conductivity (13.897 mS cm^{-1}) and the rate capability (155.56 mAh g^{-1}) are superior to the compared separator.

The most core–shell composite separators mentioned above are composed of single core which is encased in a single shell. In addition, a novel conception has also been considered that multiple cores are embedded in the shell structure. Park et al.[218] prepared a unique multicore–shell (MCS) structure of the electrospun composite fibers separators, which are consist of multiple PI core fibrils with high molecular orientation, and PVDF shell, as shown in Figure 20e. The multiple PI core fibrils contribute remarkable thermal stabilities to MCS separators, which show no shrinkage at 200 °C. The proper architecture and synergy effects of multiple PI nanofibrils as a thermally stable polymer in the PVDF shell are responsible for the superior thermal performance and high rate performances for LIBs, especially at the discharge rate of 5C and 10C, as given in Figure 20f,g.

3.4.3. Core–Shell Structure Based on Other Polymer Shell

Jiang et al.[219] prepared a core–shell structured nanofibrous separator, where SiO_2 nanoparticles are covalently bonded on the surface of bacteria cellulose (BC) nanofibers. Because of the unique SiO_2-coating structure and crosslinked 3D network, SiO_2/BC core–shell separators show significant advantages of good thermal stability up to 200 °C, high ionic conductivity, excellent coating strength, and improved battery charge–discharge performance. Dong et al.[90] reported the nanostructured surface configuration design in which PI nanofibers are encapsulated by TiO_2 nanolayer, which is fabricated by the in situ hydrolysis deposition process, as shown in **Figure 21**a–c. The PI-TiO_2 core–shell separator manifests enough pore size, outstanding wettability for electrolyte and superior thermal dimensional stability at 300 °C (see Figure 21d–f). Moreover, the cell installed in the TiO_2@PI separators separator displays a brilliant Li$^+$ transportation mechanism and high-rate property with as high as 82% capacity retention under 5C (135 mAh g^{-1}), which is superior to the cell using Celgard PP (60%, 90 mAh g^{-1}) as shown in Figure 21g,h. **Table 3** shows the important characteristics of recently developed composite separators with the core–shell structure for LIBs.

3.4.4. Section Summary

In this section, recent development in the composite separators with the core–shell structure has been discussed, including core–shell structure based on the PVDF and its co-polymers separators as well as based on the other polymer materials. The commercial separators have rarely been developed with the core–shell structure due to the difficulty for recasting commercial membranes to achieve the consistency and performance of the original materials. Core–shell composite separators based on PVDF and its co-polymers (long-chain macromolecular polymers) are designed and assembled in the LIBs, where PVDF and its co-polymers can be used as the shell structure to wrap nanoparticles or short-chain polymer molecules. The main role of nanoparticles or short-chain polymers is to improve the overall mechanical property, thermal stability, and even flame retardancy of the core–shell structure separators, thereby improving the safety of the battery during cycling. In addition of PVDF and its co-polymers, other polymers such as cellulose and PI have been regarded as the shell due to their intrinsic outstanding mechanical support and stability. The composite separators based on these polymers can also improve the ion conductivity and further rate capacity for LIBs after adding the additive core materials. The main feature of the core–shell structure is adjusting the physical and chemical properties of core materials and shell materials to achieve complementary advantages. In addition, the core–shell structure plays an important role in maintaining core's stability to avoid scattering or agglomeration of additives when lithium ions pass through the separators. Apparently, nanostructures are generally required to fabricate the core–shell structures so that nano-scale particles and polymer molecular chains need to be precisely regulated and prepared during the process. In short, the composite membrane prepared in this type of core–shell structure can greatly improve the structural stability, thermal stability, and ion conductivity, especially the stability working under high current in LIBs, thereby increasing the rate performance.

3.5. Grafting Structure Type

The structures of composite separators mentioned above enable to remedy and solve the defects of the commercial separators for LIBs by improving their thermal stability and intrinsically hydrophobic property. The composite separators with the blending form, layered structure and core–shell structure have been designed and reported above, generally exploring the polymers added with ceramic particles, polymer fibers or some novel materials, which could show exceptional wettability, excellent thermal stability and thereby exhibit excellent performances for LIBs. However, the surface modification required for fabricating those structures could increase the thickness and blocks the porous structure, leading to a decrease in energy and power density of the battery. Moreover, the heterogeneous distribution of additives and poor binding power of polymer binder would result in the detachment of particles from the separators. Therefore, in addition to three structures mentioned above, the composite separators with a graft form have also been developed because additives or some functional groups are grafted on the membrane surface without sacrificing the porous structure and increasing the thickness.

3.5.1. Models and Simulations of Grafting Composite Separators

The molecular dynamic simulations were designed to predict and prove that the excellent wettability and uptake capability
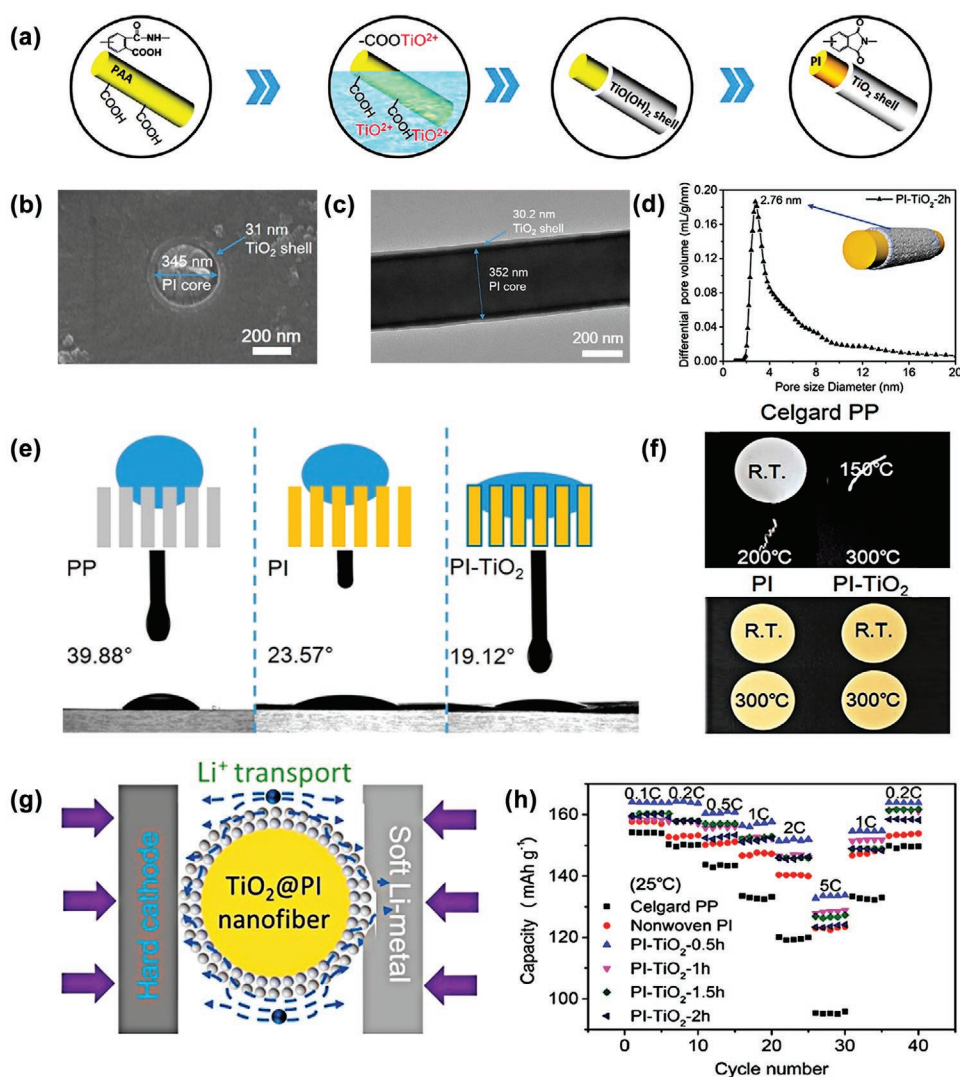
Figure 21. a) Diagram of the preparation for TiO_2-nanolayer-encapsulated PI nanofibers by in situ hydrolysis deposition process. b,c) SEM and TEM pictures of the TiO_2 encapsulated PI nanofibrous membranes. d) Pore size distribution of the TiO_2@PI separator. e) Electrolyte contact angles of Celgard PP, PI nonwoven, and TiO_2@PI separators. f) Thermal dimensional stability of Celgard PP, PI nonwoven, and TiO_2@PI core–shell separators at different temperatures. g) Li^+ transport mechanisms in the LIBs with TiO_2@PI separators. h) High-rates capability of the half-cells installed in Celgard PP, PI nonwoven, and TiO_2@PI separators. Reproduced with permission.[90] Copyright 2019, American Chemical Society.

of grafting composite separators result in high Li^+ ion transference numbers and ionic conductivity. The functional sites of grafting groups on the surface of polymers could promote the motion of Li^+ ions along and across the surface, further improving ionic conductivity of LIBs.

Zhang et al.[225] grafted the cyanoethyl groups onto the surface of chitin nanofibers through a facile Michael addition reaction, as shown in **Figure 22**a. The successful grafting of $-OCH_2CH_2CN$ groups onto chitin nanofibers was confirmed through the solid state ^{13}C NMR spectra, which shows three new peaks referred to new carbon atoms (i, ii, and iii) in $-OCH_2CH_2CN$ groups appeared as shown in Figure 22b. Li^+ ion transference numbers and ionic conductivity of the composite separators were highly promoted by the increase of nitrogen content in separators, which can be attributed to the differentiated interactions between ions and cyano groups, as shown in Figure 22c,d. To

further understand the influence of interactions on the Li^+ ion transport in cyanoethyl-chitin nanofiber (CCN) separators, they implemented the DFT calculations in Gaussian 09 to interpret the interactions between functional cyanoethyl groups and the liquid electrolyte as shown in Figure 22e. The basic repeat unit of α-chitin, that is, two N-acetylglucosamine molecules (NAG) connected with opposite conformations, was used to represent the long chain of chitin. The binding energies for Li^+ (EC) and PF_6^- with unmodified NAG are calculated as -1.54 and -0.98 eV, respectively. Li^+ with a positive charge is stabilized by the electronegative oxygen atoms in OH, CH_2OH, and carbonyl groups, while PF_6^- interacts with the OH, CH_2OH, and NH groups via hydrogen bonding. After the modification of α-chitin with acrylonitrile, both hydrogen atoms in OH or CH_2OH in the NAG unit can be substituted by cyanoethyl, leading to two different structures, namely NAG-CN1 and NAG-CN2. We find that

Table 3. The important characteristics of recently developed composite separators with the core–shell structure for LIBs.

Shell materials	Core materials	Fabrication method	Separator thickness [μm]	Thermal shrinkage [%]	Tensile Strength (MPa)	Liquid electrolyte types	Electrolyte uptake [%]	Ionic conductivity [mS cm^{-1}] at RT	Cathode/ anode	Rate performance	Refs.
PI	TiO_2	Electrospinning	17	0% at 300 °C for 1 h	27.6	LiPF$_6$-EC/ DEC/DMC	460	1.54	LiFePO$_4$/Li	135 mAh g^{-1} (82%) at 5C	[90]
PVDF-HFP	Cellulose acetate (CA)	Electrospinning	–	0% at 200 °C for 1 h	34.1	LiPF$_6$-EC/ DMC/EMC	355	6.16	LiCoO$_2$/Li	32.9 mAh g^{-1} (23.8%) at 5C	[216]
PVDF-HFP	Li$_{6.75}$La$_3$ Zr$_{1.75}$Ta$_{0.25}$O$_{12}$ (LLZTO).	Electrophoretic deposition	25	0% at 160 °C for 2 h	28.6	LiPF$_6$-EC/ DMC	150.53	0.713	LiFePO$_4$/Li	100 mAh g^{-1} (59.9%) at 5C	[81]
PVDF	PI	Electrospinning	20	0% at 200 °C for 1 h	–	LiPF$_6$-EC/PC/ DEC/VC	427	1.3	LiCoO$_2$/Li	123 mAh g^{-1} (80.4%) at 5C	[218]
Al$_2$O$_3$	PVDF-HFP	Atomic layer deposition	–	0% at 200 °C for 1 h	–	LiPF$_6$-EC/ DMC	–	1.24	LiMn$_2$O$_4$/Li	86 mAh g^{-1} (86.3%) at 5C	[215]
PVDF	PMIA	Electrospinning	45	0% at 260 °C for 1 h	18.9	LiPF$_6$-EC/ DEC/EMC	753	1.7	LiCoO$_2$/Li	125.6 mAh g^{-1} (80.6%) at 2C	[73]
PVDF-HFP	PSA	Electrospinning	40	0% at 200 °C for 0.5 h	24	LiPF$_6$-EC/ DMC	350	1.97	LiCoO$_2$/Li	103 mAh g^{-1} (73.6%) at 4C	[220]
PBS	PLA	Electrospinning	20	0% at 170 °C for 0.25 h	–	LiPF$_6$-EC/ DEC/EMC	969	1.65	LiFePO$_4$/Li	82 mAh g^{-1} (68.3%) at 10C	[91]
PDA	PVDF-HFP	Electrospinning	40	<15% at 200 °C for 0.5 h	11.2	LiPF$_6$-EC/ DEC/DMC	254	1.4	LiMn$_2$O$_4$/Li	95 mAh g^{-1} (86.9%) at 5C	[221]
PMMA	SiO_2	Solution casting	25	12.9% at 120 °C for 0.5 h	–	LiPF$_6$-EC/ DEC/DMC	89.5	1.08	LiMn$_2$O$_4$/Li	101 mAh g^{-1} (93.5%) at 5C	[222]
PZS	SiO_2	Solution casting	21	–	–	LiPF$_6$-EC/ DEC/DMC	155.2	1.04	LiCoO$_2$/Li	105 mAh g^{-1} (74.7%) at 8C	[223]
TiO$_2$	PI	In situ complexation hydrolysis	27	0% at 300 °C for 1 h	20.2	LiPF$_6$-EC/ DEC	455	1.47	LiFePO$_4$/Li	132.8 mAh g^{-1} (81%) at 10C	[224]
PVDF-HFP	Li$_{0.33}$La$_{0.557}$ TiO$_3$ (LLTO)	Electrospinning	37	1% at 300 °C for 1 h	–	LiPF$_6$-EC/ DMC/EMC	497	13.897	LiFePO$_4$/Li	37 mAh g^{-1} (23.8%) at 5C	[217]

NAG-CN1 is less stable than NAG-CN2 with a higher energy by 0.28 eV, but both derivatives show a decrease of binding abilities with both ions. Because of the lower electronegativity of CN than O, the interaction between Li$^+$ (EC) and NAG-CN1 or NAG-CN2 is significantly weakened, resulting in a significant decrease of binding energy by 0.3 eV. On the other hand, the binding energy of PF$_6^-$ only reduces by 0.12 eV because one hydrogen bond is missing. These results suggest that the cyanoethyl group modification has a relatively larger impact on weakening the binding of Li$^+$ (EC) than that of PF$_6^-$ with chitin, making the migration of Li$^+$ (EC) relatively easier.

3.5.2. Grafting Type Based on Commercial Separators

Fabricating the composite separators based on commercial polyolefin membranes with the graft surface modification could not only efficiently improve the physical properties, also guarantee the original porous structure.

Jiang et al.[226] simply grafted the vinylsilane coupling reagent on the surface of the PE separator by electron beam irradiation method and subsequent hydrolysis reaction into the Al^{3+} solution to obtain an ultrathin Al$_2$O$_3$ grafted PE micro frame-

work, as shown in **Figure 23**a. The Al$_2$O$_3$ ceramic-grafted separator (CGS) shows almost no shrinkage at 150 °C, decreasing the contact angle of the conventional electrolyte (from 46° to 21°) and robust mechanical strength compared with the bare PE separator (see Figure 23b–d). LiFePO$_4$/Li half cells show excellent rate capability at 10C. The LiFePO$_4$/C full cells with the Al$_2$O$_3$-CGSs also exhibit the better rate capability from 0.2C to 5C., indicating its promising application in LIBs with high safety and energy density as given in Figure 23e–g.

Coincidentally, Zhu et al.[69] prepared a ceramic (SiO$_2$)-grafted PE separator by electron beam irradiation (see **Figure 24**a). The SiO$_2$-grafted PE separators show similar thickness and pore structure to the bare separator, while displaying strong dimensional thermal stability at 180 °C. Besides, the grafted separators endow LIBs with high rate capacities from 0.2C to 5C, as shown in Figure 24b. Similarly, Na et al.[227] grafted SiO$_2$ nanoparticles onto a porous PE separator (Figure 24c) to improve the adhesion strength, thermal stability, and electrochemical performance of a polyolefin separator. The chemical grafting provided a much stronger adhesive strength (>2.5 N cm^{-1}) and reduced thermal shrinkage (<5% at 120 °C) than conventional physical coating of a ceramic particle-based polymer composite, as given in Figure 24d,e. LiFePO$_4$/Li cells fabricated with the
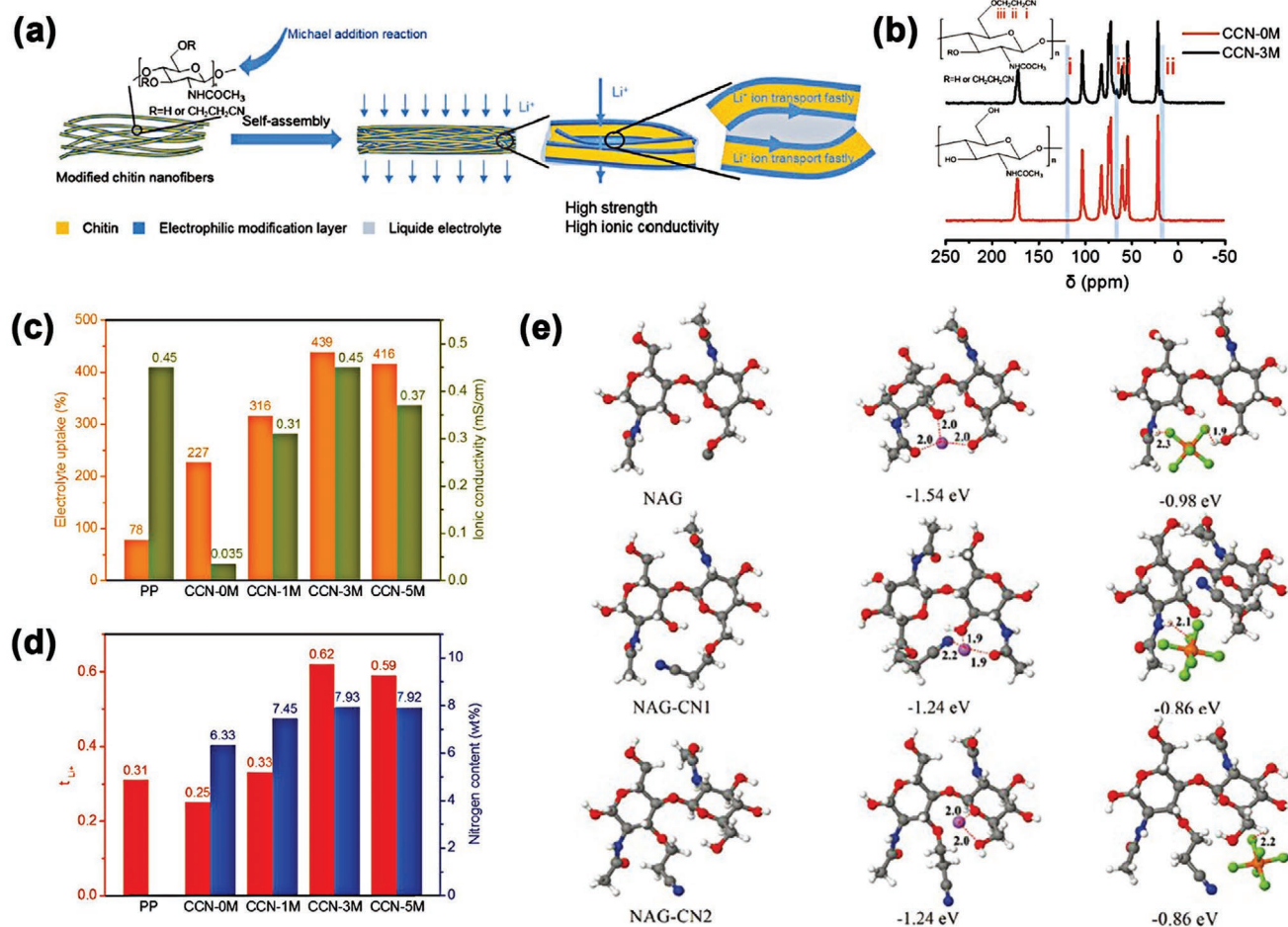
Figure 22. a) A new strategy to increase the ionic conductivity of chitin nanofiber separator through a chemical modification, and the strength is still high at the same time. b) The solid state ^{13}C NMR spectra of CCN-0M and CCN-3M separators. c) The Li$^+$ ion transference number and nitrogen content of commercial PP and CCN separators. d) The electrolyte uptake and ionic conductivities of PP and CCN separators. e) Binding energies for Li$^+$ (EC) and PF$_6^-$ with unmodified NAG, NAG-CN1 and NAG-CN2. Reproduced with permission.[225] Copyright 2019, Wiley-VCH GmbH.

SiO$_2$-grafted separator show excellent rate capabilities (68 mAh g^{-1} at 5C), as shown in Figure 24f.

In addition to ceramic grafted commercial separators, some organic polymers have been developed to graft on the surface of polyolefin separators. Most of grafted separators are prepared by radiation-induced graft polymerization, which is a well-known method for modification of polymeric material without changing mechanical properties, and is environmental-friendly due to free of catalysts or additive. Miao et al.[228] grafted polyacrylamide (PAAm) on PE separators (denoted as PE-g-PAAm) by radiation. PE-g-PAAm separators enhance the thermal stability and liquid electrolyte uptake (688.4%). The cells with the grafted separators show a higher ionic conductivity (0.76 × 10^{-3} S cm^{-1}) and more secure than cells containing PE membranes. Li et al.[229] designed polyacrylamide-grafted graphene oxide molecular brushes onto commercial PP separators. The composite separators integrate the lithiophilic feature of hairy polyacrylamide chains and fast electrolyte diffusion pathways with the excellent mechanical strength of graphene oxide nanosheets and thus enable molecular-level homogeneous and fast lithium ionic flux on the surfaces of electrodes. Dendrite free uniform

lithium deposition with a high Coulombic efficiency (98%) and ultralong-term reversible cycles at a high current density (2 mA cm^{-2}) are achieved for high safety and excellent performance LIBs. In addition, some studies have mentioned that the ceramic particles could be blended with the polymers, and then grafted on the commercial separators to enhance the mechanical strength and thermal stability. Liu et al.[230] prepared SiO$_2$/PAM-grafted PP separators. The shrinkage of the bare PP and SiO$_2$/PAM-grafted PP separators were 70% and 12% at 150 °C for 30 min, respectively. In addition, the surface contact angle of PP separator is reduced from 105° to 37° after grafting modification, thus showing better thermal stability and superior wettability of the composite separators. The cells with SiO$_2$/PAM-grafted PP separators have better rate capacities from 0.1C to 2C than those with bare PP.

3.5.3. Grafting Type Based on Other Polymers Separators

In order to improve the safety and performances of LIBs with the commercial separators, other polymers have been
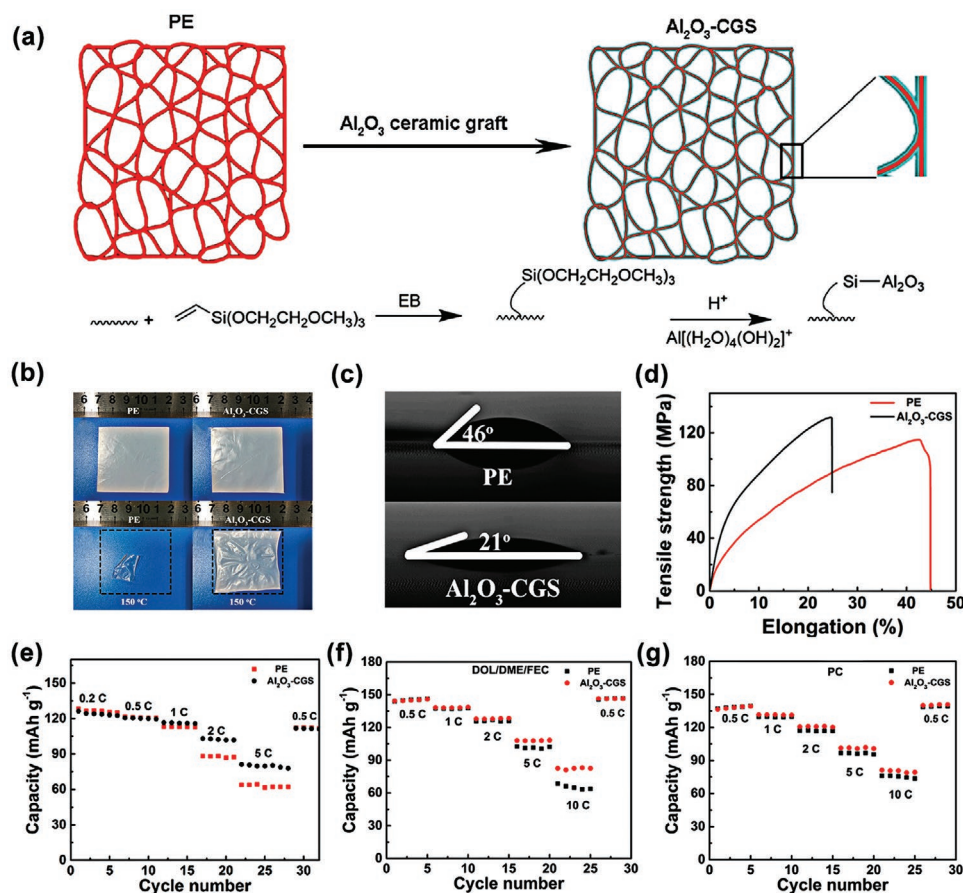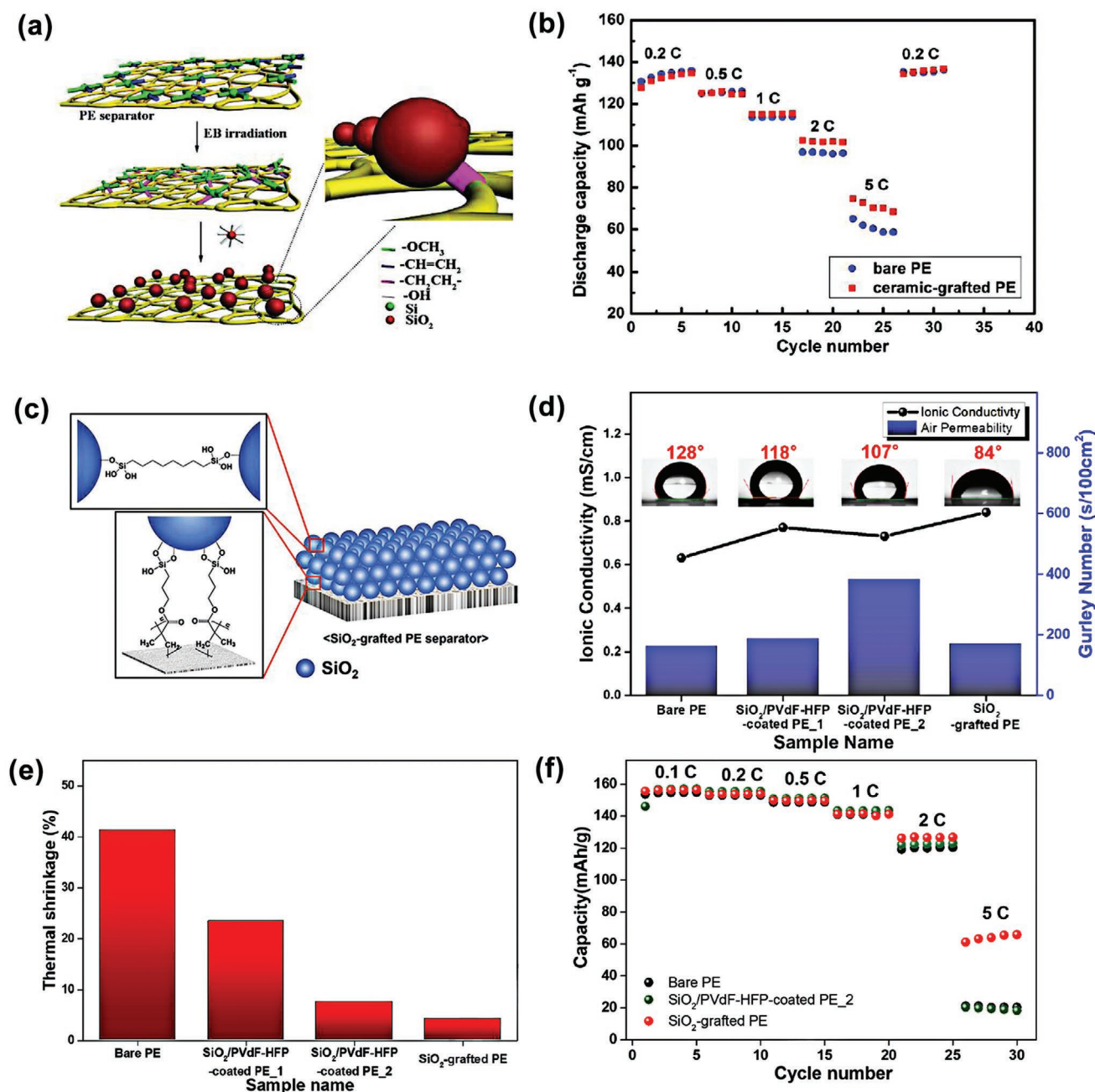
Figure 23. a) Schematic illustration and proposed mechanism of the preparation process of the Al_2O_3-CGS. b) Photographs of the PE and Al_2O_3-CGS before/after storage at 150 °C for 0.5 h. c,d) Electrolyte (EC/DEC/EMC) contact angle images and tensile curves of the PE and Al_2O_3-CGS. e) Rate capabilities of LFP/C full cells assembled with bare PE and Al_2O_3-CGS. f,g) Rate capabilities of Li/LFP half cells assembled with bare PE and Al_2O_3-CGS in DOL/DME/FEC and PC electrolyte. Reproduced with permission.[226] Copyright 2017, American Chemical Society.

reported as the substrate separators to be grafted by some additives or functional groups. Li et al.[231] synthesized Hydroxyl-terminated polybutadiene grafted methoxyl polyethylene glycol (HTPB-g-MPEG) using isophorone diisocyanate as the coupling agent, and blended with PVDF to fabricate porous separators. Compared with pure PVDF separators, the adoption of HTPB-g-MPEG could not only decrease the crystallinity, but also enhance the liquid electrolyte uptake and ion conductivity. Chen et al.[232] prepared functionalized TiO_2 grafted with 2-hydroxyethyl methacrylate by atom transfer radical polymerization technique and then blended with PI/PVDF-HFP membranes. The composite separators have a smaller fiber diameter, higher porosity, larger electrolyte uptake, smaller contact angle and more excellent thermal dimensional stability, which provides assistance for high safety LIBs.

Natural polymers are attractive sustainable raw materials to fabricate the grafted composite separators. The limitation of natural polymers, such as complicated pore-forming processes, low ionic conductivity, and relatively low mechanical strength, can be addressed by grafting. Moreover, except for the grafted particles or polymer fibers as the additives, the functional groups could be grafted on the surfaces of separators without increasing the thickness. Zhang et al.[225] proposed a

modification strategy for natural polymer nanofiber-based separators by grafting cyanoethyl groups on the surface of chitin nanofibers. The fabricated CCN separators maintain much higher thermal stability, exhibit enhanced electrolyte uptake and excellent ionic conductivity in comparison to unmodified chitin nanofiber and PP separators. Through density function theory calculations, the mechanism of high Li^+ ion transport in the CCN separator is unraveled as the weakening of the binding of Li^+ ions over that of PF^{6-} ions with chitin, via the cyanoethyl modification. The $LiFePO_4/Li_4Ti_5O_{12}$ full cells using CCN separators show much better rate capabilities from 0.1C to 3C compared to the cells with PP separators.

Polymer separators containing fluorine have also been reported as separators for LIBs, of which the common ones are PVDF, PVDF-HFP, PVDF-PTFE, and their composite separators, such as PVDF/PAN, and PVDF/PET mentioned above. They possess a good compatibility with liquid electrolytes, yet lower heat resistance. In addition to blending with other materials, grafting the functional groups containing fluorine is a promising alternative to enhance the thermostability and mechanical strength. Kong et al.[233] prepared a robust fluorinated polyimide (FPI) membrane. The thermally crosslinked FPI membranes possess considerable an excellent mechanical strength (31.7 MPa),

**ADVANCED
SCIENCE NEWS**

www.advancedsciencenews.com

**ADVANCED
FUNCTIONAL
MATERIALS**

www.afm-journal.de

Figure 24. a) Mechanism for the preparation of ceramic-grafted PE separators by irradiation grafting of SiO$_2$. b) Rate performances of the LiFePO$_4$ half cells using the bare and SiO$_2$ grafted PE separators. Reproduced with permission.[69] Copyright 2015, American Chemical Society. c) Schematic depiction of the fabrication of the SiO$_2$ grafted PE separator. d) Room temperature ionic conductivities, Gurley number, and (inset) contact angles of bare PE, SiO$_2$/PVDF-HFP-coated PE and SiO$_2$-grafted PE separators. e) Photographs of selected separators after the heat treatment at 120 °C for 30 min. f) Rate capabilities for cells fabricated with bare PE, SiO$_2$/PVDF-HFP-coated PE, and SiO$_2$-grafted PE separators. Reproduced with permission.[227] Copyright 2018, Elsevier B.V.

admirable thermal stability (no loss at 250 °C) and enhanced performance to prevent the growth and penetration of dendritic lithium. Moreover, compared with nonfluorinated PI separators (74 mAh g^{-1} at 5C), or PE separators (19 mAh g^{-1} at 5C), the cells with FPI separators exhibit an enhanced rate capacity (104 mAh g^{-1} at 5C). Furthermore, Li et al.[234] synthesized fluorinated polyether-ether-ketone (FPEEK) porous separators. The

FPEEK separators show much stronger antishrinkage properties than the commercial PP separator at 150 °C over 1 h. The FPEEK separator also exhibited a superior electrolyte uptake (559%), strong mechanical properties (27.7 MPa), high porosity (88%), and great ionic conductivity (3.12 mS cm^{-1}). More importantly, the cell assembled with this FPEEK separator presented outstanding C rate performances from 0.1C to 1C. **Table 4** shows the

ADVANCED
SCIENCE NEWS
www.advancedsciencenews.com

ADVANCED
FUNCTIONAL
MATERIALS
www.afm-journal.de

Table 4. The important characteristics of recently developed composite separators with the grafting structure for LIBs.

Materials	Grafted additives	Fabrication method	Separator thickness [μm]	Thermal shrinkage [%]	Tensile strength [MPa]	Liquid electrolyte types	Electrolyte uptake [%]	Ionic conductivity [mS cm^{-1}] at RT	Cathode/anode	Rate performance	Refs.
PE	Al$_2$O$_3$	Irradiation treated	16	0% at 150 °C for 1 h	131	LiPF$_6$-EC/DEC/EMC	–	0.53	LiFePO$_4$/graphite	80 mAh g^{-1} (61.5%) at 5C	[226]
PE	SiO$_2$	Irradiation treated	–	0% at 150 °C for 0.5 h	14.46	LiPF$_6$-EC/DEC/DMC	–	0.45	LiFePO$_4$/Li	75.4 mAh g^{-1} (58.4%) at 5C	[69]
PE	SiO$_2$	Chemical vapor deposition	16	15.23% at 150 °C for 0.5 h	–	LiPF$_6$-EC/DEC/EMC	–	0.759	LiCoO$_2$/Li	46.81 mAh g^{-1} (32%) at 5C	[70]
PE	Methylmethacrylate (MMA)	Irradiation treated	31	–	–	LiPF$_6$-EC/DMC	210	1.01	LiCoO$_2$/Li	102.5 mAh g^{-1} (74%) at 2C	[235]
PP	Octafluoropentyl methacrylate (OFPMA)	Irradiation treated	–	17.5% at 150 °C for 0.5 h	1.29	LiPF$_6$-EC/DEC	290	1.76	LiFePO$_4$/Li	130 mAh g^{-1} (87.8%) at 2C	[236]
PE	SiO$_2$	Irradiation treated	23	4.2% at 120 °C for 0.5 h	–	LiPF$_6$-EC/DEC	–	0.84	LiFePO$_4$/Li	65 mAh g^{-1} (41.7%) at 5C	[227]
PE	TiO$_2$	Irradiation treated	–	36% at 150 °C for 1 h	121.2	LiPF$_6$-EC/DEC/DMC	–	0.5	LiFePO$_4$/Li	79.8 mAh g^{-1} (60%) at 5C	[93]
PP	SiO$_2$-TEOS	Polymerization and condensation	25.6	4.6% at 150 °C for 0.5 h	–	LiPF$_6$-EC/DEC	–	1.6	LiFePO$_4$/Li	100 mAh g^{-1} (64.5%) at 8C	[94]
PE	PVDF-EC-(A-SiO$_2$)	Dip-coating	18	0% at 150 °C for 0.5 h	73	LiPF$_6$-EC/EMC	–	0.79	LiNi$_{0.5}$Mn$_{1.5}$O$_4$/Li	113 mAh g^{-1} (85.6%) at 5C	[237]
PP	SiO$_2$/PAM	Surface chemical modification	28	12% at 150 °C for 0.5 h	–	LiPF$_6$-EC/DMC	436	1.43	LiFePO$_4$/Li	88 mAh g^{-1} (50.3%) at 2C	[230]
Chitin	Cyanoethyl groups	Wet-laid	12	0% at 170 °C for 0.5 h	120	LiPF$_6$-EC/EMC/DMC	439	0.45	LiFePO$_4$/Li$_4$Ti$_5$O$_{12}$	94 mAh g^{-1} (62.3%) at 3C	[225]
MPEG	HTPB	Phase inversion	46	–	–	LiPF$_6$-EC/DMC/EMC	–	–	LiFePO$_4$/graphite	122 mAh g^{-1} (76.25%) at 1C	[231]
PPO-PEO	PDMS	Phase inversion	52.2	–	66	LiPF$_6$-EC/DMC/EMC	512	4.5	LiFePO$_4$/graphite	118 mAh g^{-1} (73.8%) at 1C	[238]
PEEK	Fluorinated groups	Electrospinning	30	0% at 150 °C for 1 h	27.7	LiPF$_6$-EC/DMC/EMC	559	3.12	LiFePO$_4$/Li	141 mAh g^{-1} (87.6%) at 1C	[234]
SiO$_2$-PVDF	PMMA	Irradiation treated	100	0% at 120 °C for 12 h	8.2	LiPF$_6$-EC/DEC	317	2.31	LiFePO$_4$/Li	130 mAh g^{-1} (83.3%) at 2C	[239]
PI	Fluorinated groups	Electrospinning + thermo-crosslinking	35	0% at 250 °C for 1 h	31.7	LiPF$_6$-EC/DMC/EMC	620.2	1.14	LiFePO$_4$/Li	103 mAh g^{-1} (64.3%) at 5C	[233]
Poly(ethylene-alt-maleic anhydride)	4-Amino-4′-trifluoromethyl bis(benzene sulfonyl)imide	Solution casting	24	5% at 325 °C for 0.5 h	15.5	LiPF$_6$-EC/PC	135	0.104	LiFePO$_4$/C	65 mAh g^{-1} (52.8%) at 5C	[240]

important characteristics of recently developed composite separators with the grafting structure for LIBs.

3.5.4. Section Summary

In this section, recent development in the composite separators with the grafting structure has been discussed including grafting structure based on the commercial separators and based on the other polymer materials, such as PVDF, PI and chitin. Through the surface modification type of grafting, the commercial separators have been modified by ceramic materials or ceramic-polymer blending materials to strengthen the thermal stability and wettability on basis of its original outstanding mechanical property. Moreover, grafted composite separators based on other polymers have also been developed because with the support of the substrate membranes, additive particles or functional groups can be added to improve the overall performances of the composite separators. The main feature of the grafting structure is that it

ADVANCED
SCIENCE NEWS
www.advancedsciencenews.com

ADVANCED
FUNCTIONAL
MATERIALS
www.afm-journal.de

could make up for the defects of the composite separators by adding the additives or functional groups. For example, the introduction of fluorine groups into the separator can form strong adsorption with the fluorine-containing electrolyte, thereby enhancing the lithium ion conductivity and further increasing the rate capacity of the battery. Moreover, another advantage of grafting structure is that additives or some functional groups are grafted on the membrane surface without sacrificing the porous structure and increasing the thickness. However, in the process of lithium ions passing through the separator, the surface of composite separators with the grafting type may also result in the detachment of particles or dissociation of groups, which depends on the binding force of the particles or functional groups to the substrate separators. Overall, under the premise of ensuring the mechanical and structure stabilities of the composite separators, this grafting type of separators can greatly improve the thermal stability and wettability compared with the commercial separators. As equipped into LIBs, the composite separators can improve the safety, ion conduction and rate performance.

4. Conclusion

Among numerous separators, composite separators have been widely concerned recently due to their improved thermal stability, mechanical strength, electrolyte uptake, surface properties through introducing additives. The performances of composite separators are closely related to the safety, stability, and rate discharge capacity of LIBs. In this review, the recent studies and developments in composite separators for safe and high rate LIBs with respect to their composite types are discussed. Composite separators can be divided into four categories according to the types of composite, including the blending structure, layer structure, core–shell structure and grafting structure. In addition, the recent progress in composite separators with these types for improving the core properties and for achieving safe and high rate LIBs have been discussed in detail.

For the blending structure type, composite separators based on commercial separators, based on PVDF and its co-polymers and based on other polymer materials have been demonstrated firstly. Although commercial polyolefin separators possess excellent mechanical strength, pore size, and good chemical stability, their inferior wettability and thermal stability are serious limitation for LIBs. As internal temperature of battery exceeds 120 °C, the commercial separators would shrink severely, causing a short circuit between positive and negative electrodes, thermal runaway, or even battery burning explosion. In addition, as lithium ions are excessively deposited on the electrode, lithium dendrites are generated and penetrate through the separator, resulting in capacity degradation and safety hazards of LIBs. Blending the ceramic particles or high melting point polymers can effectively improve the thermal stability and wettability of the commercial separators. In addition, PVDF and its co-polymers have been widely concerned due to their intrinsic good wettability, but the poor mechanical property needs to be improved by the additives for avoiding safety problems.

Other polymer materials have also been studied as the raw materials to form blending type of separators, achieving the optimal dual performance of raw materials and additives. For the type of blending structure, adjusting the proportion of the amount of raw materials and additives has become the key approach to control each performance of composite separators.

In addition to the blending structure type, the composite separators with the layered structure have also been reviewed. Commercial polyolefin separators are coated by the ceramic layer or polymer chain layer to improve the thermal stability and wettability. Other polymers, such as PVDF-HFP, PI and PET, are used as the substrate layer because of their intrinsic excellent properties. Based on the support of the substrate layer, the properties of the additive layers can be greatly highlighted in the layered composite membrane. Compared with the blending structure type, the composite separators with layered structure have unique advantages. The additive layers could be multifunctional. The conductive layers as the additives could be laminated to suppress the growth of lithium dendrites and further improve the safety of LIBs. Furthermore, the difference is also that each layer of the layered separator has different functions. For example, the upper layer introducing additives can increase mechanical properties and the lower layer can improve thermal stability. This composite separator can meet the demands of high safety and high rate LIBs.

The composite separators with the core–shell structure have been discussed. PVDF and its co-polymers, as long-chain macromolecular polymers, are usually designed as the shell structure to wrap nanoparticles or short-chain polymer molecules. The main role of the nanoparticles or short-chain polymers in the core–shell structure composite separators is to improve the mechanical strength, thermal stability, and flame retardancy. Other polymers, such as cellulose and PI, can also be used as the shell to improve the performance of composite separators after adding the additive core materials. The main feature of the core–shell structure is to maintain core's stability and avoid scattering or agglomeration of additives as lithium ions pass through the separators. Therefore, the composite separators with core–shell structure can greatly improve the structural stability under high current density in LIBs, thereby increasing the rate capacity.

The development in the composite separators with the grafting structure has been reviewed. The commercial separator-based and other polymer material-based, (PVDF, PI and chitin) grafting structures are discussed in detail. Through the surface modification type of grafting, the thermal stability and wettability of commercial separators have been greatly strengthened. Moreover, composite separators based on other polymers have also been developed to be grafted by particles or functional groups to improve the whole performance of the composite separators. Compared with other composite types, the main feature of the grafting structure is that additives or functional groups are grafted on the membrane surface without sacrificing the porous structure and increasing the thickness.

The advantages and disadvantages of four types of composite separators are shown in **Table 5**. Overall, no matter which the

**ADVANCED
SCIENCE NEWS**

www.advancedsciencenews.com

**ADVANCED
FUNCTIONAL
MATERIALS**

www.afm-journal.de

Table 5. The advantages and disadvantages of four types of composite separators.

Parameters	Blending structure	Layered structure	Core–shell structure	Grafting structure
Utilization efficiency of raw materials and additives functions	Good	Good	Fair	Good
Stability between raw materials and additives	Good	Fair	Outstanding	Good
Difficulty of preparation process	Easy	Easy	Relatively difficult	Relatively difficult
Variation of separators thickness	Controlled	Relatively big	Controlled	Least
Universality of composite types for materials	Fair	Good	Relatively poor	Fair
Optimization of separators for next generation LIBs	Outstanding	Outstanding	Good	Good

composite types of separators, only to address the potential problems of each composite types and combine their respective advantages, can they support for LIBs with high structural stability, improved thermal stability, robust mechanical strength, increased wettability, enhanced high ion conductivity, and excellent rate capacity performance.

In general, the types of composite separators are determined by the fillers. Therefore, the intrinsic properties of typical fillers are summarized in **Table 6**, including density, melting point/tolerance temperature, particle size/molecular weight, dielectric constant, cost and functionality of fillers. Composite separators can operate at high temperatures without thermal runaway because high melting point and maximum tolerance temperature of the fillers significantly improve the thermostability of the composite separators. In addition, the particle size and molecular weight of the fillers are also important for controlling the uniformity and stability of composite separators to affect the ion transport. Furthermore, the surface modification and the formation of specific structure of fillers can improve the separator wettability and dispersion in the polymer matrices. These fillers also form strong interaction with the polymer matrices to improve the tensile mechanical strength and ionic conductivity of the separators, thus enhancing the rate capacities of LIBs. In brief, the selection of fillers featured with various physical properties is particularly important to boost the physicochemical performances of composite separators and thus improve the overall electrochemical performances of LIBs.

5. Future Directions

The safe high rate capacity performances for the LIBs could be enhanced through the development of the composite separators with more superior structures and higher stability. Composite separators still have rooms for improving the thermal stability, ion transport structure, structure stability and ion conductivity.

On the basis of the analysis of recent development in separator technology, following future directions can lead toward safe and high rate LIBs:

1) Lower fabrication cost of separators: Manufacturing ultrathin separators is an effective strategy to achieve low cost because it uses less raw materials. Commercialized polyolefin separators have already reached 10 µm and the future objective is toward 5 µm. Inferior mechanical strength of ultrathin separators would be a challenge, but lower thickness is worth exploiting as it brings more benefits such as efficient packaging, higher energy density and lower impedance. Moreover, inexpensive raw materials, efficient production equipment and effective solvent recycle should also be optimized to minimize the overall cost.

2) Novel materials with high thermal stability: Conventional polyolefin separators shrink due to the elevated temperatures during long cycles or rapid charging and discharging for LIBs. This urgent problem has been explored and reported intensively and, thus, polymer materials with higher melting point are urgently needed as raw materials for the composite separators to ensure the high thermal stability of separators and to further improve sustainable development of LIBs, such as PI, PMIA, PPS, and PEEK.

3) State-of-the-art analysis of separator performances: Advanced characterization techniques, such as in situ scanning electron microscopy and in situ Raman spectroscopy, can be applied to examine the structural and chemical alteration of separators during battery operation. On the other hand, simulation methods should also be developed for investigating separators. Ab initio molecular dynamics (AIMD) simulation is a powerful tool for analyzing and understanding the ionic transport mechanisms across the separator. Artificial intelligence (AI) aided analysis models should also be designed and established to determine the necessary conditions for predicting separator performance before assembly.

4) Multifunctional separators for improving battery performances: Uncovering more separator functionalities: In the future, separator modification should not only improve the intrinsic properties of pristine separators, but also ameliorate other battery components. For example, flame retardant materials embedded within the separators can ensure battery safety by permeating out to extinguish the fire when LIBs overheat and catch fire. Also, some recent reports suggest that the introduction of positive or negative active materials into the separator decreases the interfacial impedance and provides extra capacity.

5) Sustainable and environmentally friendly technologies and materials: The components of current LIBs, including steel, Al foil, Cu foil, cathode, anode, separator, and electrolyte, can post environmental hazards. For the sustainable development of LIBs, recycling technologies for each component are of particular value. In terms of separators, more environmentally friendly separator materials and advanced recycling technologies are to be explored in the future. In particular, biodegradable polymers, such as PLA, polyhydroxyalkanoate, PBS, and polycaprolactone are expected to earn increased research interests in the separator field.

ADVANCED
SCIENCE NEWS

www.advancedsciencenews.com

ADVANCED
FUNCTIONAL
MATERIALS

www.afm-journal.de

Table 6. The main physical properties of fillers.

Fillers	Density [g cm^{-3}]	Melting point/ tolerance temperature [°C]	Particle size/ molecular weight	Dielectric constant	Cost	Functionality	Refs.
Al$_2$O$_3$	3.5	2054	20–60 nm	7.8	≈167 $ kg^{-1}, Acros Organics	Improve thermal stability, tensile strength, wettability	[123,170,214]
SiO$_2$	2.2	1723	20–40 nm	3.9	≈85 $ kg^{-1}, Sigma-Aldrich Inc.	Improve thermal stability, tensile strength, wettability	[47,119,237]
CeO$_2$	7.13	2397	25–40 nm	23	≈4000 $ kg^{-1}, Sigma-Aldrich Inc.	Improve thermal stability, tensile strength, wettability	[147]
TiO$_2$	4.26	1840	25–50 nm	85	≈150 $ kg^{-1}, Sigma-Aldrich Inc.	Improve thermal stability, tensile strength, wettability	[123,226,232]
ZrO$_2$	5.85	2700	40–50 nm	10	≈1730 $ kg^{-1}, Alfa Aesar	Improve thermal stability, tensile strength, wettability	[154,173,199]
Sb$_2$O$_3$	5.82	655	50–200 nm	2–2.5	≈260 $ kg^{-1}, Sigma-Aldrich Inc.	Improve tensile strength, wettability	[136]
hBN	2.25	3000	≈1000 nm	3.29	≈3700 $ kg^{-1}, Sigma-Aldrich Inc.	Improve wettability, suppress dendrite growth	[64,104]
Al(OH)$_3$	2.4	300	50–100 nm	2.2	≈166 $ kg^{-1}, Sigma-Aldrich Inc.	Improve tensile strength, wettability	[130]
PVDF	1.8	170	10–180 w	7.25	≈25 $ kg^{-1}, Solvay S.A.	Improve wettability	[190,231]
PVDF-HFP	1.78	143	30–60 w	8.4	≈30 $ kg^{-1}, Solvay S.A.	Improve wettability	[134,152]
PI	1.43	400	1.47–7.34 w	3.5	≈85 $ kg^{-1}, DuPont Co. Ltd.	Improve thermal stability, tensile strength, wettability	[180,224,241]
PBI	1.3	430	5–20 w	3.2	≈2000 $ kg^{-1}, DuPont Co. Ltd.	Improve thermal stability, tensile strength, wettability	[171,242]
PMIA	1.35	460	10–50 w	3.0	≈300 $ kg^{-1}, DuPont Co. Ltd.	Improve thermal stability, tensile strength, wettability	[73,212]
PMMA	1.17	160	12–100 w	4.9	≈10 $ kg^{-1}, LG. Co. Ltd.	Improve tensile strength, wettability	[129,206,222,243]
PEI	1.36	360	2000–25 000	3.3	≈25 $ kg^{-1}, DuPont Co. Ltd.	Improve thermal stability, tensile strength, wettability	[86,126]
POSS	1.37	230	2000–5000	2.47	≈155 $ kg^{-1}, DuPont Co. Ltd.	Improve wettability	[199]
PLA	1.26	176	1–20 w	2.9	≈5 $ kg^{-1}, NatureWorks	Improve tensile strength, wettability	[91]
PPTA	1.46	482	1.8–1.9 w	3.9	≈12 $ kg^{-1}, DuPont Co. Ltd.	Improve thermal stability, tensile strength, wettability	[172]
PTFE	2.2	327	10–55 w	2.02	≈30 $ kg^{-1}, DuPont Co. Ltd.	Improve thermal stability, tensile strength, wettability	[203,244]
POM	1.42	165	1–15 w	3.0	≈15 $ kg^{-1}, DuPont Co. Ltd.	Improve wettability	[165,245]
PU	1.25	170	200–10 000	5.6	≈6.5 $ kg^{-1}, Bayer Co. Ltd.	Improve wettability	[86,161,246]
Cellulose	2	274	5–250 w	3.2	≈5 $ kg^{-1}, DuPont Co. Ltd.	Improve thermal stability, tensile strength, wettability	[2,6,13,16,41,247]
Zeolite	1.75	1000	1.7–300 μm	2.56	≈480 $ kg^{-1}, Sigma-Aldrich Inc.	Improve thermal stability, tensile strength, wettability	[208]
Clay	2.7	1780	2–50 μm	9.5	–	Improve thermal stability, tensile strength, wettability	[134]
Hydroxyapatite	3.16	1670	50–500 nm	0.42	≈200 $ kg^{-1}, Sigma-Aldrich Inc.	Improve thermal stability, tensile strength, wettability	[29,157]
Glass fiber	2.56	1135	–	11.6	≈300 $ kg^{-1}, Sigma-Aldrich Inc.	Improve thermal stability, tensile strength, wettability	[118,162]

Acknowledgements

Conflict of Interest

The authors declare no conflict of interest.

Keywords

[1] F. Y. Cheng, J. Liang, Z. L. Tao, J. Chen, *Adv. Mater.* **2011**, *23*, 1695.
[2] Y. M. Zhao, F. S. Yue, S. C. Li, Y. Zhang, Z. R. Tian, Q. Xu, S. Xin, Y. G. Guo, *InfoMat.* **2021**, *3*, 460.
[3] G. Harper, R. Sommerville, E. Kendrick, L. Driscoll, P. Slater, R. Stolkin, A. Walton, P. Christensen, O. Heidrich, S. Lambert, A. Abbott, K. S. Ryder, L. Gaines, P. Anderson, *Nature* **2019**, *575*, 75.
[4] D. J. Chen, K. C. Wen, W. Q. Lv, Z. H. Wei, W. D. He, *Phys. Status Solidi-R.* **2018**, *12*, 13.
[5] S. K. Jung, I. Hwang, D. Chang, K. Y. Park, S. J. Kim, W. M. Seong, D. Eum, J. Park, B. Kim, J. Kim, J. H. Heo, K. Kang, *Chem. Rev.* **2020**, *120*, 6684.
[6] Z. Q. Zeng, X. W. Liu, X. Y. Jiang, Z. J. Liu, Z. Q. Peng, X. M. Feng, W. H. Chen, D. G. Xia, X. P. Ai, H. Yang, Y. L. Cao, *InfoMat.* **2020**, *2*, 984.
[7] J. B. Goodenough, K. S. Park, *J. Am. Chem. Soc.* **2013**, *135*, 1167.
[8] T. Sasaki, Y. Ukyo, P. Novak, *Nat. Mater.* **2013**, *12*, 569.
[9] J. P. Liu, L. W. Dong, D. J. Chen, Y. P. Han, Y. F. Liang, M. Q. Yang, J. C. Han, C. H. Yang, W. D. He, *Small Methods* **2020**, *4*, 8.
[10] E. S. Fan, L. Li, Z. P. Wang, J. Lin, Y. X. Huang, Y. Yao, R. J. Chen, F. Wu, *Chem. Rev.* **2020**, *120*, 7020.
[11] T. Y. Lei, W. Chen, W. Q. Lv, J. W. Huang, J. Zhu, J. W. Chu, C. Y. Yan, C. Y. Wu, Y. C. Yan, W. D. He, J. Xiong, Y. R. Li, C. L. Yan, J. B. Goodenough, X. F. Duan, *Joule* **2018**, *2*, 2091.
[12] M. Armand, J. M. Tarascon, *Nature* **2008**, *451*, 652.
[13] S. S. Zhang, *InfoMat.* **2020**, *2*, 942.
[14] B. Scrosati, J. Hassoun, Y. K. Sun, *Energy Environ. Sci.* **2011**, *4*, 3287.
[15] J. N. Liu, X. Y. Shi, B. Boateng, Y. P. Han, D. J. Chen, W. D. He, *ChemSusChem* **2019**, *12*, 908.
[16] Y. F. Zhao, J. C. Guo, *InfoMat.* **2020**, *2*, 866.
[17] D. J. Chen, Z. Q. Zhou, C. Feng, W. Q. Lv, Z. H. Wei, K. H. L. Zhang, B. Lin, S. H. Wu, T. Y. Lei, X. Y. Guo, G. L. Zhu, X. Jian, J. Xiong, E. Traversa, S. X. Dou, W. D. He, *Adv. Energy Mater.* **2019**, *9*, 11.
[18] C. F. J. Francis, I. L. Kyratzis, A. S. Best, *Adv. Mater.* **2020**, *32*, 1904205.
[19] W. J. Lu, Z. Z. Yuan, Y. Y. Zhao, H. Z. Zhang, H. M. Zhang, X. F. Li, *Chem. Soc. Rev.* **2017**, *46*, 2199.
[20] G. M. Zhou, L. Xu, G. W. Hu, L. Q. Mai, Y. Cui, *Chem. Rev.* **2019**, *119*, 11042.
[21] Y. X. Tang, Y. Y. Zhang, W. L. Li, B. Ma, X. D. Chen, *Chem. Soc. Rev.* **2015**, *44*, 5926.
[22] H. Lee, M. Yanilmaz, O. Toprakci, K. Fu, X. W. Zhang, *Energy Environ. Sci.* **2014**, *7*, 3857.
[23] M. Waqas, S. Ali, C. Feng, D. J. Chen, J. C. Han, W. D. He, *Small* **2019**, *15*, 44.
[24] M. R. Asghar, M. T. Anwar, A. Naveed, *Membranes* **2019**, *9*, 37.
[25] X. Wang, Q. H. Weng, Y. J. Yang, Y. Bando, D. Gotberg, *Chem. Soc. Rev.* **2016**, *45*, 4042.
[26] K. Liu, Y. Y. Liu, D. C. Lin, A. Pei, Y. Cui, *Sci. Adv.* **2018**, *4*, eaas9820.
[27] Y. H. Song, K. J. Wu, T. W. Zhang, L. L. Lu, Y. Guan, F. Zhou, X. X. Wang, Y. C. Yin, Y. H. Tan, F. Li, T. Tian, Y. Ni, H. B. Yao, S. H. Yu, *Adv. Mater.* **2019**, *31*, 1905711.
[28] Z. Chen, P. C. Hsu, J. Lopez, Y. Z. Li, J. W. F. To, N. Liu, C. Wang, S. C. Andrews, J. Liu, Y. Cui, Z. N. Bao, *Nat. Energy* **2016**, *1*, 8.
[29] H. Li, S. T. Guo, L. B. Wang, J. Wu, Y. J. Zhu, X. L. Hu, *Adv. Energy Mater.* **2019**, *9*, 12.
[30] C. J. Orendorff, T. N. Lambert, C. A. Chavez, M. Bencomo, K. R. Fenton, *Adv. Energy Mater.* **2013**, *3*, 314.
[31] M. Baginska, B. J. Blaiszik, R. J. Merriman, N. R. Sottos, J. S. Moore, S. R. White, *Adv. Energy Mater.* **2012**, *2*, 583.
[32] X. R. Lin, M. Salari, L. M. R. Arava, P. M. Ajayan, M. W. Grinstaff, *Chem. Soc. Rev.* **2016**, *45*, 5848.
[33] W. C. Ren, Y. N. Zheng, Z. H. Cui, Y. S. Tao, B. X. Li, W. T. Wang, *Energy Storage Mater.* **2021**, *35*, 157.
[34] X. R. Chen, B. C. Zhao, C. Yan, Q. Zhang, *Adv. Mater.* **2021**, *33*, 2004128.
[35] Z. Y. Wang, Z. X. Lu, W. Guo, Q. Luo, Y. H. Yin, X. B. Liu, Y. S. Li, B. Y. Xia, Z. P. Wu, *Adv. Mater.* **2021**, *33*, 2006702.
[36] M. F. Lagadec, R. Zahn, V. Wood, *Nat. Energy* **2019**, *4*, 16.
[37] Q. W. Lu, Y. B. He, Q. P. Yu, B. H. Li, Y. V. Kaneti, Y. W. Yao, F. Y. Kang, Q. H. Yang, *Adv. Mater.* **2017**, *29*, 8.
[38] J. X. Zheng, M. S. Kim, Z. Y. Tu, S. Choudhury, T. Tang, L. A. Archer, *Chem. Soc. Rev.* **2020**, *49*, 2701.
[39] S. O. Tung, S. Ho, M. Yang, R. L. Zhang, N. A. Kotov, *Nat. Commun.* **2015**, *6*, 6152.
[40] M. D. Tikekar, S. Choudhury, Z. Y. Tu, L. A. Archer, *Nat. Energy* **2016**, *1*, 16114.
[41] Z. H. Wei, Y. Q. Ren, J. Sokolowski, X. D. Zhu, G. Wu, *InfoMat.* **2020**, *2*, 483.
[42] B. Boateng, Y. P. Han, C. Zhen, G. F. Zeng, N. Chen, D. J. Chen, C. Feng, J. C. Han, J. Xiong, X. F. Duan, W. D. He, *Nano Lett.* **2020**, *20*, 2594.
[43] C. L. Jiang, Y. Fang, J. H. Lang, Y. B. Tang, *Adv. Energy Mater.* **2017**, *7*, 6.
[44] J. Y. Zhao, D. J. Chen, B. Boateng, G. F. Zeng, Y. P. Han, C. Zhen, J. B. Goodenough, W. D. He, *J. Power Sources* **2020**, *451*, 9.
[45] B. Kang, G. Ceder, *Nature* **2009**, *458*, 190.
[46] Y. Y. Liu, Y. Y. Zhu, Y. Cui, *Nat. Energy* **2019**, *4*, 540.
[47] K. Liu, D. Zhuo, H. W. Lee, W. Liu, D. C. Lin, Y. Y. Lu, Y. Cui, *Adv. Mater.* **2017**, *29*, 6.
[48] J. W. Liu, D. X. Xie, W. Shi, P. Cheng, *Chem. Soc. Rev.* **2020**, *49*, 1624.
[49] C. Z. Zhao, P. Y. Chen, R. Zhang, X. Chen, B. Q. Li, X. Q. Zhang, X. B. Cheng, Q. Zhang, *Sci. Adv.* **2018**, *4*, eaat3446.
[50] Z. D. Hao, Q. Zhao, J. D. Tang, Q. Q. Zhang, J. B. Liu, Y. H. Jin, H. Wang, *Mater. Horiz.* **2021**, *8*, 12.
[51] F. Zou, A. Manthiram, *Adv. Energy Mater.* **2020**, *10*, 2002508.
[52] J. Nunes-Pereira, C. M. Costa, S. Lanceros-Mendez, *J. Power Sources* **2015**, *281*, 378.
[53] Z. F. Qiu, S. Yuan, Z. Y. Wang, L. Y. Shi, J. H. Jo, S. T. Myung, J. F. Zhu, *J. Power Sources* **2020**, *472*, 228445.
[54] Z. H. Wang, R. J. Pan, C. Q. Ruan, K. Edstrom, M. Stromme, L. Nyholm, *Adv. Sci.* **2018**, *5*, 1700663.
[55] M. Waqas, S. Ali, D. J. Chen, B. Boateng, Y. P. Han, M. Zhang, J. C. Han, J. B. Goodenough, W. D. He, *Compos. Part B-Eng.* **2019**, *177*, 10.
[56] C. Feng, X. C. Wang, G. F. Zeng, D. J. Chen, W. Q. Lv, Y. P. Han, X. Jian, S. X. Dou, J. Xiong, W. D. He, *Phys. Status Solidi-R.* **2020**, *14*, 8.

ADVANCED
SCIENCE NEWS
www.advancedsciencenews.com

ADVANCED
FUNCTIONAL
MATERIALS
www.afm-journal.de

[57] Y. C. Zhang, Z. H. Wang, H. F. Xiang, P. C. Shi, H. H. Wang, *J. Membr. Sci.* **2016**, *509*, 19.

[58] C. Q. Zhu, J. X. Zhang, J. Xu, X. Z. Yin, J. Wu, S. H. Chen, Z. M. Zhu, L. X. Wang, H. Wang, *J. Membr. Sci.* **2019**, *588*, 8.

[59] M. Kim, J. H. Park, *Adv. Energy Mater.* **2013**, *3*, 1417.

[60] L. Li, M. Yu, C. Jia, J. X. Liu, Y. Y. Ly, Y. H. Liu, Y. Zhou, C. T. Liu, Z. Q. Shao, *ACS Appl. Mater. Interfaces* **2017**, *9*, 20885.

[61] C. M. Costa, M. Kundu, V. F. Cardoso, A. V. Machado, M. M. Silva, S. Lanceros-Mendez, *J. Membr. Sci.* **2018**, *564*, 842.

[62] M. N. Wang, X. Chen, H. Wang, H. B. Wu, X. Y. Jin, C. Huang, *J. Mater. Chem. A* **2017**, *5*, 311.

[63] C. J. Zhang, Y. F. Xia, K. H. Zuo, Y. P. Zeng, *J. Appl. Polym. Sci.* **2014**, *131*, 6.

[64] A. C. M. de Moraes, W. J. Hyun, N. S. Luu, J. M. Lim, K. Y. Park, M. C. Hersam, *ACS Appl. Mater. Interfaces* **2020**, *12*, 8107.

[65] Y. Kim, W. Y. Lee, K. J. Kim, J. S. Yu, Y. J. Kim, *J. Power Sources* **2016**, *305*, 225.

[66] Y. N. Wang, L. Y. Shi, H. L. Zhou, Z. Y. Wang, R. Li, J. F. Zhu, Z. F. Qiu, Y. Zhao, M. H. Zhang, S. Yuan, *Electrochim. Acta* **2018**, *259*, 386.

[67] Y. S. Zhu, F. X. Wang, L. L. Liu, S. Y. Xiao, Z. Chang, Y. P. Wu, *Energy Environ. Sci.* **2013**, *6*, 618.

[68] S. Li, K. Gao, *Ionics* **2010**, *16*, 555.

[69] X. M. Zhu, X. Y. Jiang, X. P. Ai, H. X. Yang, Y. L. Cao, *ACS Appl. Mater. Interfaces* **2015**, *7*, 24119.

[70] Y. Choi, J. I. Kim, J. Moon, J. Jeong, J. H. Park, *Appl. Surf. Sci.* **2018**, *444*, 339.

[71] Y. F. Li, Q. H. Li, Z. C. Tan, *J. Power Sources* **2019**, *443*, 20.

[72] Y. Xu, J. W. Zhu, J. B. Fang, X. Li, M. Yu, Y. Z. Long, *J. Nanomater.* **2020**, *2020*, 10.

[73] L. Y. Wang, N. P. Deng, J. G. Ju, G. Wang, B. W. Cheng, W. M. Kang, *Electrochim. Acta* **2019**, *300*, 263.

[74] F. H. Cui, W. D. Han, J. L. Ge, X. H. Wu, H. Kim, B. Ding, *Compos. Commun.* **2018**, *10*, 175.

[75] J. L. Pan, Z. Zhang, H. Zhang, P. P. Zhu, J. C. Wei, J. X. Cai, J. Yu, N. Koratkar, Z. Y. Yang, *ACS Appl. Energy Mater.* **2018**, *1*, 4794.

[76] M. Yanilmaz, X. W. Zhang, *Polymers* **2015**, *7*, 629.

[77] M. Yanilmaz, Y. Lu, Y. Li, X. W. Zhang, *J. Power Sources* **2015**, *273*, 1114.

[78] R. Liu, F. Wong, W. T. Duan, A. Sen, *Adv. Mater.* **2013**, *25*, 6997.

[79] L. H. Ye, K. C. Wen, Z. X. Zhang, F. Yang, Y. C. Liang, W. Q. Lv, Y. K. Lin, J. M. Gu, J. H. Dickerson, W. D. He, *Adv. Energy Mater.* **2016**, *6*, 15.

[80] Y. P. Han, L. H. Ye, B. Boateng, Q. W. Sun, C. Zhen, N. Chen, X. Y. Shi, J. H. Dickerson, X. Li, W. D. He, *J. Mater. Chem. A* **2019**, *7*, 1410.

[81] T. J. He, G. F. Zeng, C. Feng, X. Jian, N. Chen, Y. P. Han, Q. W. Sun, D. J. Chen, S. X. Dou, W. D. He, *J. Power Sources* **2020**, *448*, 8.

[82] Q. Xu, Q. S. Kong, Z. H. Liu, X. J. Wang, R. Z. Liu, J. J. Zhang, L. P. Yue, Y. L. Duan, G. L. Cui, *ACS Sustainable Chem. Eng.* **2014**, *2*, 194.

[83] H. S. Jeong, E. S. Choi, S. Y. Lee, *Electrochim. Acta* **2012**, *86*, 317.

[84] Z. H. Wang, H. F. Xiang, L. J. Wang, R. Xia, S. P. Nie, C. H. Chen, H. H. Wang, *J. Membr. Sci.* **2018**, *553*, 10.

[85] J. J. Zhang, Z. H. Liu, Q. S. Kong, C. J. Zhang, S. P. Pang, L. P. Yue, X. J. Wang, J. H. Yao, G. L. Cui, *ACS Appl. Mater. Interfaces* **2013**, *5*, 128.

[86] Y. Y. Zhai, K. Xiao, J. Y. Yu, B. Ding, *Electrochim. Acta* **2015**, *154*, 219.

[87] L. Q. Jiang, X. F. Zhang, Y. J. Chen, L. Qiao, X. L. Lu, X. Tian, *Mater. Chem. Phys.* **2018**, *219*, 368.

[88] C. Zhang, L. Shen, J. Q. Shen, F. Liu, G. Chen, R. Tao, S. X. Ma, Y. T. Peng, Y. F. Lu, *Adv. Mater.* **2019**, *31*, 8.

[89] M. Kim, G. Y. Han, K. J. Yoon, J. H. Park, *J. Power Sources* **2010**, *195*, 8302.

[90] G. Q. Dong, B. X. Liu, L. S. Kong, Y. A. Wang, G. F. Tian, S. L. Qi, D. Z. Wu, *ACS Sustainable Chem. Eng.* **2019**, *7*, 17643.

[91] X. Y. Jiang, L. F. Xiao, X. P. Ai, H. X. Yang, Y. L. Cao, *J. Mater. Chem. A* **2017**, *5*, 23238.

[92] K. Liu, W. Liu, Y. C. Qiu, B. A. Kong, Y. M. Sun, Z. Chen, D. Zhuo, D. C. Lin, Y. Cui, *Sci. Adv.* **2017**, *3*, e1601978.

[93] X. M. Zhu, X. Y. Jiang, X. P. Ai, H. X. Yang, Y. L. Cao, *J. Membr. Sci.* **2016**, *504*, 97.

[94] P. Zhao, J. P. Yang, Y. M. Shang, L. Wang, M. Fang, J. L. Wang, X. M. He, *J. Energy Chem.* **2015**, *24*, 138.

[95] C. E. Lin, H. Zhang, Y. Z. Song, Y. Zhang, J. J. Yuan, B. K. Zhu, *J. Mater. Chem. A* **2018**, *6*, 991.

[96] X. N. Feng, M. G. Ouyang, X. Liu, L. G. Lu, Y. Xia, X. M. He, *Energy Storage Mater.* **2018**, *10*, 246.

[97] X. Liu, D. S. Ren, H. J. Hsu, X. N. Feng, G. L. Xu, M. H. Zhuang, H. Gao, L. G. Lu, X. B. Han, Z. Y. Chu, J. Q. Li, X. M. He, K. Amine, M. G. Ouyang, *Joule* **2018**, *2*, 2047.

[98] I. Esho, K. Shah, A. Jain, *Appl. Therm. Eng.* **2018**, *145*, 287.

[99] A. Latz, J. Zausch, *J. Power Sources* **2011**, *196*, 3296.

[100] H. Li, X. B. Kong, C. Y. Liu, J. B. Zhao, *Appl. Therm. Eng.* **2019**, *161*, 114144.

[101] J. T. Hu, W. Li, Y. D. Duan, S. H. Cui, X. H. Song, Y. D. Liu, J. X. Zheng, Y. Lin, F. Pan, *Adv. Energy Mater.* **2017**, *7*, 1601894.

[102] A. Keller, D. Stark, H. Fierz, E. Heinzle, K. Hungerbuhler, *J. Loss Prev. Process Ind.* **1997**, *10*, 31.

[103] M. H. Ryou, Y. M. Lee, J. K. Park, J. W. Choi, *Adv. Mater.* **2011**, *23*, 3066.

[104] M. Waqas, S. Ali, W. Q. Lv, D. J. Chen, B. Boateng, W. D. He, *Adv. Mater. Interfaces* **2019**, *6*, 10.

[105] Z. X. Pan, J. E. Zhu, H. Y. Xu, T. Sedlatschek, X. W. Zhang, W. Li, T. Gao, Y. Xia, T. Wierzbicki, *Extreme Mech. Lett.* **2020**, *37*, 100705.

[106] M. H. Moghim, A. N. Bayani, R. Eqra, *Polym. Int.* **2020**, *69*, 545.

[107] H. Y. Xu, C. Bae, *J. Power Sources* **2019**, *430*, 67.

[108] J. C. Zheng, J. F. Yin, D. H. Zhang, G. J. Li, D. C. Bock, T. Tang, Q. Zhao, X. T. Liu, A. Warren, Y. Deng, S. Jin, A. Marschilok, E. S. Takeuchi, K. J. Takeuchi, C. D. Rahn, L. A. Archer, *Sci. Adv.* **2020**, *6*, eabb1122.

[109] E. P. Roth, D. H. Doughty, D. L. Pile, *J. Power Sources* **2007**, *174*, 579.

[110] S. S. Zhang, *J. Power Sources* **2007**, *164*, 351.

[111] X. S. Huang, *J. Solid State Electrochem.* **2011**, *15*, 649.

[112] J. H. Chen, H. J. Hu, S. Li, Y. L. He, *J. Appl. Polym. Sci.* **2018**, *135*, 46441.

[113] N. S. Selyutina, I. I. Argatov, G. S. Mishuris, *Mech. Res. Commun.* **2015**, *67*, 24.

[114] S. Beyer, O. Kobsch, D. Pospiech, F. Simon, C. Peter, K. Nikolowski, M. Wolter, B. Voit, *J. Adhes. Sci. Technol.* **2020**, *34*, 849.

[115] A. Schilling, S. Wiemers-Meyer, V. Winkler, S. Nowak, B. Hoppe, H. H. Heimes, K. Droder, M. Winter, *Energy Technol.* **2020**, *8*, 1900078.

[116] A. Lundblad, B. Bergman, *J. Electrochem. Soc.* **1997**, *144*, 984.

[117] M. S. Wu, T. L. Liao, Y. Y. Wang, C. C. Wan, *J. Appl. Electrochem.* **2004**, *34*, 797.

[118] B. Zhang, Q. F. Wang, J. J. Zhang, G. L. Ding, G. J. Xu, Z. H. Liu, G. L. Cui, *Nano Energy* **2014**, *10*, 277.

[119] B. Boateng, G. L. Zhu, W. Q. Lv, D. J. Chen, C. Feng, M. Waqas, S. Ali, K. C. Wen, W. D. He, *Phys. Status Solidi-R.* **2018**, *12*, 6.

[120] M. Shokrollahi, D. Semnani, M. Morshed, B. Rezaei, M. Mirsoofian, *J. Mater. Eng. Perform.* **2013**, *22*, 3639.

[121] M. Park, X. C. Zhang, M. D. Chung, G. B. Less, A. M. Sastry, *J. Power Sources* **2010**, *195*, 7904.

[122] L. S. Wang, H. B. Wu, S. R. Desai, L. Lou, *Phys. Rev. B* **1996**, *53*, 8028.

[123] S. Ali, C. Tan, M. Waqas, W. Q. Lv, Z. H. Wei, S. H. Wu, B. Boateng, J. N. Liu, J. Ahmed, J. Xiong, J. B. Goodenough, W. D. He, *Adv. Mater. Interfaces* **2018**, *5*, 10.

[124] N. Bizmark, M. A. Ioannidis, *Langmuir* **2015**, *31*, 9282.

ADVANCED
SCIENCE NEWS
www.advancedsciencenews.com

ADVANCED
FUNCTIONAL
MATERIALS
www.afm-journal.de

[125] M. S. Li, Y. H. Liao, Q. Y. Liu, J. X. Xu, F. B. Chen, J. H. Huang, W. S. Li, *Solid State Ionics* **2018**, *325*, 57.

[126] Z. Y. Wang, F. L. Guo, C. Chen, L. Y. Shi, S. Yuan, L. N. Sun, J. F. Zhu, *ACS Appl. Mater. Interfaces* **2015**, *7*, 3314.

[127] S. Y. Hu, S. D. Lin, Y. Y. Tu, J. W. Hu, Y. Wu, G. J. Liu, F. Li, F. M. Yu, T. T. Jiang, *J. Mater. Chem. A* **2016**, *4*, 3513.

[128] H. Chen, M. Ling, L. Hencz, H. Y. Ling, G. R. Li, Z. Lin, G. Liu, S. Q. Zhang, *Chem. Rev.* **2018**, *118*, 8936.

[129] Q. S. Fu, G. Lin, X. D. Chen, Z. X. Yu, R. S. Yang, M. T. Li, X. G. Zeng, J. Chen, *Energy Technol.* **2018**, *6*, 144.

[130] J. Q. Cui, J. Q. Liu, C. F. He, J. Li, X. F. Wu, *J. Membr. Sci.* **2017**, *541*, 661.

[131] M. Waqas, C. Tan, W. Q. Lv, S. Ali, B. Boateng, W. J. Chen, Z. H. Wei, C. Feng, J. Ahmed, J. B. Goodenough, W. D. He, *ChemElectroChem* **2018**, *5*, 2722.

[132] X. Y. Shi, Q. W. Sun, B. Boateng, Y. H. Niu, Y. D. Han, W. Q. Lv, W. D. He, *J. Power Sources* **2019**, *414*, 225.

[133] R. P. Luo, C. Wang, Z. X. Zhang, W. Q. Lv, Z. H. Wei, Y. N. Zhang, X. Y. Luo, W. D. He, *ACS Appl. Energy Mater.* **2018**, *1*, 921.

[134] M. Kim, J. K. Kim, J. H. Park, *Adv. Funct. Mater.* **2015**, *25*, 3399.

[135] K. Bicy, S. Suriyakumar, P. A. Paul, A. S. Anu, N. Kalarikkal, A. M. Stephen, V. G. Geethamma, D. Rouxel, S. Thomas, *New J. Chem.* **2018**, *42*, 19505.

[136] L. Wang, Z. Wang, Y. Sun, X. Liang, H. Xiang, *J. Membr. Sci.* **2019**, *572*, 512.

[137] W. S. Chen, H. P. Yu, S. Y. Lee, T. Wei, J. Li, Z. J. Fan, *Chem. Soc. Rev.* **2018**, *47*, 2837.

[138] J. J. Zhang, L. P. Yue, Q. S. Kong, Z. H. Liu, X. H. Zhou, C. J. Zhang, Q. Xu, B. Zhang, G. L. Ding, B. S. Qin, Y. L. Duan, Q. F. Wang, J. H. Yao, G. L. Cui, L. Q. Chen, *Sci. Rep.* **2014**, *4*, 8.

[139] X. H. Cao, C. L. Tan, M. Sindoro, H. Zhang, *Chem. Soc. Rev.* **2017**, *46*, 2660.

[140] S. L. Chen, Z. X. Zhang, L. Li, W. H. Yuan, *ChemistrySelect* **2018**, *3*, 13365.

[141] J. Shayapat, O. H. Chung, J. S. Park, *Electrochim. Acta* **2015**, *170*, 110.

[142] M. Yanilmaz, M. Dirican, X. W. Zhang, *Electrochim. Acta* **2014**, *133*, 501.

[143] Y. Z. Liang, Z. Lin, Y. P. Qiu, X. W. Zhang, *Electrochim. Acta* **2011**, *56*, 6474.

[144] M. H. Ryou, D. J. Lee, J. N. Lee, Y. M. Lee, J. K. Park, J. W. Choi, *Adv. Energy Mater.* **2012**, *2*, 645.

[145] S. S. Ma, H. Lin, L. Y. Yang, Q. S. Tong, F. Pan, J. Z. Weng, S. N. Zheng, *Electrochim. Acta* **2019**, *320*, 8.

[146] C. Y. Chao, Y. F. Feng, K. Hua, H. Li, L. J. Wu, Y. S. Zhou, Z. W. Dong, *J. Appl. Polym. Sci.* **2018**, *135*, 7.

[147] X. Y. Luo, Y. H. Liao, Y. M. Zhu, M. S. Li, F. B. Chen, Q. M. Huang, W. S. Li, *J. Power Sources* **2017**, *348*, 229.

[148] M. Yanilmaz, Y. Lu, M. Dirican, K. Fu, X. W. Zhang, *J. Membr. Sci.* **2014**, *456*, 57.

[149] J. W. Zhang, Y. K. Xiang, M. I. Jamil, J. G. Lu, Q. H. Zhang, X. L. Zhan, F. Q. Chen, *J. Membr. Sci.* **2018**, *564*, 753.

[150] C. Y. Cao, L. Tan, W. W. Liu, J. Q. Ma, L. Li, *J. Power Sources* **2014**, *248*, 224.

[151] X. S. Huang, *J. Power Sources* **2016**, *323*, 17.

[152] M. R. Asghar, Y. Zhang, A. M. Wu, X. H. Yan, S. Y. Shen, C. C. Ke, J. L. Zhang, *J. Power Sources* **2018**, *379*, 197.

[153] C. J. Fang, S. L. Yang, X. F. Zhao, P. F. Du, J. Xiong, *Mater. Res. Bull.* **2016**, *79*, 1.

[154] K. J. Kim, H. K. Kwon, M. S. Park, T. Yim, J. S. Yu, Y. J. Kim, *Phys. Chem. Chem. Phys.* **2014**, *16*, 9337.

[155] H. L. Chen, X. N. Jiao, *Solid State Ionics* **2017**, *310*, 134.

[156] H. Zhang, J. Liu, M. Guan, Z. Shang, Y. W. Sun, Z. H. Lu, H. L. Li, X. Y. An, H. B. Liu, *ACS Sustainable Chem. Eng.* **2018**, *6*, 4838.

[157] H. Li, D. B. Wu, J. Wu, L. Y. Dong, Y. J. Zhu, X. L. Hu, *Adv. Mater.* **2017**, *29*, 11.

[158] Q. Xu, C. Z. Wei, L. L. Fan, S. Peng, W. L. Xu, J. Xu, *Cellulose* **2017**, *24*, 1889.

[159] Q. F. Wang, *Electrochim. Acta* **2015**, *182*, 334.

[160] J. L. Shi, H. S. Hu, Y. G. Xia, Y. Z. Liu, Z. P. Liu, *J. Mater. Chem. A* **2014**, *2*, 9134.

[161] Y. Y. Zhai, K. Xiao, J. Y. Yu, J. M. Yang, B. Ding, *J. Mater. Chem. A* **2015**, *3*, 10551.

[162] S. Zhang, J. Cao, Y. M. Shang, L. Wang, X. M. He, J. J. Li, P. Zhao, Y. W. Wang, *J. Mater. Chem. A* **2015**, *3*, 17697.

[163] J. M. Kim, C. Kim, S. Yoo, J. H. Kim, J. H. Kim, J. M. Lim, S. Park, S. Y. Lee, *J. Mater. Chem. A* **2015**, *3*, 10687.

[164] M. Yanilmaz, Y. Lu, J. D. Zhu, X. W. Zhang, *J. Power Sources* **2016**, *313*, 205.

[165] J. C. Liu, K. Yang, Y. D. Mo, S. J. Wang, D. M. Han, M. Xiao, Y. Z. Meng, *J. Power Sources* **2018**, *400*, 502.

[166] G. Zainab, X. F. Wang, J. Y. Yu, Y. Y. Zhai, A. A. Babar, K. Xiao, B. Ding, *Mater. Chem. Phys.* **2016**, *182*, 308.

[167] Y. S. Oh, G. Y. Jung, J. H. Kim, J. H. Kim, S. H. Kim, S. K. Kwak, S. Y. Lee, *Adv. Funct. Mater.* **2016**, *26*, 7074.

[168] Y. C. Wen, X. S. Wang, Y. Yang, M. Z. Liu, W. Q. Tu, M. Q. Xu, G. Z. Sun, S. Kawaguchi, G. Z. Cao, W. S. Li, *J. Mater. Chem. A* **2019**, *7*, 26540.

[169] G. H. Feng, Z. H. Li, L. W. Mi, J. Y. Zheng, X. M. Feng, W. H. Chen, *J. Power Sources* **2018**, *376*, 177.

[170] Y. S. Jung, A. S. Cavanagh, L. Gedvilas, N. E. Widjonarko, I. D. Scott, S. H. Lee, G. H. Kim, S. M. George, A. C. Dillon, *Adv. Energy Mater.* **2012**, *2*, 1022.

[171] D. Li, D. Q. Shi, Z. Z. Yuan, K. Feng, H. M. Zhang, X. F. Li, *J. Membr. Sci.* **2017**, *542*, 1.

[172] L. Y. He, T. Qiu, C. J. Xie, X. L. Tuo, *J. Appl. Polym. Sci.* **2018**, *135*, 9.

[173] W. X. Xu, Z. Y. Wang, L. Y. Shi, Y. Ma, S. Yuan, L. N. Sun, Y. Zhao, M. H. Zhang, J. F. Zhu, *ACS Appl. Mater. Interfaces* **2015**, *7*, 20678.

[174] G. F. Zeng, J. Y. Zhao, C. Feng, D. J. Chen, Y. Meng, B. Boateng, N. Lu, W. D. He, *ACS Appl. Mater. Interfaces* **2019**, *11*, 26402.

[175] M. S. Gonzalez, Q. Z. Yan, J. Holoubek, Z. H. Wu, H. Y. Zhou, N. Patterson, V. Petrova, H. D. Liu, P. Liu, *Adv. Mater.* **2020**, *32*, 9.

[176] C. H. Zhu, T. Nagaishi, J. Shi, H. Lee, P. Y. Wong, J. H. Sui, K. Hyodo, I. S. Kim, *ACS Appl. Mater. Interfaces* **2017**, *9*, 26400.

[177] K. Peng, B. A. Wang, C. C. Ji, *J. Appl. Polym. Sci.* **2017**, *134*, 7.

[178] Q. Z. Liu, M. Xia, J. H. Chen, Y. F. Tao, Y. D. Wang, K. Liu, M. F. Li, W. W. Wang, D. Wang, *Electrochim. Acta* **2015**, *176*, 949.

[179] X. X. Liang, Y. Yang, X. Jin, Z. H. Huang, F. Y. Kang, *J. Membr. Sci.* **2015**, *493*, 1.

[180] G. H. Sun, G. Q. Dong, L. S. Kong, X. N. Yan, G. F. Tian, S. L. Qi, D. Z. Wu, *Nanoscale* **2018**, *10*, 22439.

[181] S. Y. Xiao, Y. Q. Yang, M. X. Li, F. X. Wang, Z. Chang, Y. P. Wu, X. Liu, *J. Power Sources* **2014**, *270*, 53.

[182] R. J. Pan, R. Sun, Z. H. Wang, J. Lindh, K. Edstrom, M. Stromme, L. Nyholm, *Nano Energy* **2019**, *55*, 316.

[183] R. J. Pan, R. Sun, Z. H. Wang, J. Lindh, K. Edstrom, M. Stromme, L. Nyholm, *Energy Storage Mater.* **2019**, *21*, 464.

[184] J. K. Pi, G. P. Wu, H. C. Yang, C. G. Arges, Z. K. Xu, *ACS Appl. Mater. Interfaces* **2017**, *9*, 21971.

[185] H. Y. Liu, J. Xu, B. H. Guo, X. M. He, *Ceram. Int.* **2014**, *40*, 14105.

[186] J. H. Wu, X. X. Zuo, Q. Y. Chen, X. Deng, H. Y. Liang, T. M. Zhu, J. S. Liu, W. J. Li, J. M. Nan, *Electrochim. Acta* **2019**, *320*, 11.

[187] D. Yeon, Y. Lee, M. H. Ryou, Y. M. Lee, *Electrochim. Acta* **2015**, *157*, 282.

[188] J. H. Dai, C. Shi, C. Li, X. Shen, L. Q. Peng, D. Z. Wu, D. H. Sun, P. Zhang, J. B. Zhao, *Energy Environ. Sci.* **2016**, *9*, 3252.

[189] Y. Liu, Y. S. Jiang, F. F. Li, B. Xue, X. W. Cao, *J. Electrochem. Soc.* **2019**, *166*, A1082.

[190] M. Y. An, H. T. Kim, D. R. Chang, *J. Solid State Electrochem.* **2014**, *18*, 1807.

[191] S. W. Kim, K. Y. Cho, *J. Mater. Chem. A* **2016**, *4*, 5069.

[192] X. D. Ma, X. X. Zuo, J. H. Wu, X. Deng, X. Xiao, J. S. Liu, J. M. Nan, *J. Mater. Chem. A* **2018**, *6*, 1496.

[193] C. Shi, J. H. Dai, X. Shen, L. Q. Peng, C. Li, X. Wang, P. Zhang, J. B. Zhao, *J. Membr. Sci.* **2016**, *517*, 91.

[194] Y. Lee, H. Lee, T. Lee, M. H. Ryou, Y. M. Lee, *J. Power Sources* **2015**, *294*, 537.

[195] J. L. Shi, Y. G. Xia, S. J. Han, L. F. Fang, M. Z. Pan, X. X. Xu, Z. P. Liu, *J. Power Sources* **2015**, *273*, 389.

[196] J. Liu, Y. B. Liu, W. X. Yang, Q. Ren, F. Y. Li, Z. Huang, *J. Power Sources* **2018**, *396*, 265.

[197] P. Zhang, L. X. Chen, C. Shi, P. T. Yang, J. B. Zhao, *J. Power Sources* **2015**, *284*, 10.

[198] X. F. Mao, L. Y. Shi, H. J. Zhang, Z. Y. Wang, J. F. Zhu, Z. F. Qiu, Y. Zhao, M. H. Zhang, S. Yuan, *J. Power Sources* **2017**, *342*, 816.

[199] M. M. Chi, L. Y. Shi, Z. Y. Wang, J. F. Zhu, X. F. Mao, Y. Zhao, M. H. Zhang, L. N. Sun, S. Yuan, *Nano Energy* **2016**, *28*, 1.

[200] Z. X. Zhang, W. H. Yuan, L. Li, *Particuology* **2018**, *37*, 91.

[201] Y. S. Zhu, S. Y. Xiao, Y. Shi, Y. Q. Yang, Y. Y. Hou, Y. P. Wu, *Adv. Energy Mater.* **2014**, *4*, 9.

[202] J. Q. Zhang, S. Q. Chen, X. Q. Xie, K. Kretschmer, X. D. Huang, B. Sun, G. X. Wang, *J. Membr. Sci.* **2014**, *472*, 133.

[203] M. Xiong, H. L. Tang, Y. D. Wang, Y. Lin, M. L. Sun, Z. F. Yin, M. Pan, *J. Power Sources* **2013**, *241*, 203.

[204] H. S. Jeong, E. S. Choi, J. H. Kim, S. Y. Lee, *Electrochim. Acta* **2011**, *56*, 5201.

[205] W. Xiao, J. J. Wang, H. Wang, Y. Q. Gong, L. N. Zhao, J. G. Liu, C. W. Yan, *J. Solid State Electrochem.* **2016**, *20*, 2847.

[206] J. H. Cho, J. H. Park, J. H. Kim, S. Y. Lee, *J. Mater. Chem.* **2011**, *21*, 8192.

[207] M. Xia, Q. Z. Liu, Z. Zhou, Y. F. Tao, M. F. Li, K. Liu, Z. H. Wu, D. Wang, *J. Power Sources* **2014**, *266*, 29.

[208] W. Xiao, Z. G. Gao, S. L. Wang, J. G. Liu, C. W. Yan, *Mater. Lett.* **2015**, *145*, 177.

[209] J. Lee, C. L. Lee, K. Park, I. D. Kim, *J. Power Sources* **2014**, *248*, 1211.

[210] C. Shi, P. Zhang, S. H. Huang, X. Y. He, P. T. Yang, D. Z. Wu, D. H. Sun, J. B. Zhao, *J. Power Sources* **2015**, *298*, 158.

[211] M. Y. Zhang, M. X. Li, Z. Chang, Y. F. Wang, J. Gao, Y. S. Zhu, Y. P. Wu, W. Huang, *Electrochim. Acta* **2017**, *245*, 752.

[212] Y. Y. Zhai, N. Wang, X. Mao, Y. Si, J. Y. Yu, S. S. Al-Deyab, M. El-Newehy, B. Ding, *J. Mater. Chem. A* **2014**, *2*, 14511.

[213] S. R. Park, Y. C. Jung, W. K. Shin, K. H. Ahn, C. H. Lee, D. W. Kim, *J. Membr. Sci.* **2017**, *527*, 129.

[214] Y. Yang, X. P. Huang, Z. Y. Cao, G. Chen, *Nano Energy* **2016**, *22*, 301.

[215] X. Shen, C. Li, C. Shi, C. C. Yang, L. Deng, W. Zhang, L. Q. Peng, J. H. Dai, D. Z. Wu, P. Zhang, J. B. Zhao, *Appl. Surf. Sci.* **2018**, *441*, 165.

[216] F. L. Huang, Y. F. Xu, B. Peng, Y. F. Su, F. Jiang, Y. L. Hsieh, Q. F. Wei, *ACS Sustainable Chem. Eng.* **2015**, *3*, 932.

[217] F. L. Huang, W. T. Liu, P. Y. Li, J. X. Ning, Q. F. Wei, *Materials* **2016**, *9*, 11.

[218] S. Park, C. W. Son, S. Lee, D. Y. Kim, C. Park, K. S. Eom, T. F. Fuller, H. I. Joh, S. M. Jo, *Sci. Rep.* **2016**, *6*, 8.

[219] F. J. Jiang, Y. Nie, L. Yin, Y. Feng, Q. C. Yu, C. Y. Zhong, *J. Membr. Sci.* **2016**, *510*, 1.

[220] X. H. Zhou, L. P. Yue, J. J. Zhang, Q. S. Kong, Z. H. Liu, J. H. Yao, G. L. Cui, *J. Electrochem. Soc.* **2013**, *160*, A1341.

[221] C. Shi, J. H. Dai, S. H. Huang, C. Li, X. Shen, P. Zhang, D. Z. Wu, D. H. Sun, J. B. Zhao, *J. Membr. Sci.* **2016**, *518*, 168.

[222] P. T. Yang, P. Zhang, C. Shi, L. X. Chen, J. H. Dai, J. B. Zhao, *J. Membr. Sci.* **2015**, *474*, 148.

[223] W. T. Fu, R. J. Xu, X. Q. Zhang, Z. Q. Tian, H. H. Huang, J. Y. Xie, C. H. Lei, *J. Power Sources* **2019**, *436*, 6.

[224] G. Q. Dong, B. X. Liu, G. H. Sun, G. F. Tian, S. L. Qi, D. Z. Wu, *J. Membr. Sci.* **2019**, *577*, 249.

[225] T. W. Zhang, J. L. Chen, T. Tian, B. Shen, Y. D. Peng, Y. H. Song, B. Jiang, L. L. Lu, H. B. Yao, S. H. Yu, *Adv. Funct. Mater.* **2019**, *29*, 9.

[226] X. Y. Jiang, X. M. Zhu, X. P. Ai, H. X. Yang, Y. L. Cao, *ACS Appl. Mater. Interfaces* **2017**, *9*, 25970.

[227] W. Na, K. H. Koh, A. S. Lee, S. Cho, B. Ok, S. W. Hwang, J. H. Lee, C. M. Koo, *J. Membr. Sci.* **2019**, *573*, 621.

[228] X. L. Miao, J. H. Li, Q. Xiang, J. Q. Xu, L. F. Li, J. Y. Li, *Nucl. Sci. Tech.* **2017**, *28*, 7.

[229] C. F. Li, S. H. Liu, C. G. Shi, G. H. Liang, Z. T. Lu, R. W. Fu, D. C. Wu, *Nat. Commun.* **2019**, *10*, 9.

[230] M. H. Liu, P. P. Zhang, L. T. Gou, Z. Y. Hou, B. Huang, *Mater. Lett.* **2017**, *208*, 98.

[231] H. Li, D. H. Niu, H. Zhou, C. Y. Chao, L. J. Wu, P. L. Han, *Appl. Surf. Sci.* **2018**, *440*, 186.

[232] W. Y. Chen, Y. B. Liu, Y. Ma, W. X. Yang, *J. Power Sources* **2015**, *273*, 1127.

[233] L. Y. Kong, Y. R. Yan, Z. M. Qiu, Z. Q. Zhou, J. Q. Hu, *J. Membr. Sci.* **2018**, *549*, 321.

[234] H. Li, B. Zhang, W. Liu, B. Lin, Q. Q. Ou, H. Wang, M. L. Fang, D. Liu, S. Neelakandan, L. Wang, *Electrochim. Acta* **2018**, *290*, 150.

[235] K. Gao, X. G. Hu, T. F. Yi, C. S. Dai, *Electrochim. Acta* **2006**, *52*, 443.

[236] X. F. Li, J. L. He, D. Z. Wu, M. Z. Zhang, J. W. Meng, P. H. Ni, *Electrochim. Acta* **2015**, *167*, 396.

[237] X. X. Zuo, J. H. Wu, X. D. Ma, X. Deng, J. X. Cai, Q. Y. Chen, J. S. Liu, J. M. Nan, *J. Power Sources* **2018**, *407*, 44.

[238] H. Li, H. Zhang, Z. Y. Liang, Y. M. Chen, B. K. Zhu, L. P. Zhu, *Electrochim. Acta* **2014**, *116*, 413.

[239] C. L. Yang, Z. H. Li, W. J. Li, H. Y. Liu, Q. Z. Xiao, G. T. Lei, Y. H. Ding, *J. Membr. Sci.* **2015**, *495*, 341.

[240] Q. Y. Pan, Y. Z. Chen, Y. F. Zhang, D. L. Zeng, Y. B. Sun, H. S. Cheng, *J. Power Sources* **2016**, *336*, 75.

[241] J. V. Facinelli, S. L. Gardner, L. Dong, C. L. Sensenich, R. M. Davis, J. S. Riffle, *Macromolecules* **1996**, *29*, 7342.

[242] Y. Yuan, F. Johnson, I. Cabasso, *J. Appl. Polym. Sci.* **2009**, *112*, 3436.

[243] T. Kawaguchi, L. V. J. Lassila, A. Tokue, Y. Takahashi, P. K. Vallittu, *J. Mech. Behav. Biomed. Mater.* **2011**, *4*, 1846.

[244] U. Lappan, U. Geissler, L. Haussler, G. Pompe, U. Scheler, *Macromol. Mater. Eng.* **2004**, *289*, 420.

[245] D. Q. Liu, S. H. Zhang, H. F. Cheng, R. F. Peng, Z. J. Luo, *Sci. Rep.* **2019**, *9*, 18107.

[246] S.-H. Sur, P.-J. Choi, J.-W. Ko, J.-Y. Lee, Y.-H. Lee, H.-D. Kim, *Int. J. Polym. Sci.* **2018**, *2018*, 7370852.

[247] X. D. Wang, C. H. Yao, F. Wang, Z. D. Li, *Small* **2017**, *13*, 19.
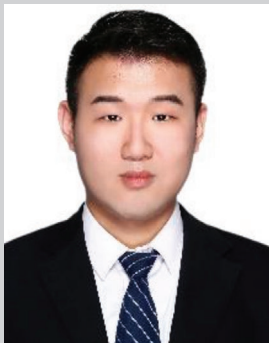
Botao Yuan is a Ph.D. student in the Center for Composite Materials and Structures, Harbin Institute of Technology, and is researching separators for lithium ion batteries. He received his bachelor's degree in 2016 and master's degree in 2019 both from University of Electronic Science and Technology of China. His research involves the development of composite separators for high performance lithium ion batteries and the synthesis of advanced energy materials for lithium based batteries.

Weidong He is a professor in the Center for Composite Materials and Structures, Harbin Institute of Technology, leading a group of researchers working on synthesis, property analysis, and theoretical simulations of energy materials for batteries and fuel cells. He received his Ph.D. from Vanderbilt University in 2012. He then went to Pacific Northwest National Laboratory for his postdoctoral research. His research involves designing efficient battery/fuel cell systems with preevaluated electrodes, electrolytes, and operating conditions.